September 14, 1973

PIO-01-06

ANALYSIS REPORT

STRUCTURAL ANALYSES OF MAIN STEAM CHECK & ISOLATION VALVES FOR PRAIRIE ISLAND, UNIT 1

Prepared for

Pioneer Service & Engineering Company

by

Nuclear Services Corporation

CAMPBELL, CALIFORNIA

Prepared by: C. E. Willey

A. J. Elliott

K. C. Wang

R. G. Petersen

Approved by: G. A. Randall

Issued by: R. E. Keever

Date: 9/15/73

September 14, 1973

PIO-01-06

ANALYSIS REPORT

STRUCTURAL ANALYSES OF MAIN STEAM CHECK & ISOLATION VALVES FOR PRAIRIE ISLAND, UNIT 1

Prepared for

Pioneer Service & Engineering Company

by

Nuclear Services Corporation

CAMPBELL, CALIFORNIA

Prepared by: C. E. Willey

A. J. Elliott

K. C. Wang

R. G. Petersen

Approved by: G. A. Randall

Issued by: R. E. Keever

Date: 9/15/73

ABSTRACT

The main steam isolation and check valve, manufactured by Schutte & Koerting Company for Prairie Island Unit 1, were analyzed to verify the ability to withstand the dynamic effects of the closure event following a postulated pipe rupture. Elastic-plastic finite element techniques were utilized with both static and nonlinear dynamic analyses. The valve components examined (the disc, tail link, rock shaft, and valve body seat area) were shown to meet the design criteria. Additional analyses were performed for the isolation valve to evaluate the effects of spurious closures on the ability of the valve to withstand a closure following pipe rupture. A measurable limit was established for the allowable permanent deformation caused by spurious closures.

TABLE OF CONTENTS

1.0 INTRODUCTION

This report, prepared for Pioneer Service and Engineering Company, presents the results of the structural analyses performed by Nuclear Services Corporation on the Prairie Island Unit 1 main steam check and isolation valves for closure following a postulated pipe rupture. The isolation valve was also investigated to determine the effects of spurious trips upon closure following a pipe rupture.

The components analyzed were the rotating assembly, which includes the disc, the tail link, the rock shaft and the valve body seat area. The effects of closure on the valve body proper, attached piping system and other components of the valve were not a part of this analysis.

The primary load conditions imposed on the valve assembly are a result of the kinetic energy developed during valve closure. This closure results in a centrifugal force on the tail link and an impact force between the disc and valve body. The kinetic energy and angular velocities of the closure assembly were determined by Nuclear Services Corporation, and are reported in Reference 1. Secondary loading conditions, such as the pressure acting on the disc, asymmetry at impact, and post impact effects, were also considered in the analyses.

For the tail link, disc, and valve body seat area finite element models were developed and static elastic-plastic analyses were performed to

determine load, deflection, and strain relationships. The total energy absorbed by the disc and valve seat as a function of the impact force was then determined from the combined static load-deflection characteristics of the disc and valve seat.

A multi-dimensional, nonlinear dynamic model was developed to determine the distribution of valve seat loading upon disc impact. It served to check the assumption of axisymmetric deformation employed in the finite element calculations.

A one dimensional, nonlinear dynamic model was used to determine response characteristics, including rebound radial acceleration. A similar model was used to determine dynamic response of the tail link during angular closure.

Structural analyses were also performed on the rock shaft and the shaft portion of the disc where the tail link is attached. Both of these areas were examined when the rotating assembly was subjected to the peak centrifugal force.

2.0 DESIGN ANALYSIS CRITERIA

The design criteria as defined for the main steam check and isolation valves following a pipe break is established to insure that the valve disc, body seat area, tail link and rock shaft survive the closure and perform the intended function of preventing further steam flow. The valve is considered to meet the design criteria if, following a pipe break:

1. The maximum material strain level within the components is less than 50 percent of the ultimate strain;

and

2. The resulting centerline offset between the disc and valve body is less than the specified disc to seat overlap of 0.625 inches.

3.0 DESCRIPTION OF CHECK VALVE COMPONENTS AND MATERIALS

The main steam check and isolation valves for Prairie Island Unit 1 are supplied by Schutte & Koerting Company (S&K). The general configuration of these valves and their principal components (valve body, disc, tail link and rock shaft) are shown in Figure 3-1. Closure of the isolation valve is initiated by a release mechanism which forces the disc into the flow, thus allowing the steam to accelerate the disc towards its seated position.

Table 3-1 identifies each of the components which were analyzed and the drawing number defining the appropriate design. The check and isolation valves are identical except for the tail link. The tail link for the check valve is slightly stronger as a result of the additional thickness for the limit stop (Figure 3-1). In addition, Table 3-1 identifies the material of each component. The material properties are defined in Figures E-1 to E-5 of Appendix E. Except for the seat welds, material properties from lot tests at room temperatures and properties at the operating temperature for the disc were supplied by Pioneer Service & Engineering Company (References 2 and 3). All other properties were obtained by Nuclear Services Corporation from the references noted in the figures. As can be seen from the stress-strain curves, the materials utilized for the valve components are ductile and can absorb large amounts of energy by plastic deformation.

TABLE 3-1

COMPONENT	S&K DRAWING NO.	MATERIAL	MATERIAL PROPERTIES
Check & Isolation Valve	70-XA-16	N/A	N/A
Disc Body	73-E-49	410 CB	Figure E-1
Disc Seat		E-306-CL-15	Figure E-2
Tail Link-Isolation	70-E-14*	A216 WCB	Figure E-3
Tail Link-Check	70-E-85*		
Rock Shaft	68-G-118	416	Figure E-4
	69-E-56		
Valve Body	sketch (See Figure 3-2)	A216 WCB	Figure E-3
Valve Body Seat		316	Figure E-5

* It is assumed that the tail links will be machined to fit the disc defined in Drawing Number 73-E-49.

Nuclear Services Corporation
CAMPBELL, CALIFORNIA

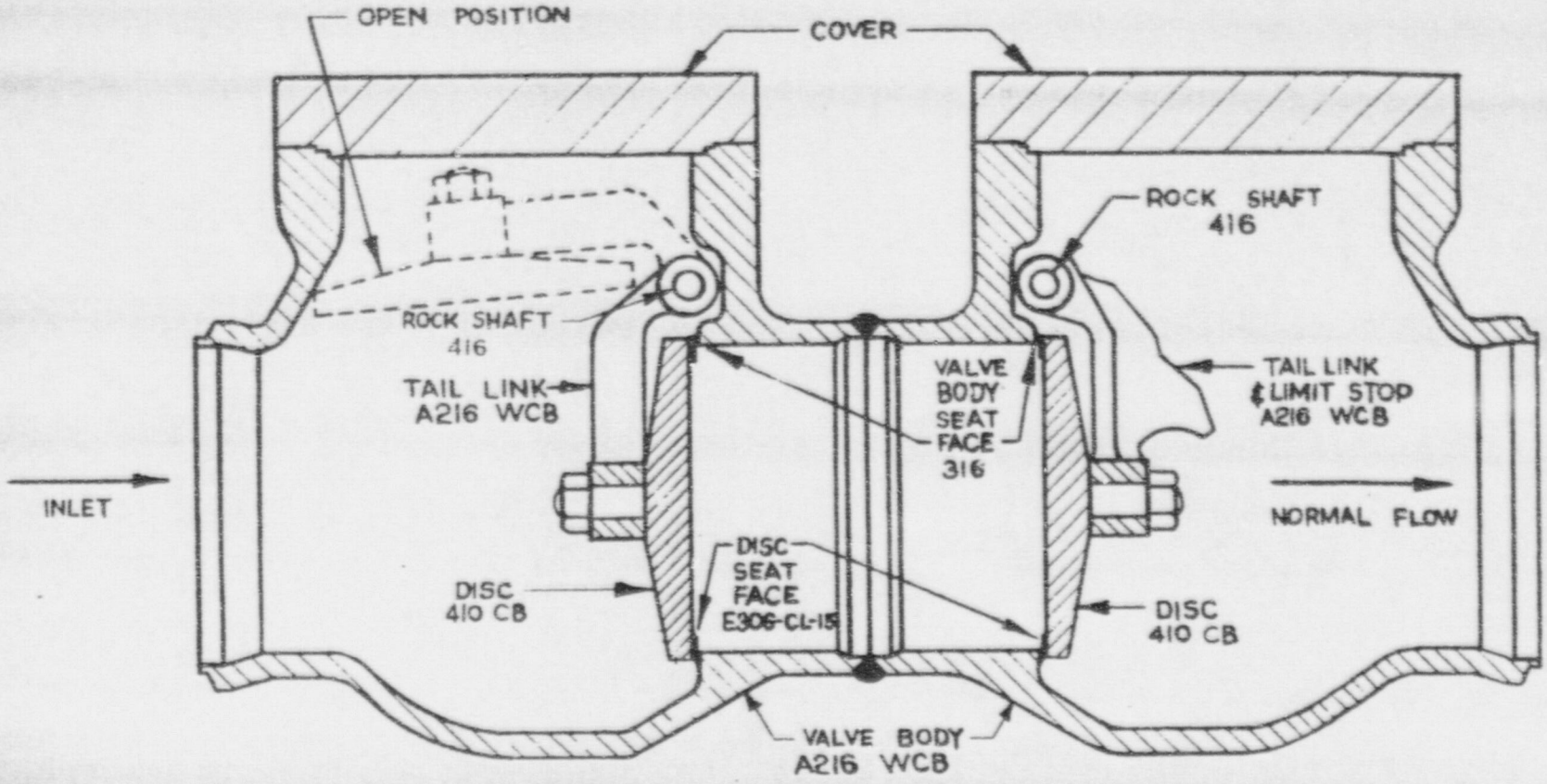

FIGURE 3-1

MS ISOLATION VALVE MS CHECK VALVE

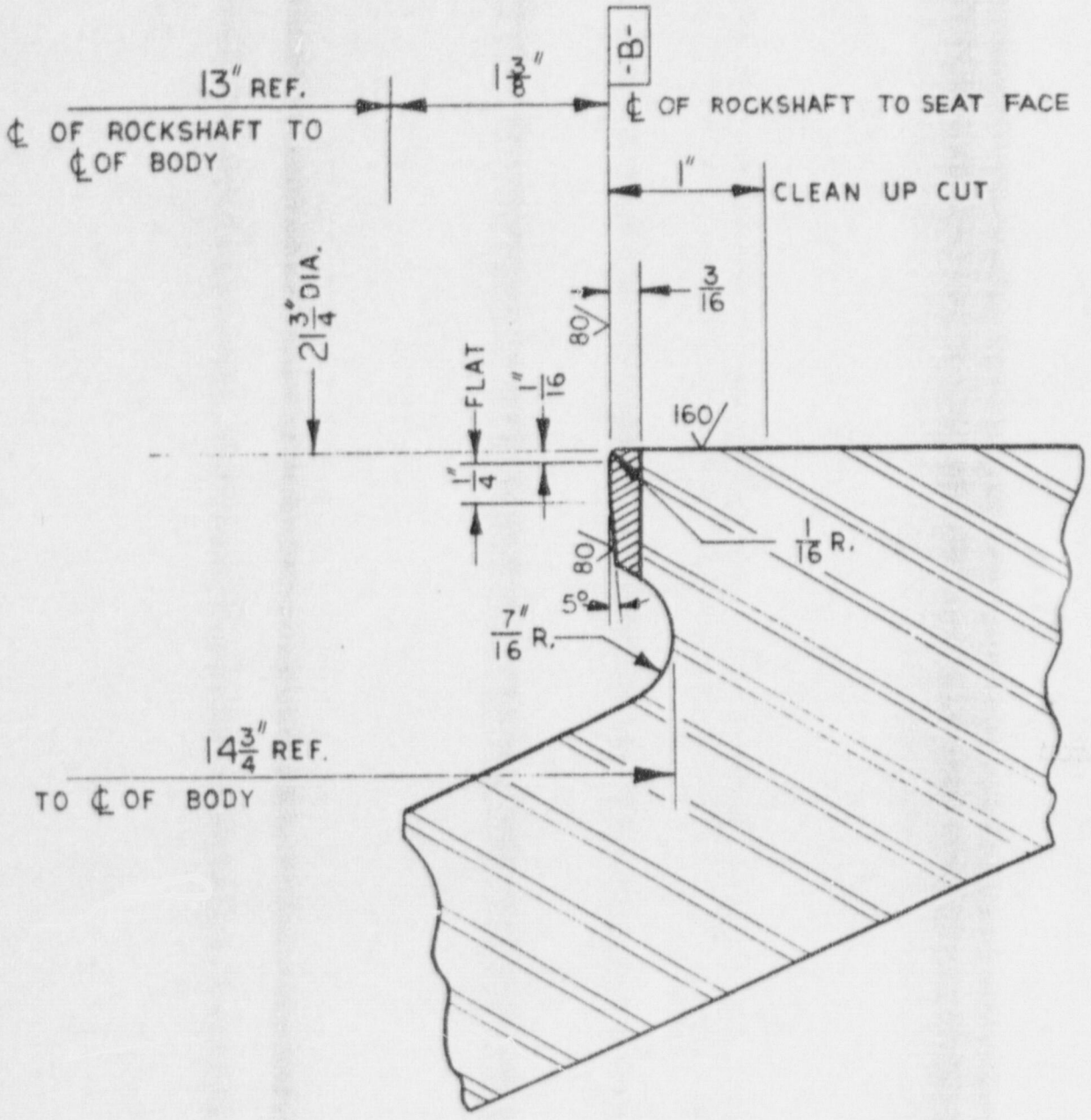

FIGURE 3-2

VALVE BODY SEAT AREA

4.0 LOADING CONDITIONS

The primary load conditions imposed on the valve assembly are a direct result of the kinetic energy which is developed during valve closure. Energy levels and associated angular velocities are given in Reference 1.

In comparing the check and isolation valves, it can be seen from Reference 1 that the highest energy levels and associated angular velocities are experienced by the isolation valve with the check valve in the full open position. These worse case levels were utilized in the analyses for the isolation valve and are identified in Table 4-1. The design pipe break level includes a 12% safety factor per Reference 4.

Resolution of the energy generated by the closure results in two primary loading cases: (1) impact force between the disc and the valve body seat area and, (2) centrifugal force in the tail link. In addition, a number of secondary load conditions are present, including centrifugal reaction at the rock shaft, centrifugal reaction at the disc shaft attachment, restraint reaction on the link due to restricted arc travel after impact, pressure on the disc, and rebound forces.

TABLE 4-1

KINETIC ENERGY & ANGULAR VELOCITY

DEVELOPED BY THE ISOLATION

VALVE DURING CLOSURE

Operating Condition	Disc Angular Travel, °	Angular Velocity, ω (Rad/Sec)	Input Energy, E (10^6 (in.-lbs)
Pipe Break [1]	80	93.9	1.20
Design Pipe Break [2]	80	99.6	1.35
Spurious Trip, 130% Normal Full Load Flow Transient [1]	80	32.8	0.15

1. Reference 1.
2. Includes 12% safety factor per Reference 4.

5.0 DESIGN ANALYSIS METHODS

5.1 Analysis Method Summary

The analyses were performed in the following steps.

A. A finite element analysis of the disc and valve seat area assuming static conditions and axisymmetry was performed. Impact load, deflection and strain relationships were developed from the results of this analysis. By combining the load deflection characteristics of the valve and disc and equating input kinetic energy to strain energy, a relationship between impact load and kinetic energy was determined.

B. A nonlinear, single degree of freedom analysis was performed for the disc to valve impact. The purpose was to determine the potential for separation between the disc and valve following initial impact. A separation would result in an additional energy input which was not considered in the previous static energy analysis. An additional objective was to determine the post impact rebound velocities so that the effect of the rebound centrifugal force on the tail link could be determined.

C. A nonlinear, multi-degree of freedom model of the disc to valve impact was utilized to confirm the assumption of axisymmetry of impact loads utilized in the finite element analysis.

D. The disc pin attachment to the tail link and the rock shaft were analyzed when the disc was subjected to the maximum centrifugal force.

E. A single degree of freedom, nonlinear dynamic analysis was performed on the tail link with the disc mass during the angular acceleration prior to impact. The purpose was to determine the influence of the dynamic time dependent centrifugal force upon the tail link reaction load in comparison to a static centrifugal force.

F. A finite element analysis of the isolation tail link was performed. Both the effects of the centrifugal force prior to impact and the effect of the disc restraint upon the free arc travel of the tail link following impact were examined.

5.2 Static

Elastic-plastic analyses methods were utilized since the available elastic strain energy is insufficient to balance the input kinetic energy and the applied centrifugal forces are above yield. The finite element computer program MARC-CDC (Reference 5), which has the capability to perform elastic-plastic analysis, was used in the stress analyses. A portion of the theoretical basis of this computer program is described in a paper by Marcal and King, Reference 6.

Yielding is governed by the von Mises criterion, and plastic flow is

governed by the Prandtl-Reuss stress-strain relations. Isotropic strain hardening effects are taken into account, and the analysis follows an incremental procedure. Initially, the program performs an elastic analysis to determine the element with the maximum strain. The loads are subsequently scaled so that this element is at incipient yiel. The loads are then increased in specified increments. With each increment, results are obtained which show the change of plastic deformation within the structure. The method utilizes small deflection theory.

In describing the structure, the cross section is broken into quadrilateral and triangular constant strain elements. The element type used to analyze the disc and valve body was the axisymmetric, quadrilateral ring element which allows only axisymmetric applied loads.

The element type used to analyze the tail link was the plane stress quadrilateral. A plane solution allowed incorporation of both plasticity and shear. Thus, the elements representing the tail link flange and circular attachment area for the rock shaft had adjusted moduli and yield strength values to correctly simulate their structural contributions.

The finite element models for the disc, valve body, and tail link are shown on Figures A.1-1, A.2-1, and B.1-1, respectively. Appendices A and B describe this portion of the analysis in greater detail.

5.3 Dynamic Nonlinear Analysis

Dynamic nonlinear analyses techniques were utilized to assess the symmetry of disc impact, rebound characteristics and effect of the time dependent radial acceleration upon the tail link during closure. All dynamic analyses were conducted with the aid of the computer program PIPERUP (Reference 7). The PIPERUP computer program performs nonlinear, elastic-plastic analysis of three dimensional systems subjected to dynamic time history forcing functions. The program computes and outputs restraint spring reaction forces and system deflections as a function of time.

PIPERUP is an adaptation of the finite element method. The three dimensional system is mathematically modeled as an assembly of weightless structural members connecting discrete nodal points. Weight of the system including the distributed weight and concentrated weights is lumped at selected model mass points. An incremental procedure is used to account for the nonlinear effects of plastic deformation of the system and restraints.

Stress-strain characteristics of the members which connect node points are idealized by three linear segments. The first portion represents linear and perfectly elastic behavior, the second represents linear strain hardening, with the third portion representing perfectly plastic behavior. In situations where stress reversal and unloading occur, an isotropic strain hardening model is used; that is, unloading is always along the elastic line. (Figure 5-1).

The method used in the program to account for the change in system stiffness during plastic deformation is to represent each member connecting two nodes by three parallel subelements which have a total stiffness equal to the elastic stiffness of the system. Upon transition from the elastic to the linear strain hardening region, one of the three subelements is hinged, such that it can sustain no increase in load, leaving two subelements which are defined to have a sum stiffness equal to the strain hardening stiffness of the system. At the second transition the process is repeated leaving a single subelement with a very small stiffness.

Restraint springs are modeled in PIPERUP with an initial gap and a trilinear stiffness curve. Again, the first stiffness represents linear elastic behavior, the second stiffness models linear strain hardening, with the third stiffness modeling perfectly plastic behavior. (Figure 5-2).

For this analysis, the yield and plastic criteria used in PIPERUP for bending is given by:

$$M^2 = M_m^2$$

where M = Resultant moment in system

$$= \sqrt{M_1^2 + M_2^2}$$

$M_m = M_y$ = Yield moment for first stage hinge (strain hardening)

$M_m = M_u$ = Ultimate moment for second stage hinge (plastic hinge).

Two single degree of freedom systems were modeled. For one, the disc and a portion of the tail link was the mass, and the tail link "radial" stiffness was the spring. The time dependent radial acceleration due to angular velocity was inputed for the maximum energy condition. In the other system the disc impact was modeled, thus the spring included the effective stiffness of the disc and valve combined. From this analysis, rebound velocities and peak loads were determined.

In addition, a multi-degree of freedom system was modeled. The disc was simulated with several bar elements connected to a pivot and the system was accelerated about the pivot to assess the symmetry of impact upon the valve seat.

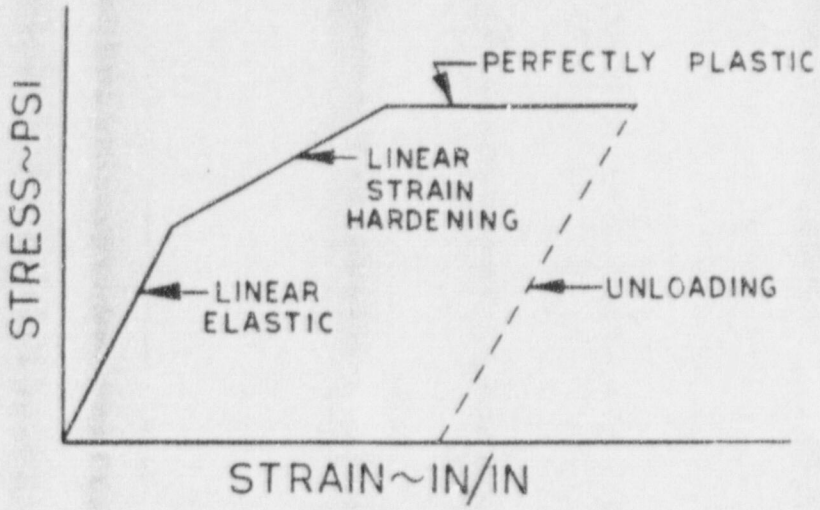

FIGURE 5-1

DYNAMIC SYSTEM STRESS-STRAIN CHARACTERISTICS

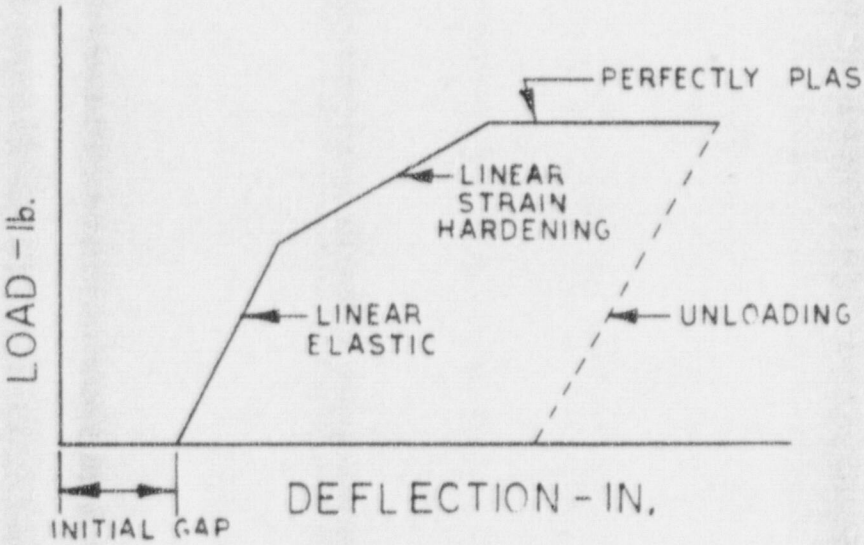

FIGURE 5-2

RESTRAINT SPRING LOAD DEFLECTION CHARACTERISTICS

6.0 RESULTS

The results of the analyses are given in Appendices A through D. Appendix A summarizes the analyses performed on the disc and valve body seat area. Appendix B includes finite element and dynamic analyses of the tail link. Appendix C and D contain analyses of the pin attachment area of the disc and the rock shaft.

The total maximum strains at several representative operating conditions given in Reference 1 for the disc, tail link, valve body seat area, and rock shaft are identified in Table 6-1. As can be seen, all trips produce some plastic deformation. Design pipe break, the worst condition, results in maximum strains which are all below the allowables as shown in Table 6-2. (See Appendix A.1, A.2 and B.1).

The tail link when subjected to the maximum centrifugal force of 148.9 kips which corresponds to an input energy of 1.35×10^6 in.-lbs extends 0.52 inches as shown in Figure B.1-6. This is less than the allowable of .625 inch.

The results in Appendix A.3 and B.2 show that the isolation valve will meet the design critieria for a design pipe break, assuming the measured maximum permanent deformation at the center of the disc following any combination of spurious closures is less than 0.19 inches. In addition, the valve will meet the criteria if three or less worse case spurious trips, as defined in Table 4-1, have occurred previous to a design pipe break closure.

Analyses of the disc pin attachment to the tail link as shown in Appendix C indicates that it was not yielded due to radial acceleration prior to impact.

The analysis of the rock shaft as shown in Appendix D showed that the stress did not reach yield during the worst case angular acceleration.

The results of the one dimensional non-linear dynamic analysis in Figures A.4.1-3 and A.4.1-6 show that the disc impacts the valve body, moves back slightly and stabilizes but does not separate from the valve after initial impact. This confirms the static energy analysis assumption that separation would not occur as a result of the rebound energy.

Other results of the dynamic analysis summarized in Table A.4-1 show the low rebound angular velocities of the disc after impact. As can be seen from Figure B.1-4 the angular velocity produces a low centrifugal force in the tail link. The strain force results in Figure B.1-3 for the tail link show that the rebound centrifugal force would not produce any additional plastic deformation.

The results of the multidimensional, non-linear dynamic analysis of the disc impact indicated that the compliance between the disc and the valve seat was sufficient to distribute the peak loads reasonably uniform around the circumference. This can be seen by examining the peak response of the eight springs representing the valve body in Figures A.4.2-2 to

A.4.2 6. This confirmed the validity of the assumption of axisymmetry loading utilized in the finite element analyses of the disc and valve body.

Centrifugal forces from static analysis were utilized to determine plastic strains in the tail link. However, this is conservative since as shown by the dynamic analyses results in Figure B.2-3, the peak dynamic reaction is 21% less than the maximum centrifugal force predicted from static analysis as shown in Figure E.1-4.

The total strain reported in Table 6.1 for the tail link is based on the conservative assumption that the tail link is constrained to deflect the same amount as the center line axial displacement of the disc. With respect to this assumption, two analyses were performed. The displacement-strain results in Figure B.1-9 are from the first case with the tail link initially stress free which corresponds to a spurious trip. The displacement-strain results in Figure B.1-11 are from the second case with the tail link initially subjected to a strain state corresponding to the centrifugal force from a design pipe break trip. For both cases, maximum strain levels were greater than the strain levels from the centrifugal force only case.

TABLE 6-1

SUMMARY OF RESULTS

OPERATING CONDITIONS	INPUT ENERGY $\times 10^6$ (in.lbs)	MAXIMUM TOTAL PLASTIC STRAIN							
		DISC	DISC FACE WELD	TAIL LINK			VALVE BODY	VALVE SEAT WELD	ROCK SHAFT
				CENTRIFUGAL FORCE	AXIAL DISPLACEMENT AFTER IMPACT	TOTAL			
Pipe Break (1)	1.20	8.0	3.8	3.4	-	~8.5 (3)	7.0	7.9	0.0
Design Pipe Break (2)	1.35	8.9	4.2	4.6	4.9	9.5	7.3	8.3	0.0
Spurious Trip (1) 130% Normal Full Load Flow Transient	0.15	1.8	1.4	0.0	2.2	2.2	5.0	5.9	0.0

(1) Reference 1

(2) Includes 12% Safety Factor per Reference 4

(3) Conservative Estimate Based on Analysis Results for Design Pipe Break in Figure B.1-11

TABLE 6-2

SUMMARY OF RESULTS FOR DESIGN PIPE BREAK

Component	Maximum Total Strain	Allowable Strain	Percent of Allowable Strain
Disc	8.9%	9.0%	99%
Disc Face Weld	4.2%	10.0%	42%
Tail Link	9.5%	12.0%	79%
Valve Body	7.3%	12.0%	61%
Valve Seat Weld	8.3%	20.%	41 %
Rock Shaft	*	-	-

* less than yield

7.0 CONCLUSIONS

For the check valve, the analyses demonstrated that the components examined (the disc, valve seat, tail link and rock shaft) meet the specified design criteria for a postulated pipe rupture.

For the isolation valve, the analyses demonstrates that the components examined meet the specified design criteria for a postulated pipe rupture, assuming that the measured maximum permanent deformation at the center of the valve disc following any combination of spurious closurec is less than 0.19 inch. Furthermore, tbe components will meet the specified criteria if three or less worst case spurious trips have occured previous to a design pipe break closure.

8.0 REFERENCES

1. Nuclear Services Corporation, "Analysis Report: Maximum Energy of Disc Impact Following Pipe Rupture Main Steam Check and Isolation Values for Kewaunee Unit 1", KEW-01-01, July 30, 1973, Revised September 6, 1973.

2. Personal Communication from A. J. Elliott, Nuclear Services Corporation, to C. Didier, Pioneer Service & Engineering Company, on July 27, 1973, concerning lot test data for valve materials.

3. Personal Communication from C. Didier, Pioneer Service & Engineering Company, to G. R. Randall, Nuclear Service Corporation on August 28, 1973.

4. Personal Communication from C. Didier, Pioneer Service & Engineering Company, to G. R. Randall, Nuclear Service Corporation on July 30, 1973.

5. Marc Analysis Corporation, MARC-CDC: Non-linear Finite Element Analysis Program", 1971.

6. Marcal, V. P. and King, I. P., "Elastic-Plastic Analysis of Two-Dimensional Stress Systems by the Finite Element Method," Int. J. Mech. Sci., Vol 9, pp 143-155, 1967.

7. Nuclear Services Corporation, "PIPERUP: A Computer Program for Analysis of Piping Systems Subject to Pipe Rupture Loads".

8. Personal Communication from C. Didier, Pioneer Service & Engineering Company, to G. R. Randall, Nuclear Service Corporation on July 28,1973.

9. "Steels for Elevated Temperature Service," United States Steel Corp., Pittsburgh, Pa.

10. Aerospace Structural Metals Handbook, 1973 Publication, Mechanical Properties Data Center, Belfour Stulen, Inc. AF ML-TR-68-115.

11. Designer's Guide for Welded Construction, The Lincoln Electric Company, Cleveland, Ohio, No. 1100.1.

12. Personal Communication from A. J. Elliott, Nuclear Services Corporation, to R. Sabertino, Shutte & Koerting Company on July 27,1973.

13. "Steel for Nuclear Applications", United States Steel Corporation, Pittsburgh, Pennsylvania, 1967.

APPENDIX A

Analysis of Disc and Valve Body Seat Area

TABLE OF CONTENTS

A-1 Disc - Static

The finite element computer code MARC - CDC, which incorporates elastic-plastic analysis with strain hardening, was used for the static stress analysis of the disc. The model (Figure A.1-1) was constructed from 296 axisymmetric quadrilateral and triangular ring elements to simulate the disc geometry. Analytical accuracy in the area of the impact face weld was enhanced by the use of a very fine mesh with the appropriate material properties.

For the purpose of the disc analysis, the boundary between the disc face weld and the valve seat face weld was modeled by fixing one degree of freedom for a single node (Figure A.1-2). This restraint provided an axisymmetric reaction for the applied loads but allowed the disc to rotate freely without developing shear at the contact surface, thus realistically simulating the zero shear and zero tension interface.

The disc inertia loads were simulated by applying an equivalent axisymmetric pressure as indicated in Figure A.1-2. The pressure distribution corresponded to the actual mass distribution of the disc with an amplification near the center to account for the effect of the tail link mass. The elastic-plastic stress analysis preceded by incrementally increasing the pressure amplitudes in a manner that perserved the shape of the distribution. The total "impact" load for a given increment equals the integrated area of the pressure distribution. For each increment a point

on a total force - equivalant deflection curve can be determined. The strains for each element of the disc model can then be related to the total force.

The total force applied versus equivalant deflection is shown in Figure A.1-3. This curve was generated by equating the summation of external work done at the pressure boundary (equivalant to the strain energy) to the external work done by the total force moving through a distance equal to an equivalant deflection. The above relationships are given by

$$\text{Total Force} = 2\pi \int p_r . r . dr$$

and

$$\text{Equivalant Deflection} = \frac{\text{Total External Work}}{\text{Total Force}}$$

$$= \frac{2\pi \int p_r . \delta_r . r . dr}{2\pi \int p_r . r . dr} .$$

The total energy absorbed (strain energy) by the disc at a given load is equal to the area under that portion of the total force-equivalant deflection curve. The total strain at two locations of interest (face weld contact and extreme tensile element) as a function of the total force is shown in Figure A.1-4. The sequence of growth of the plastic zone with increasing total applied load is described schematically in Figure A.1-5. The predicted actual deflection at the center of the disc as a function of applied total load is given in Figure A.1-6.

As a result of the large deflections encountered and the accompanying convergence problems, it was necessary to extrapolate the data beyond load increment nine (2,616 kips). The dashed extension of the curves represent this extrapolated data.

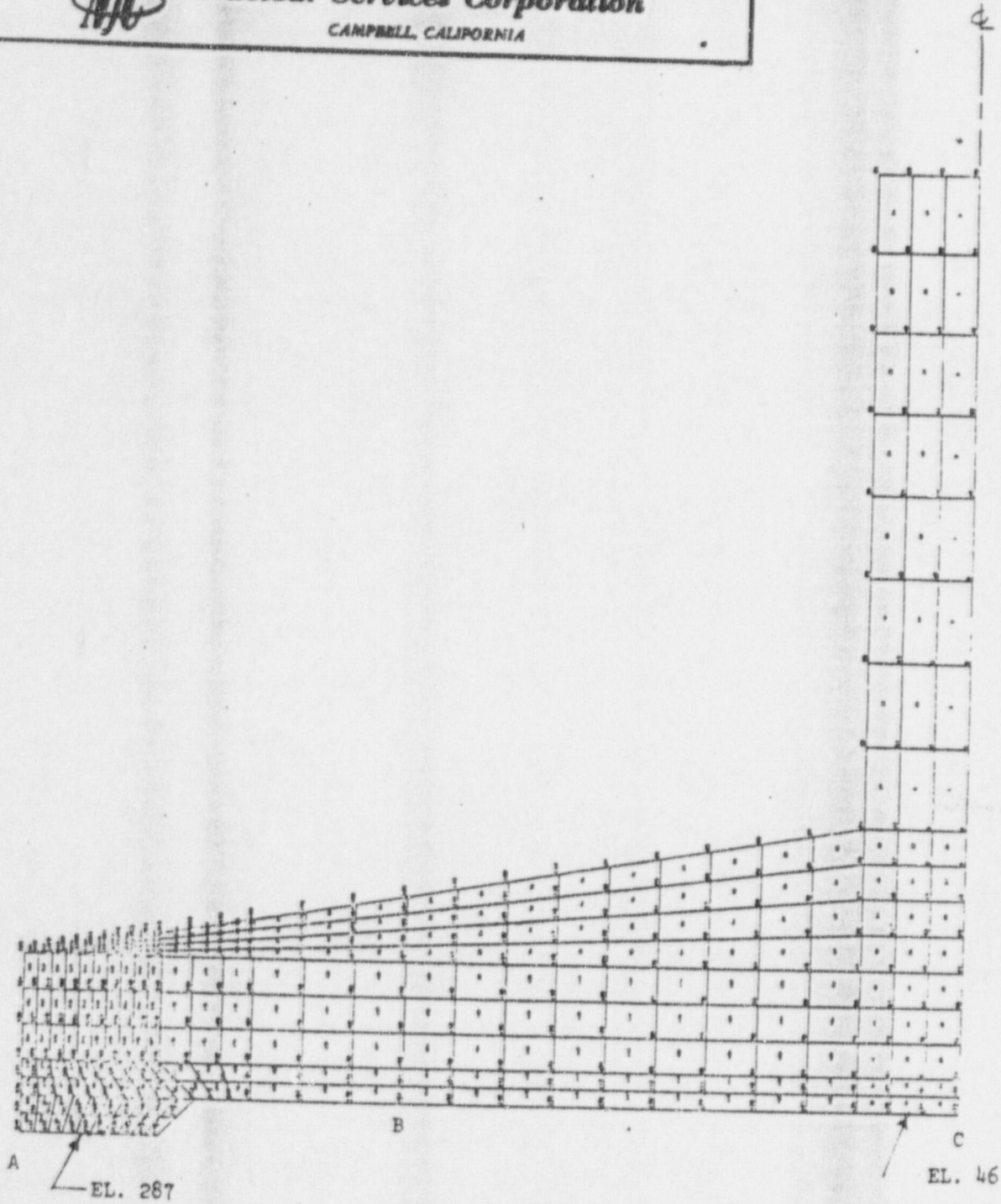

FINITE ELEMENT MODEL OF DISC

Figure A.1-1

Figure A.1-2

APPLIED PRESSURE DISTRIBUTION - EQUIVALENT TO BODY FORCES

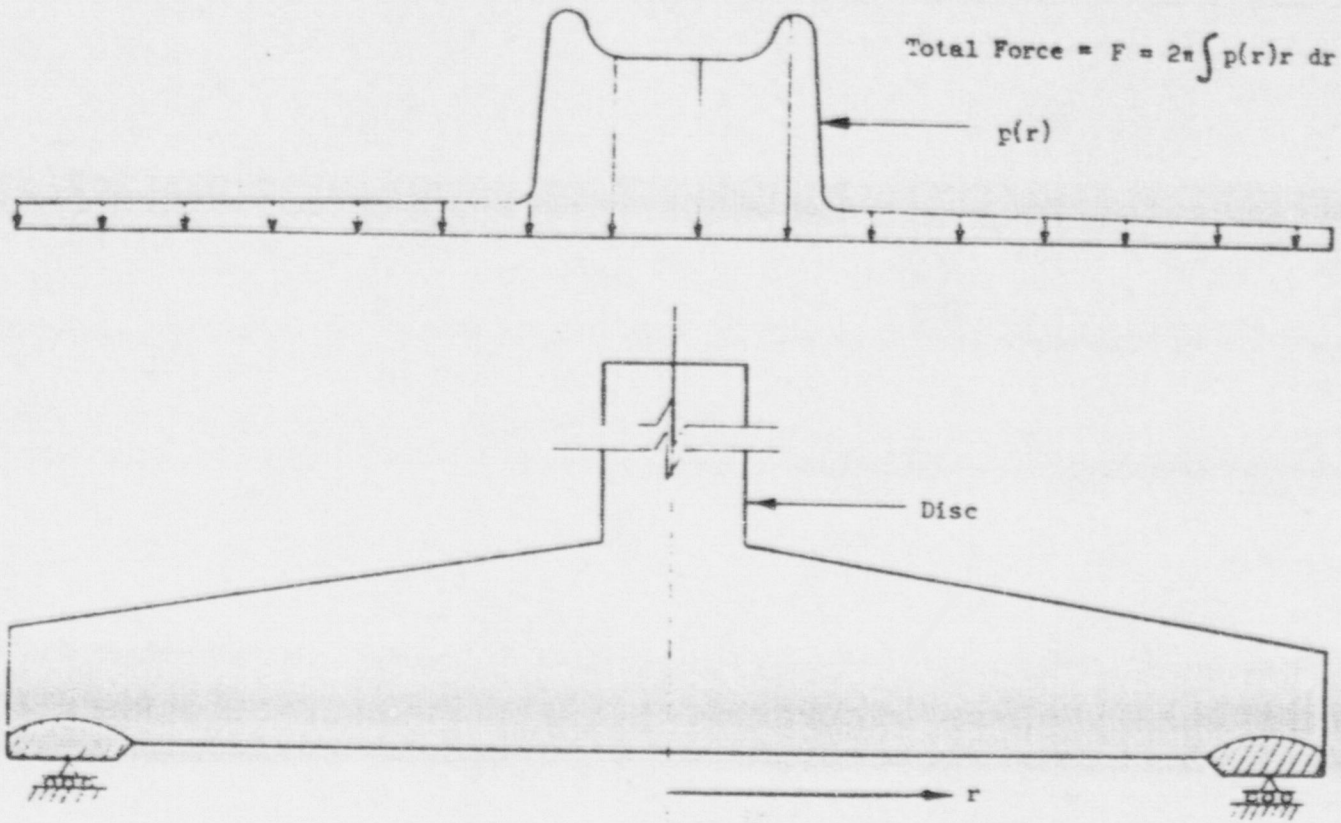

Nuclear Services Corporation
CAMPBELL, CALIFORNIA

Figure A.1-3

TOTAL FORCE EQUIVALENT DEFLECTION CURVE FOR THE DISC

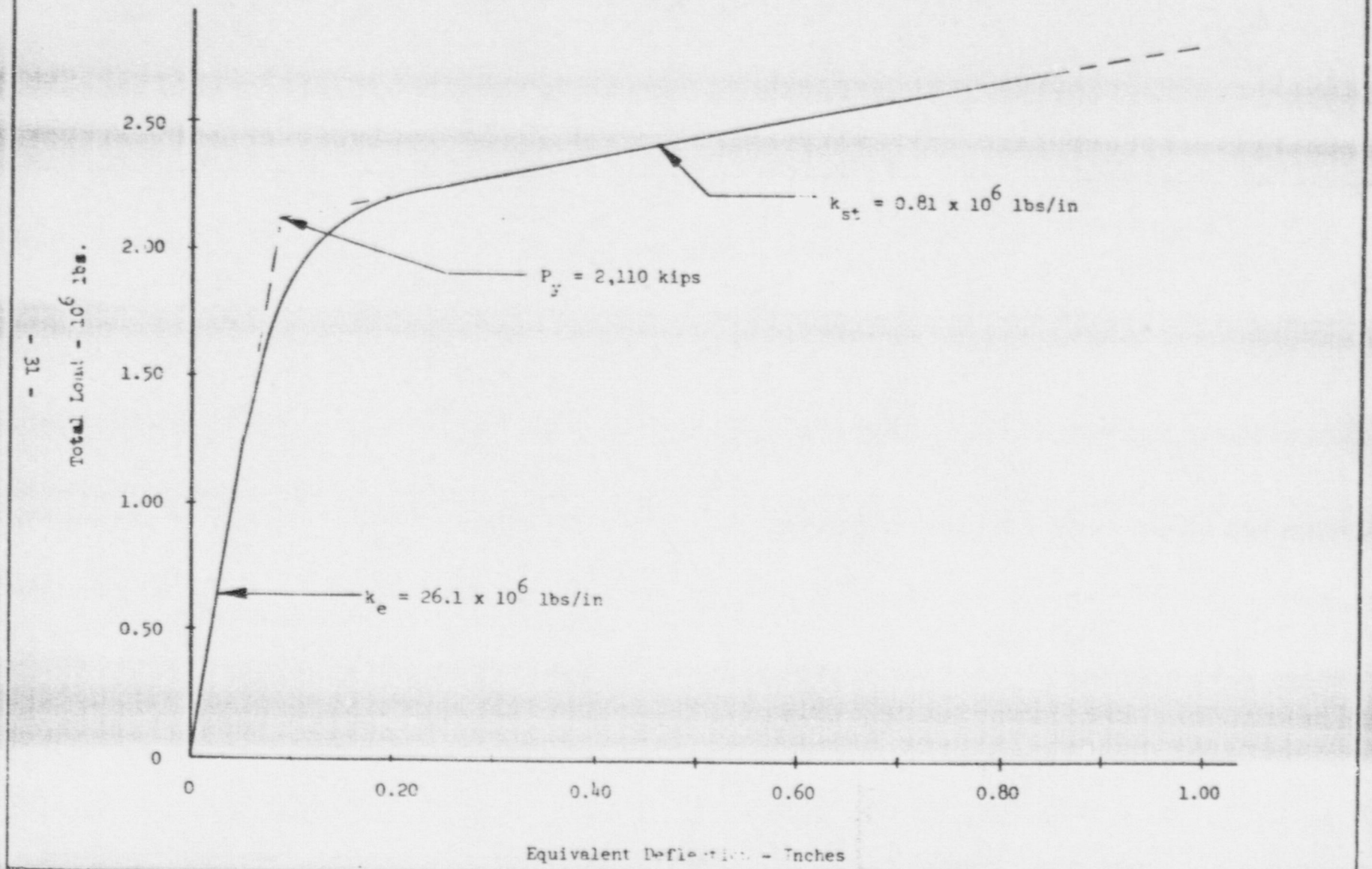

Nuclear Services Corporation
CAMPBELL, CALIFORNIA

Figure A.1-4
DISC STRAINS AS A FUNCTION
OF TOTAL APPLIED LOAD

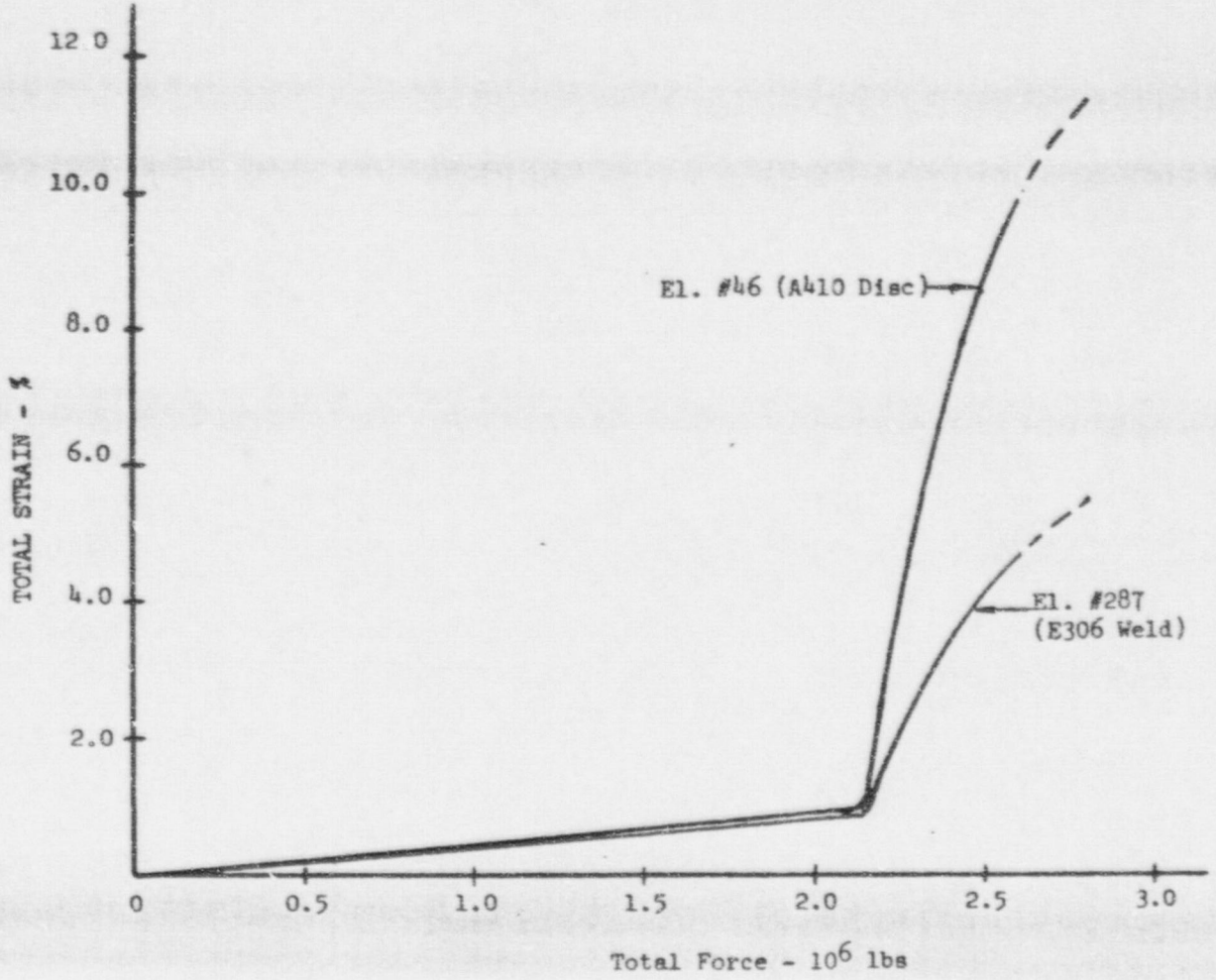

Nuclear Services Corporation
CAMPBELL, CALIFORNIA

Figure A.1-5

SEQUENCE OF GROWTH OF THE PLASTIC ZONE AS A FUNCTION OF INCREASING LOAD

Load Increment	Total Applied Load (kips)
1	1,120
2	1,307
3	1,494
4	1,681
5	1,868
6	2,055
7	2,242
8	2,429
9	2,616

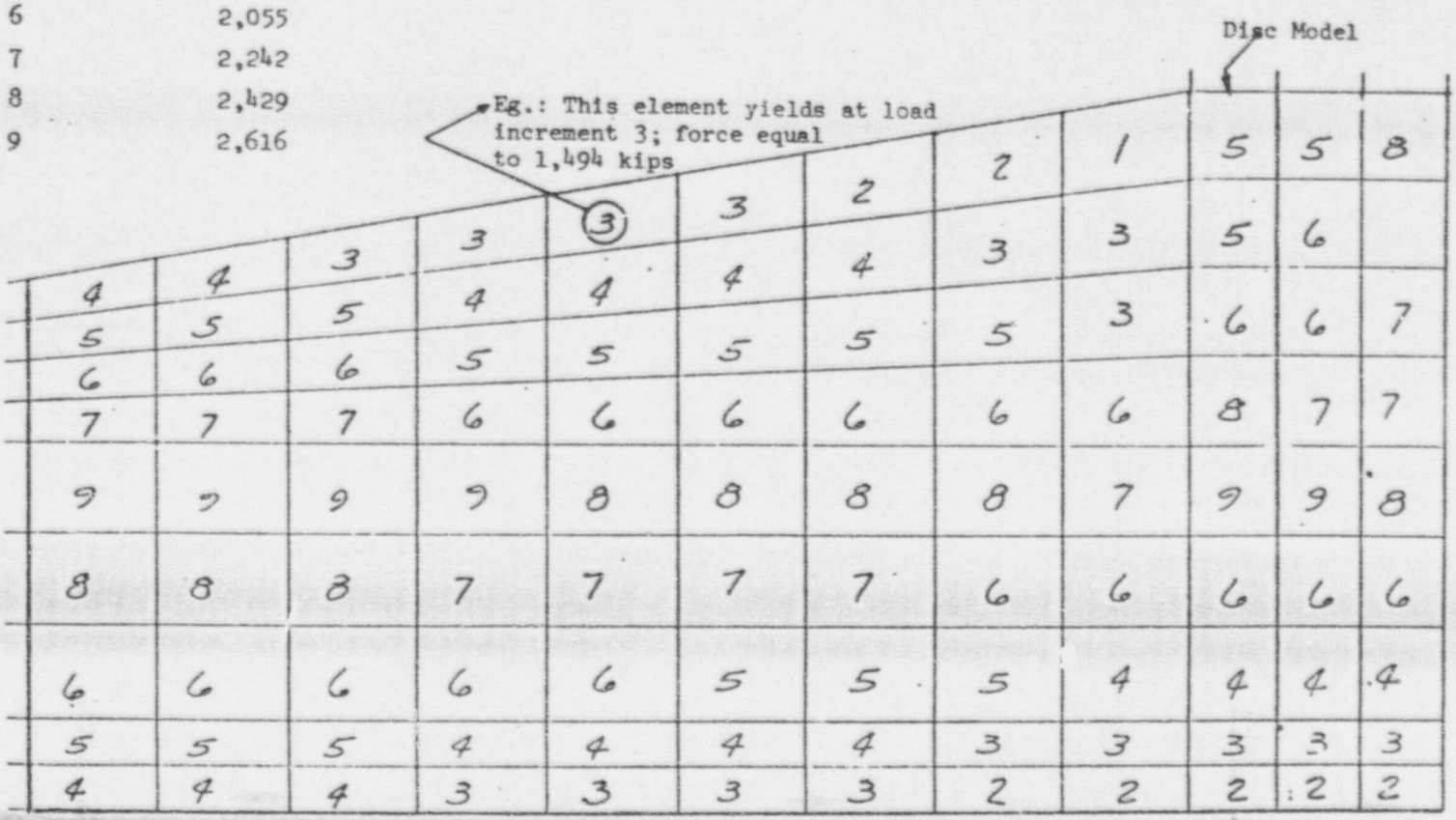

Figure Continued on the Next Page

Figure A.1-5 (Continued)

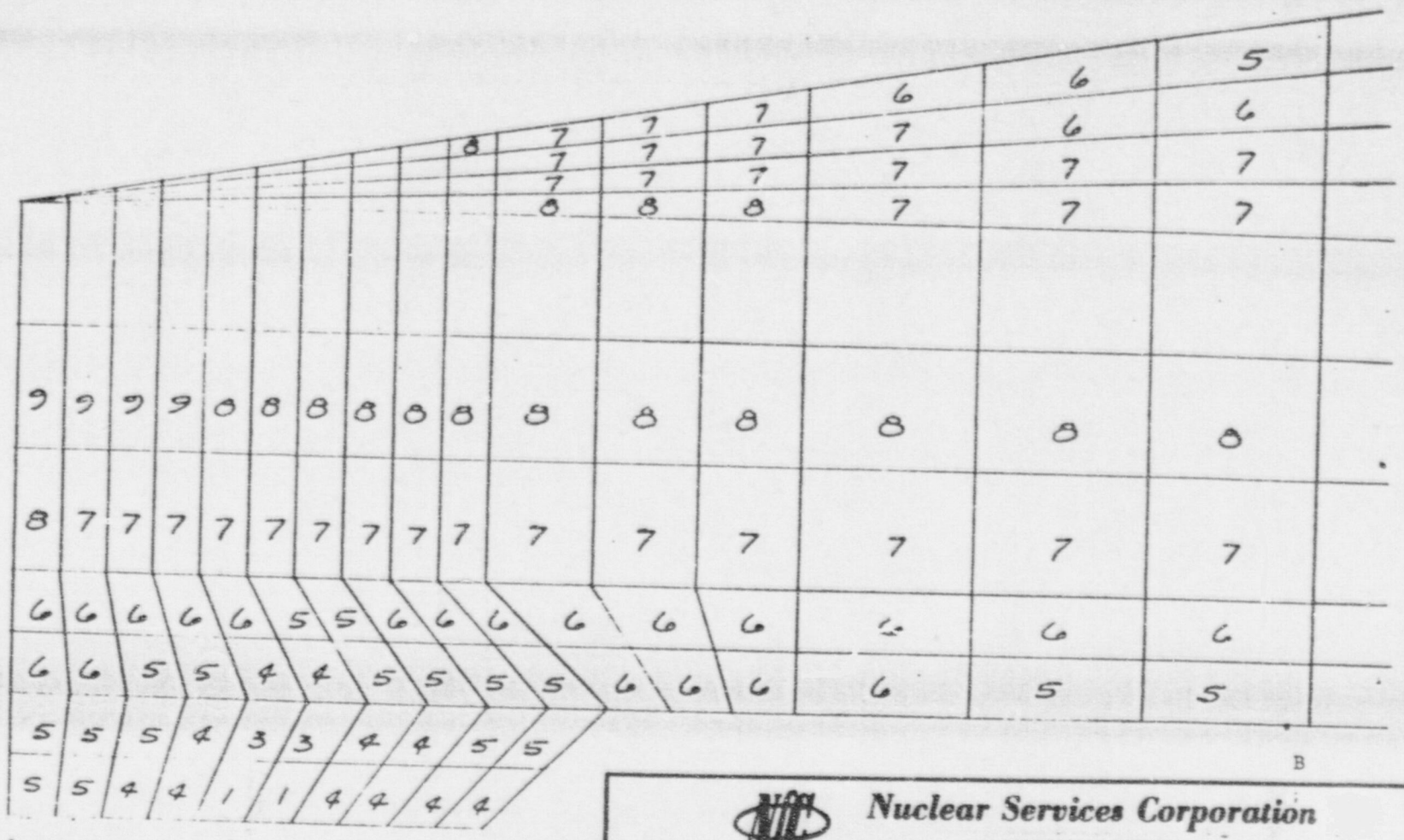

Nuclear Services Corporation
CAMPBELL, CALIFORNIA

Nuclear Services Corporation
CAMPBELL, CALIFORNIA

Figure A.1-6
CENTER DEFLECTION OF DISC AS
A FUNCTION OF TOTAL APPLIED LOAD

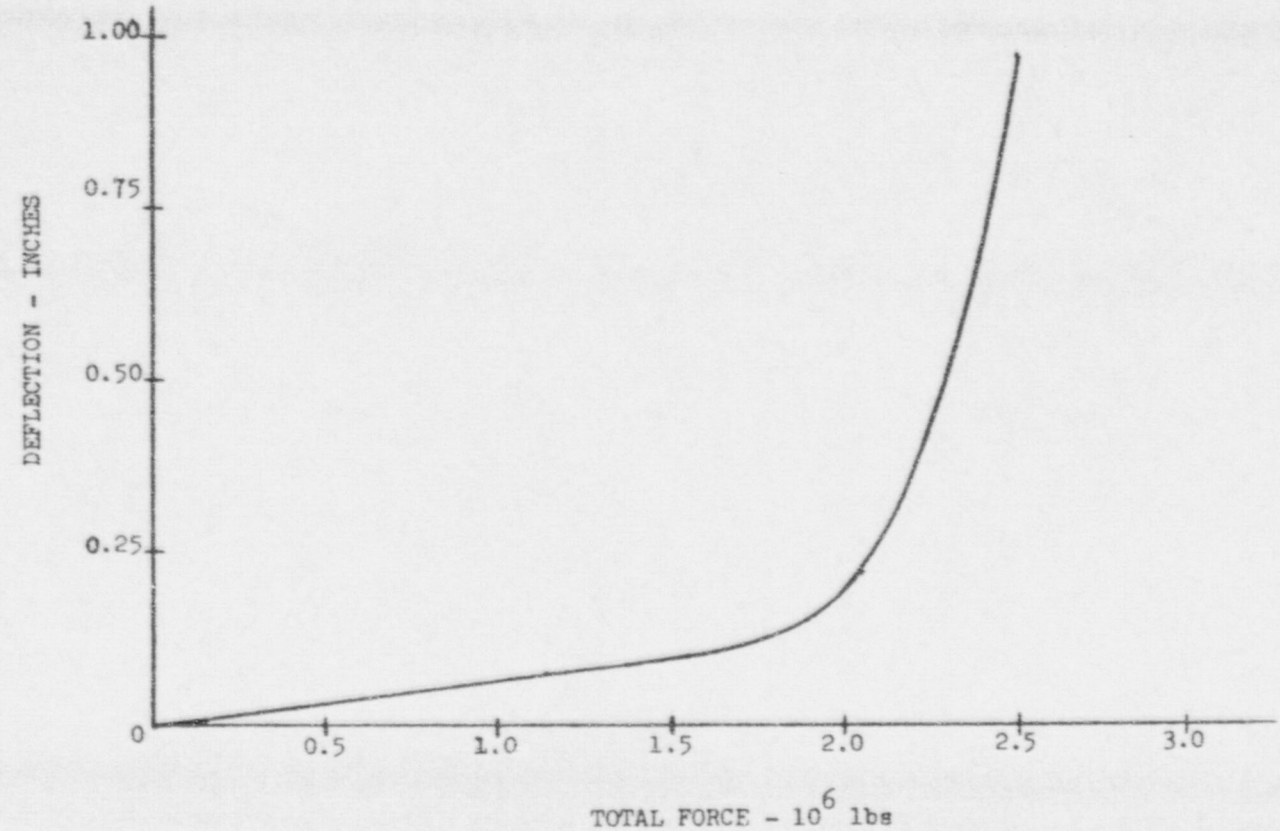

A.2 Valve Body Seat Area - Static

An axisymmetric, elastic-plastic, strain hardening stress analysis utilizing the finite element computer code MARC - CDC was performed to obtain the equivalant static response of the valve seat upon disc impact. The model (Figure A.2.1) incorporated 125 axisymmetric quadrilateral and triangular ring elements to simulate the seat geometry. An increased density mesh was utilized in the area of the face weld in order to enhance the accuracy of localized compressive strain predictions.

The disc impact load was applied to the seat as an axisymmetric annular pressure distributed linearly over a radial distance of 0.156 inches, as shown in Figure A.2-1. This distribution corresponded to the reaction distribution on the disc as predicted per Section A.1. The distribution was determined by examining the stress state of the elements at the boundary of the disc while the disc was loaded and constrained by the boundary conditions of Section A.1.

The geometry of the finite element model of the valve body was truncated both upstream and downstream from the valve seat. Fixed boundary conditions for reacting the impact load were established along line A-B (Figure A.2-1) which lies 3.6 inches downstream from the face weld surface. In addition, the boundary along C-D, upstream, was fixed. One criterion for selection of these boundaries included consideration of the anticipated plastic zone. Based on the extent of the plastic zone indicated in Figure A.2-4, the

boundaries were sufficiently distant from the load point to prevent spurious predictions of the plastic strain. An additional boundary selection criterion was based on the effects of the reactive restraint provided by the large inertia of the valve both upstream and downstream of the valve seat area. These inertias will tend to produce a fixed condition during the high velocity impact of the disc upon the valve seat area.

Since the stress in the valve body in the seat region resulting from an internal pressure of 1000 psi was negligible when compared to the impact stresses, it was not included in the analysis.

The results of the finite element analysis of the valve seat are presented in Figures A.2-2 through A.2-4. The force-equivalent deflection curve of Figure A.2-2 was generated with the same procedure described in Section A.1. The maximum total strain as a function of total applied load for wo areas of interest, the face weld and the valve body parent material adjacent to the weld, is shown in Figure A.2-3. The growth of the plastic zone as a function of the applied load increment is shown schematically in Figure A.2-4.

Figure A.2-1

FINITE ELEMENT MODEL

VALVE SEAT

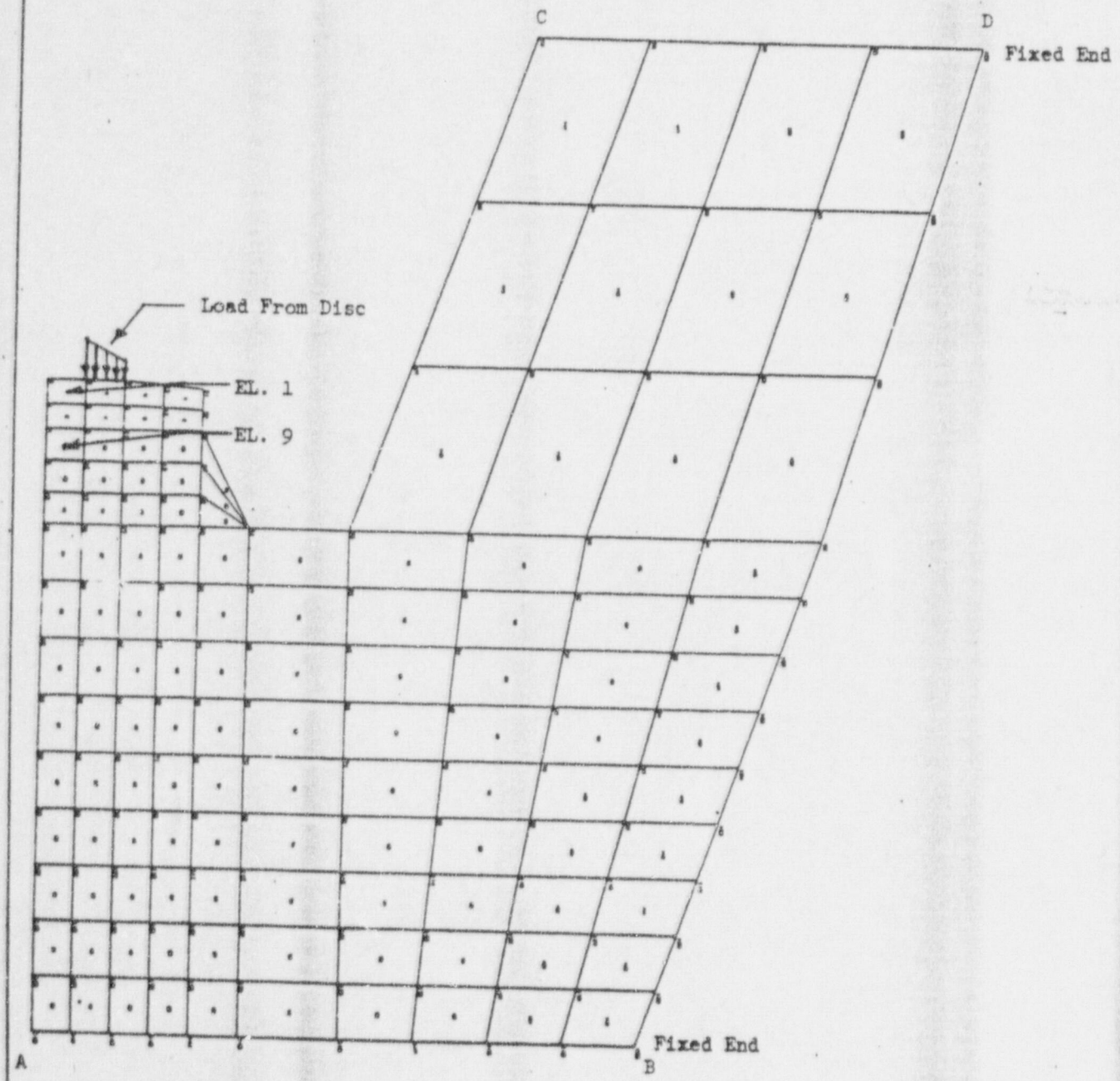

Figure A.2-2

TOTAL FORCE VERSUS EQUIVALENT DEFLECTION
VALVE SEAT

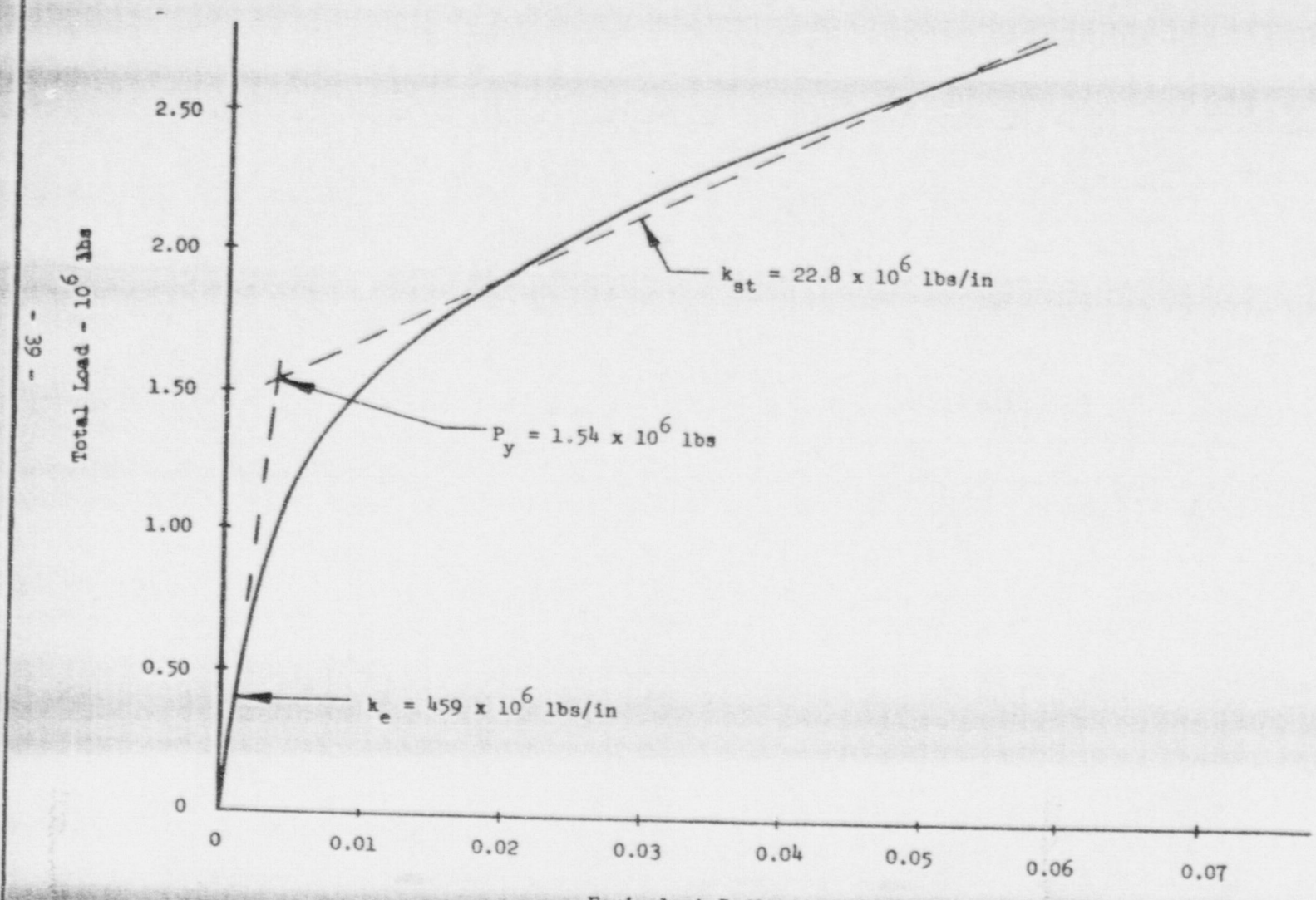

Nuclear Services Corporation
CAMPBELL, CALIFORNIA

Figure A.2-3

VALVE SEAT STRAINS AS

A FUNCTION OF TOTAL APPLIED LOAD

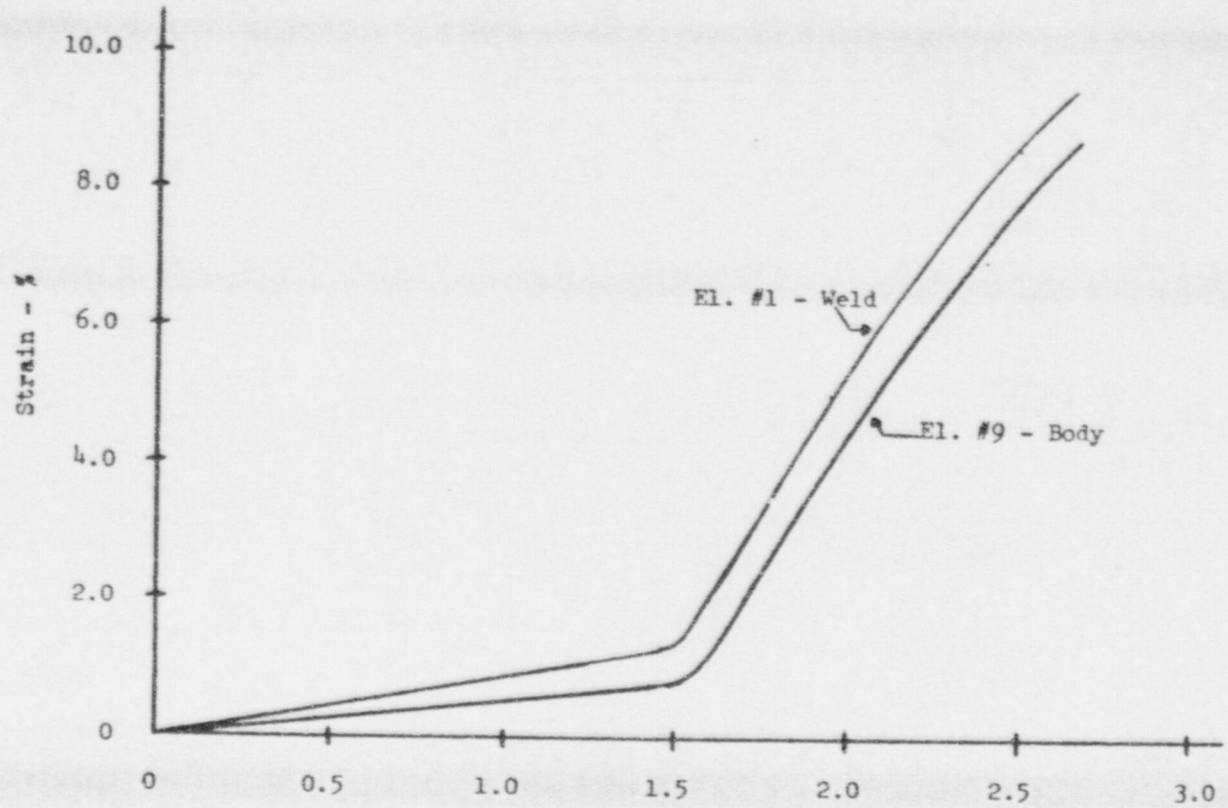

Figure A.2-4

SEQUENCE OF GROWTH OF THE PLASTIC ZONE

AS A FUNCTION OF INCREASING LOAD

VALVE BODY

Load Increment	Load (Kips)
1	573
2	688
3	802
4	917
5	1,032
6	1,147
7	1,262
8	1,376
9	1,491
10	1,606
11	1,720
12	1,835
13	1,950
14	2,064
15	2,179
16	2,294
17	2,408
18	2,523
19	2,638
20	2,752

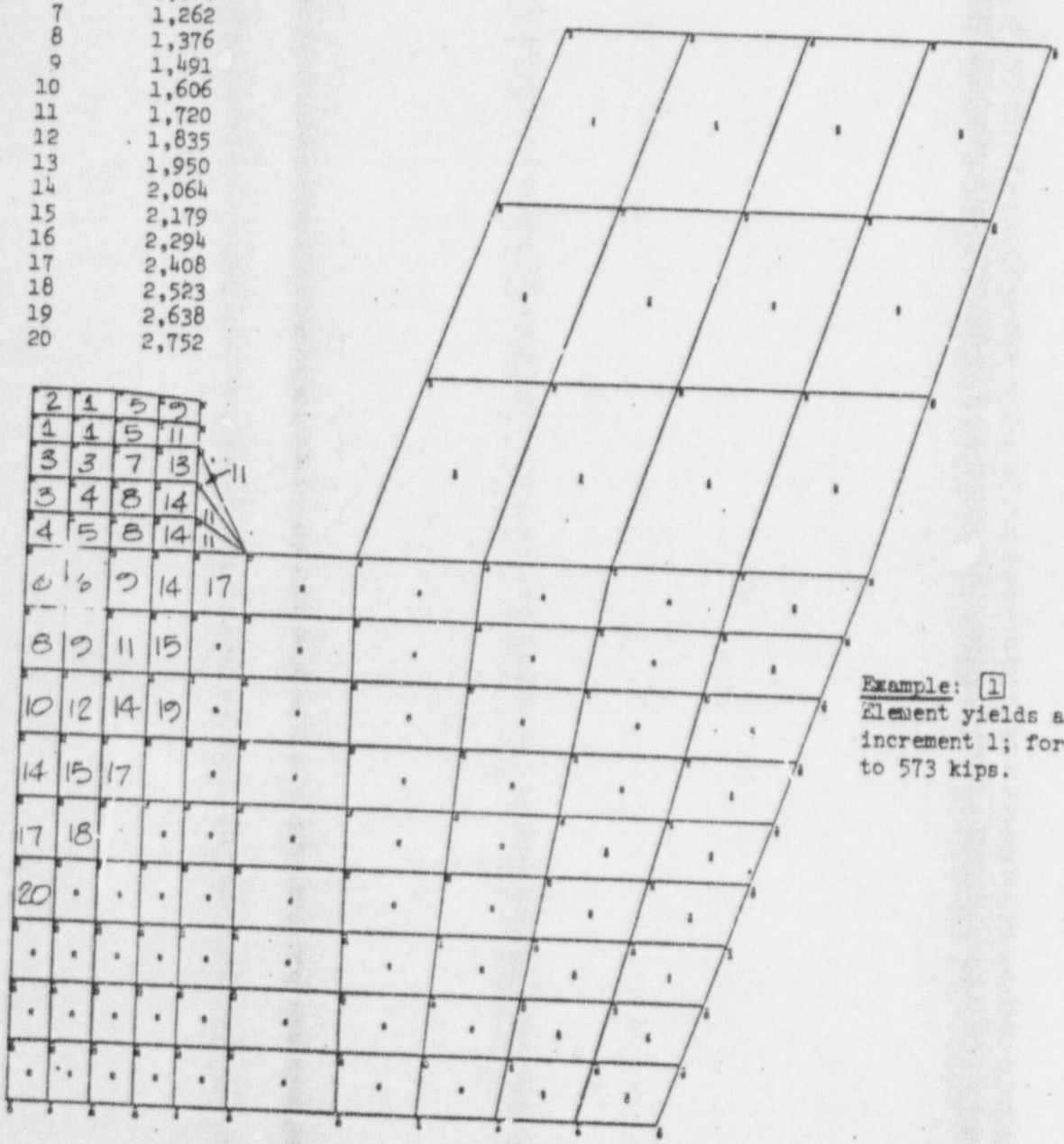

Example: [1]
Element yields at load increment 1; force equal to 573 kips.

A.3 Disc and Valve Body Interaction - Static

In order to determine the total energy absorbed by the combination of the disc and valve seat as a function of the impact force, it was necessary to combine the static models of the two components. This was accomplished by idealizing the respective force-equivalent deflection curves as bilinear, elastic and strain hardening, and then combining the two according to the law of linear springs in series (i.e. $k = \frac{k_a k_b}{k_a + k_b}$) to obtain a single force-deflection curve for the disc-valve seat system. The resulting curve, Figure A.3-1, was composed of three linear segments corresponding to the following conditions: (1) both components elastic, (2) disc elastic and valve seat yielded, and (3) both components yielded. The combined F-δ curve is useful for the purpose of determining strain energy, however the deflections do not directly relate physically to any portion of the structure.

The area under the combined total force-equivalent deflection curve for a particular impact force represents the energy absorbed by the system at that force. A plot of the impact force versus input energy is given in Figure A.3-2.

By utilizing this relationship between force and energy and recalling the relationships between force and strain determined in Appendices A.1 and A.2, the maximum strain as a function of input energy at regions of interest for each component was determined and is provided in Figure A.3-3.

In order to evaluate the isolation valve system for the effects of repeated spurious trips, it is necessary to consider the strain energy lost to strain hardening as a result of the spurious trip(s). This energy loss is dependent of the input energy of each individual trip. Since the input energy for each spurious trip is a random variable, the determination of acceptable conditions at any given time was accomplished by utilizing a limiting solution. For this analysis two bounds were determined.

The first bound was based on the 130% full load spurious trip (kinetic energy = 0.15×10^6 in.-lbs, Table 4.1) and represents the minimum number of allowable spurious trips. The allowable number of spurious trips was determined by recognizing that the capability of the valve to meet the design criteria at a given point in time is dependent on three energy values; that is, (1) the initial available strain energy, (2) the kinetic energy generated for the design trip, and (3) the energy loss during spurious trips. By applying the principle of isotropic hardening, the energy loss as a function of the number of spurious trips was determined and is shown in Figure A.3-4. It is required that:

$$U_A \geq (K.E.)_D + U_L\,(n)$$

where

U_A = the initial available strain energy for a given allowable strain as determined from Figure A.3-3

$(K.E.)_D$ = the kinetic energy for the design pipe break condition (1.35×10^6 in.-lbs)

$U_L(n)$ = the strain energy lost to hardening after n spurious trips as determined from Figure A.3-4

In particular, using the allowable strain of 9%, the appropriate quantities for the disc are as follows

ϵ_a = 9%

U_A = 1.40×10^6 in.-lbs

$U_L(n) \leq (1.40 - 1.35) \times 10^6 = 0.05 \times 10^6$ in.-lbs

hence

n = 3 (Figure A.3-4).

Therefore, the conclusion is that the isolation valve disc can be subjected to at least three spurious trips before the capability to sustain the design criteria for the design pipe break is jeopardized.

The second bound was based on the occurrence of a number of spurious trips with undefined input energies and represents the allowable upper limit of permanent deformation at the center of the disc. As in the previous case, isotropic hardening is assumed and the energy loss must be less than or equal to 0.05×10^6 in.-lbs. The allowable permanent set in the disc was obtained by first determining, from Figure A.3-1, the apparent impact force at the point where energy losses equal 0.05×10^6 in.-lbs. Utilizing the above force value in conjunction with the curve in Figure A.1-6, the total centerline deflection (0.31 inches) of the

disc was obtained for the allowable energy loss condition. When the elastic deflection (0.12 inches) is taken from the total deflection, 0.19 inches is the resulting permanent (plastic) deflection. Therefore, it is concluded that the isolation valve will sustain the design criteria for the design pipe break if the permanent centerline deflection of the disc is less than 0.19 inches after a number of spurious trips at unspecified energy levels.

Nuclear Services Corporation
CAMPBELL, CALIFORNIA

Figure A.3-1

TOTAL FORCE VS. EQUIVALENT DEFLECTION

DISC AND VALVE SEAT SYSTEM

Segment AB: Disc and Seat Elastic
Segment BC: Disc Elastic, Seat Yielded
Segment CD: Disc and Seat Yielded

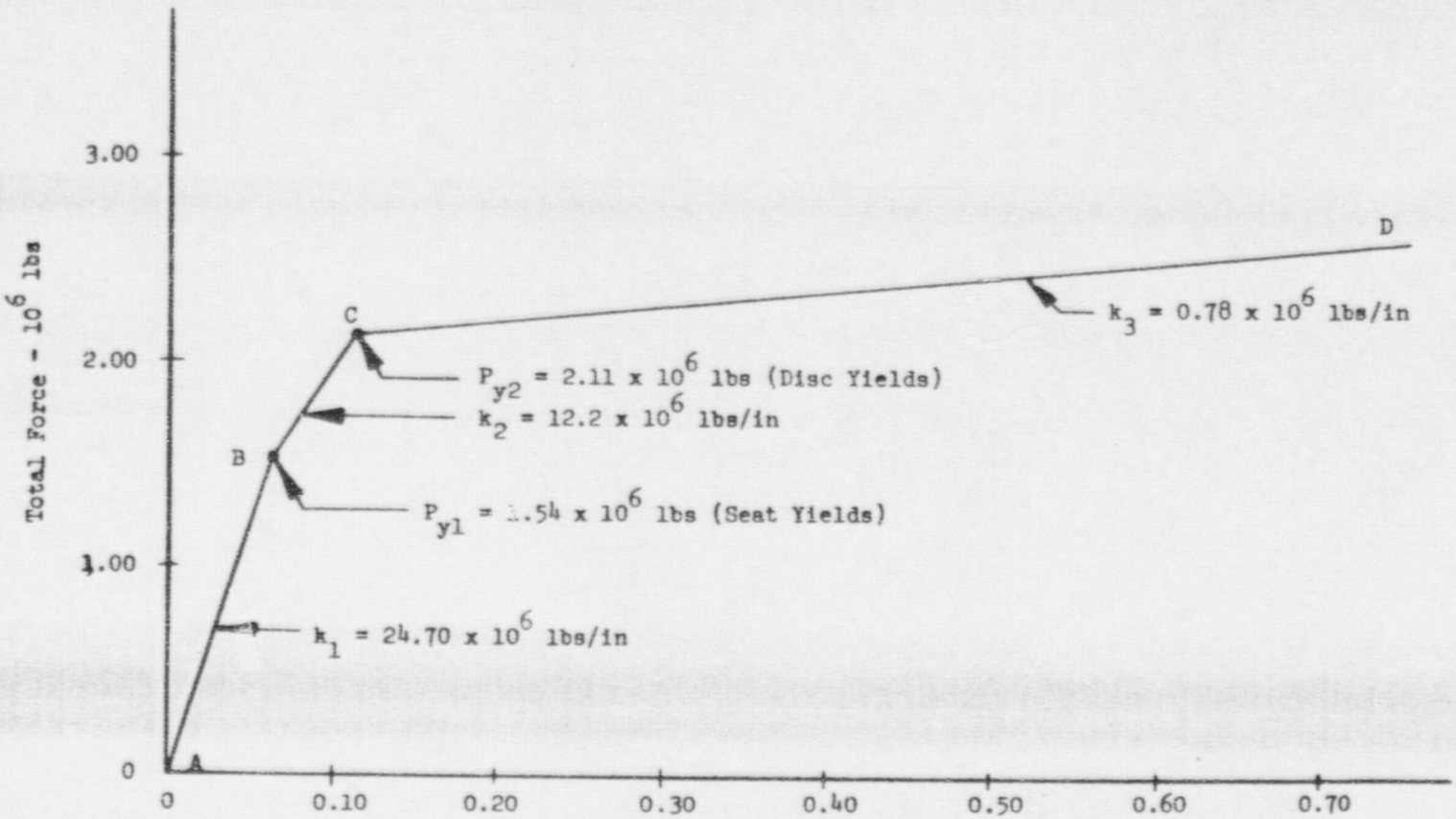

(Used Only to Calculate Strain Energy)

Figure A.3-2

IMPACT FORCE VERSUS INPUT ENERGY

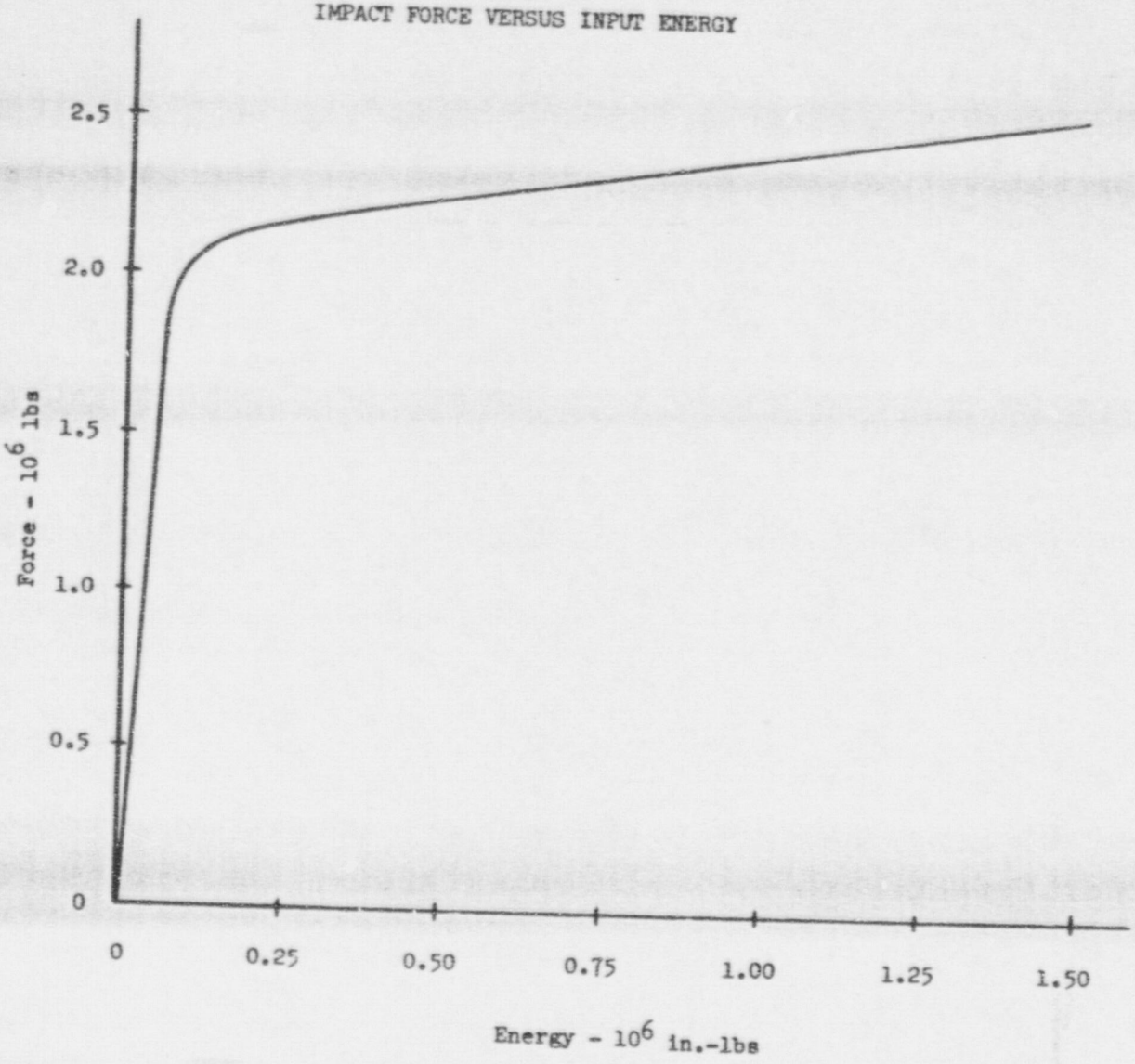

Figure A.3-3

Nuclear Services Corporation
CAMPBELL, CALIFORNIA

TOTAL STRAIN VERSUS INPUT ENERGY

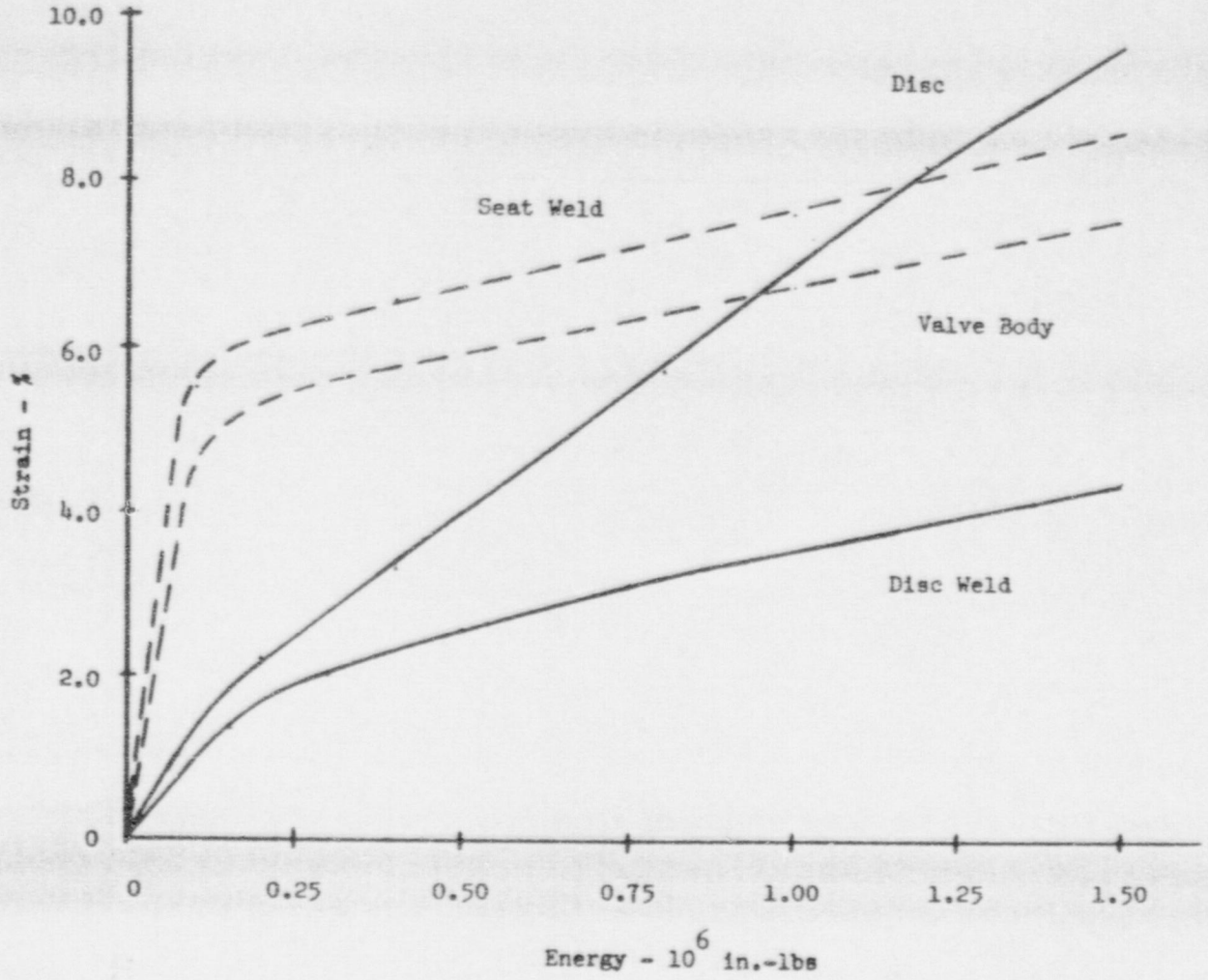

Nuclear Services Corporation
CAMPBELL, CALIFORNIA

Figure A.3-4

POTENTIAL ENERGY LOSS

VERSUS

NUMBER OF SPURIOUS TRIPS

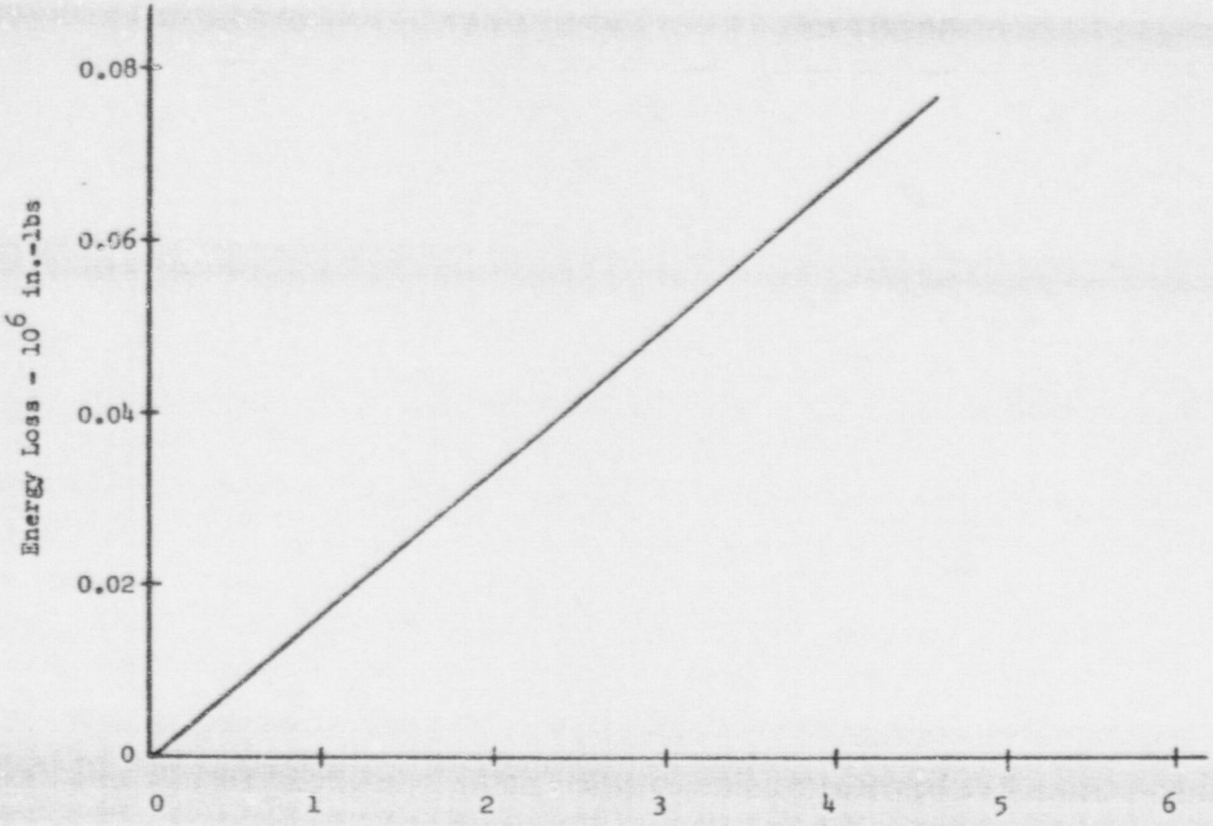

A.4 Disc and Valve Body Interaction - Dynamic

A.4.1 Single Degree of Freedom Model

A nonlinear single degree of freedom analysis was performed on the disc to valve impact. The purpose was to determine the post impact rebound velocities so the effect of the rebound centrifugal force upon the tail link could be analyzed. An additional purpose was to determine the potential for separation between the disc and valve following initial impact. A separation would result in an additional energy input which was not considered in the equivalent static analyses of Appendix A.3.

The model is as shown in Figure A.4.1-1. The spring stiffness used is shown in Figure A.4.1-2 and is a bilinear representation of the disc and valve body combined stiffness of Figure A.3-1. The combined stiffness was obtained from the static finite element analyses discussed in Appendix A. A constant forcing function of 358,538 lbs. was utilized. This force correspondes to the pressure at impact of 965 psi per Reference 1 and the 21.75 inch inside diameter of the valve body. The initial gap between the mass and spring was determined in correlation with the impact energy and the forcing function.

The disc response for the spurious trip and closure following a design pipe break is shown in Figures A.4.1-3 to A.4.1-6. It should be noted

that the disc deflections before impact in Figures A.4.1-4 and A.4.1-6 only represent the model gap necessary for the impact energy. The resulting rebound angular velocities are shown in Table A.4.1-1. It can be seen that no separation occurs, thus maximum loads predicted by the static energy analysis are not altered by rebound. The rebound angular velocities are so low that additional plastic deformation of the tail link will not occur, thus the effectiveness of the seal will not be degraded by misalignment upon final seating.

TABLE A.4.1-1

DYNAMIC DISC-VALVE IMPACT RESULT

OPERATING CONDITIONS	ENERGY in.-lbs	INITIAL GAP in.	PEAK LOAD lb	REBOUND VELOCITY in./sec	REBOUND ANGULAR VELOCITY rad/sec
Design Pipe Break	1.35×10^6	4.1769	2.70×10^6	206.4	13.1
Spurious Trip	$.15 \times 10^6$	.4211	2.15×10^6	186.6	11.8

Figure A.4.1-1

MODEL OF DISC VALVE BODY IMPACT

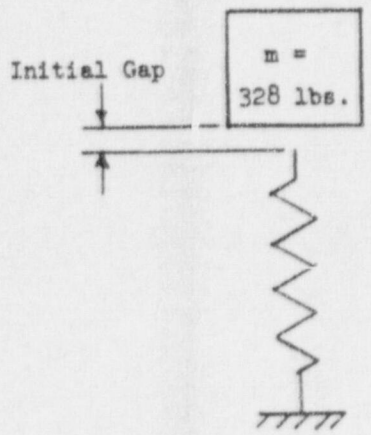

Figure A.4.1-2

SPRING REPRESENTING DISC AND VALVE BODY

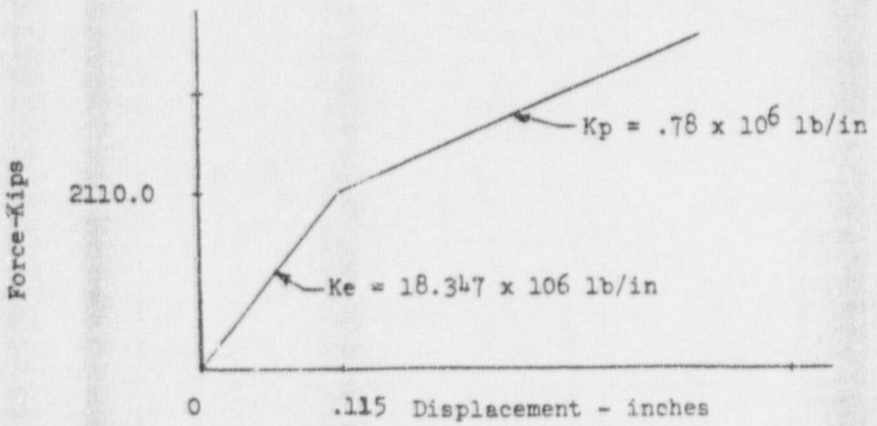

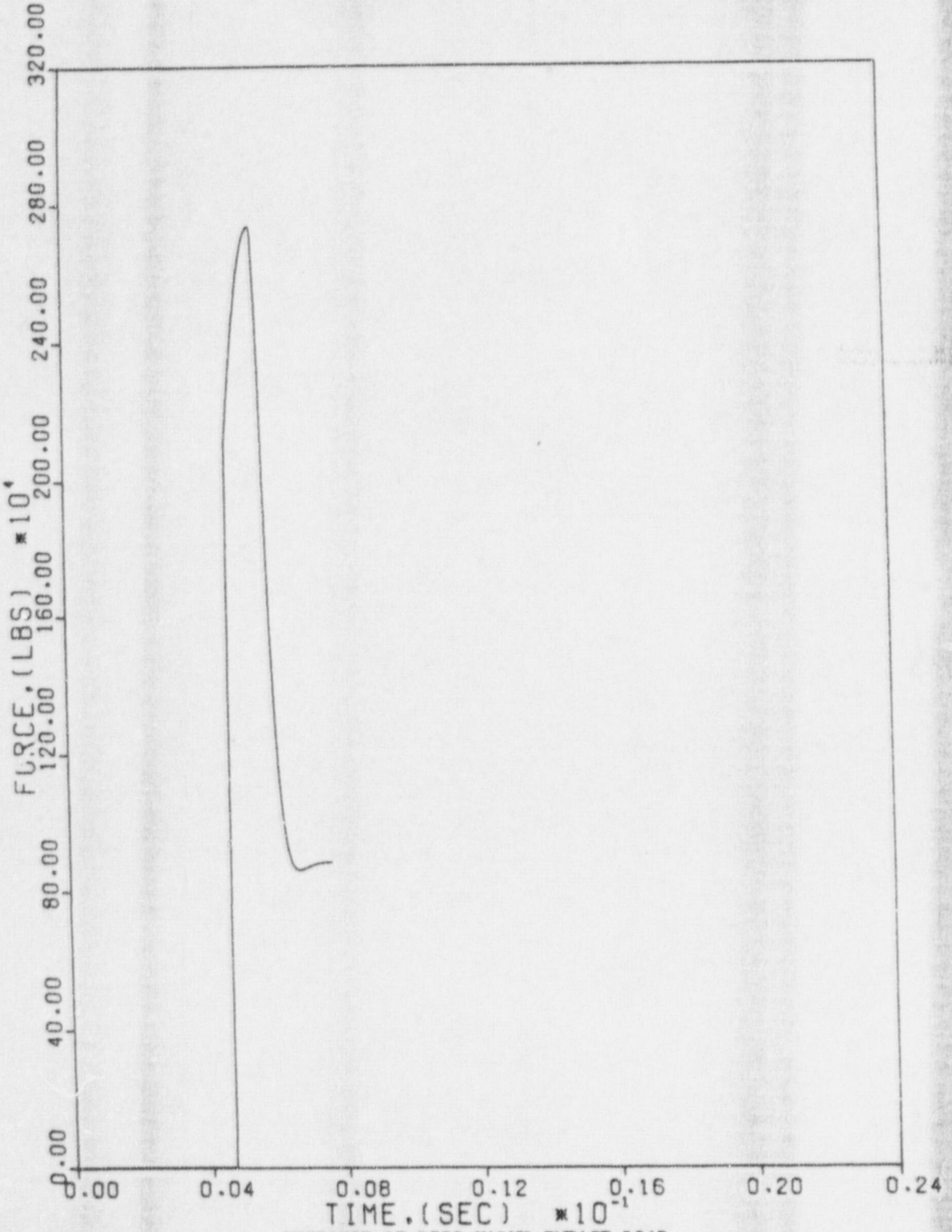

RESPONSE OF DISC-VALVE IMPACT LOAD
FOR ENERGY OF 1.35 x 10^6 in.-lbs

Figure A.4.1-3

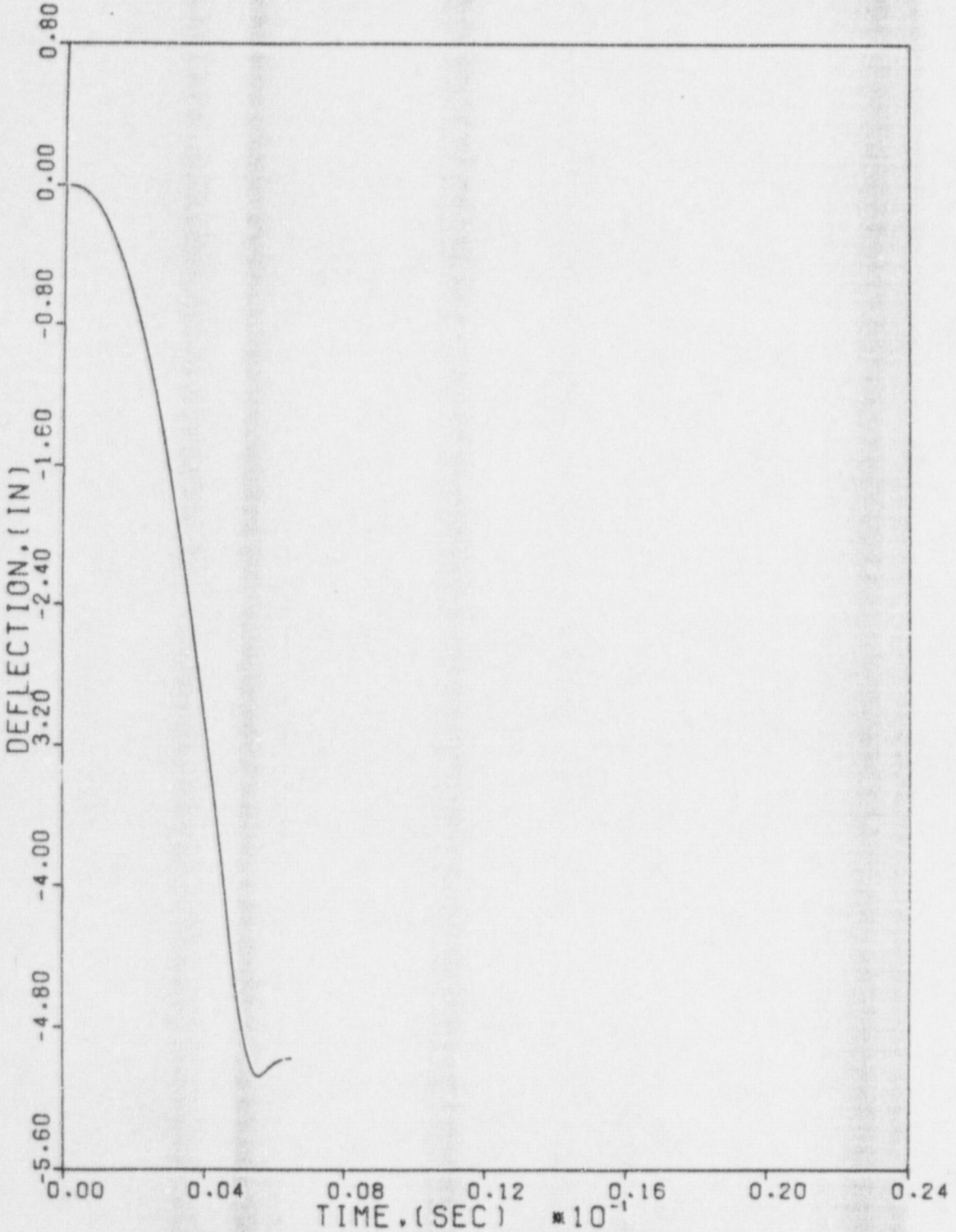

RESPONSE OF MODEL MASS (DISC) DISPLACEMENT
FOR ENERGY OF 1.35×10^6 in.-lbs
Figure A.4.1-4

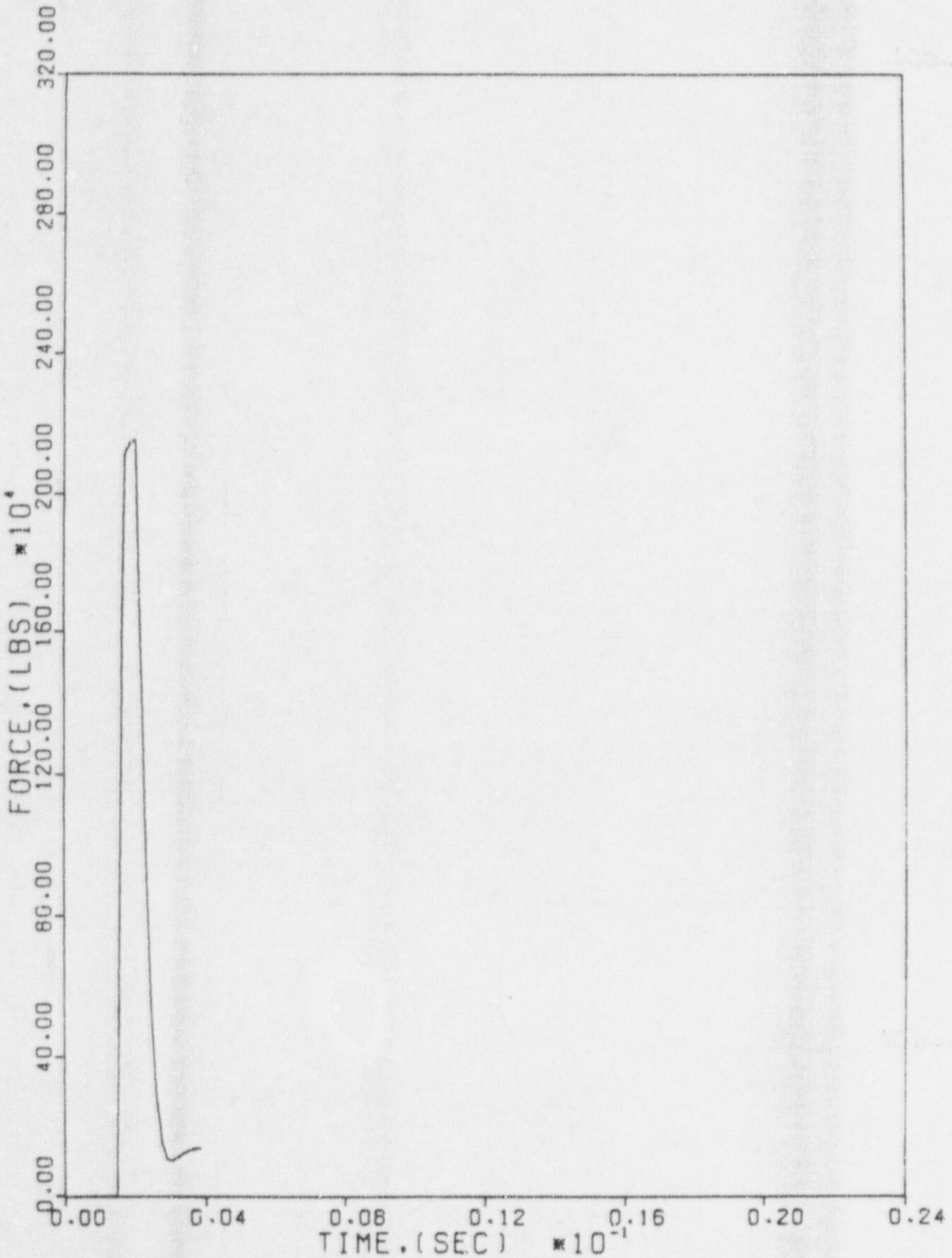

RESPONSE OF DISC-VALVE IMPACT LOAD
FOR ENERGY OF .15 x 10^6 in.-lbs

Figure A.4.1-5

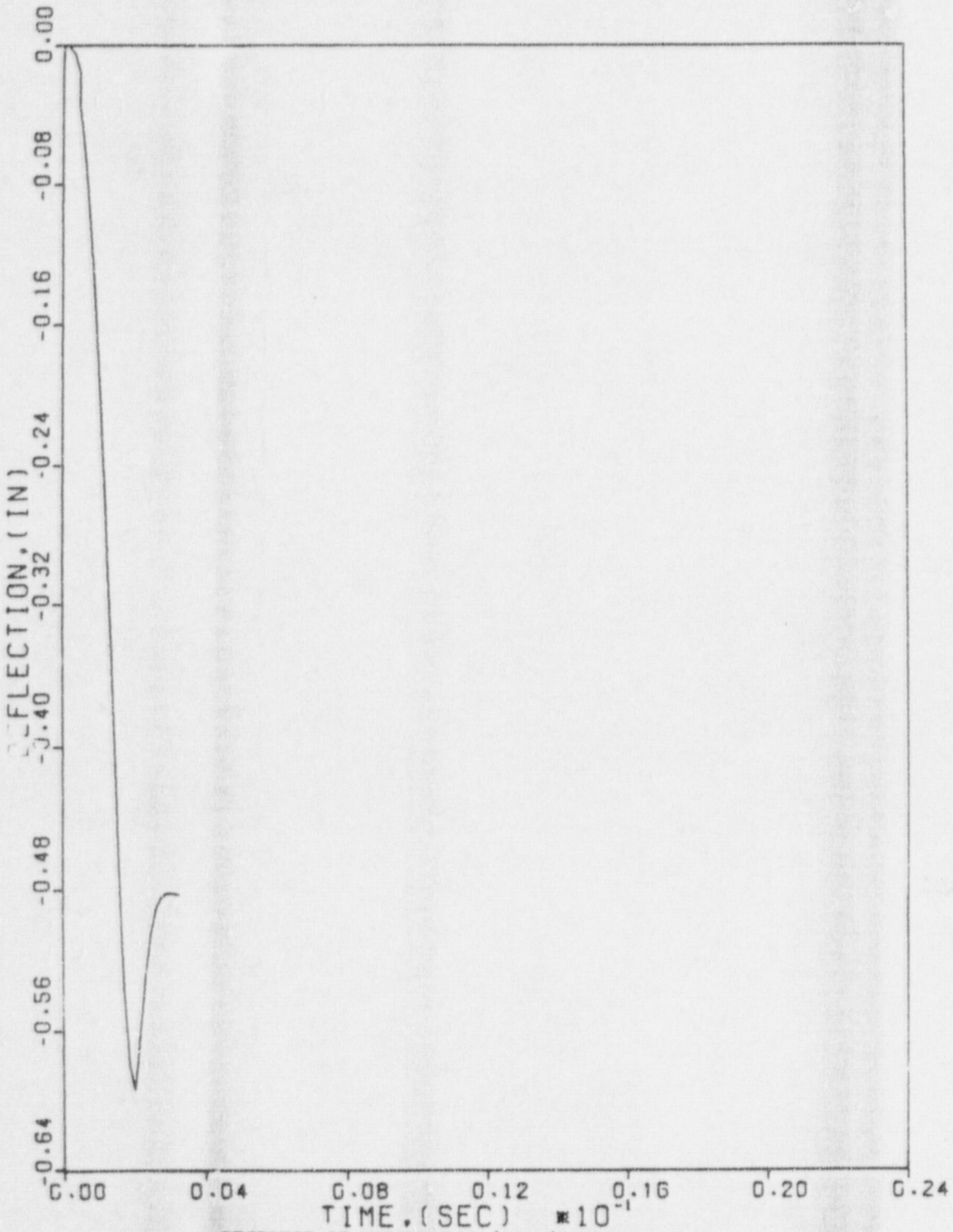

RESPONSE OF MODEL MASS (DISC) DISPLACEMENT
FOR ENERGY OF .15 x 10^6 in.-lbs
Figure A.4.1-6

A.4.2 Multi-Degree of Freedom Model

A more complex, nonlinear, dynamic analysis with multi-degrees of freedom was performed on the disc and valve body to determine the symmetry of impact loads.

The model used is shown in Figure A.4.2-1. The model consists of three basic segments. The disc is represented by four identical crossed bars which are uniformly spaced. The valve body is simulated by eight discrete springs located vertically beneath the terminal points of the bars. A bar element representing the tail link connects the disc to a pivot.

Appropriate stiffnesses have been associated with the various segments. The four crossed bars representing the disc have the effective disc stiffness as shown in Figure A.1-3. The mass of the disc was conservatively concentrated at the center in order to simplify modeling of the effective stiffness. The eight discrete springs in parallel have the effective valve body stiffness as shown in Figure A.2-2. The stiffness of the tail link was determined by matching the effective elongation with the finite element analysis of the tail link as shown in Appendix B.1.

The forcing function applied to the center of the model is the same as that utilized for the single degree of freedom model, Appendix A.4.1. The gap used for the springs located on the Z-axis (11 and 15), two of

the eight representing the valve body, was determined in correlation with an energy input of 0.55×10^6 in.-lbs. The other gaps were subsequently calculated based on the resultant angle determined by the initial gap of Nodes 11 and 15.

The results of the analysis are shown in Figures A.4.2-2 to A.4.2-6. It can be seen that the maximum valve body loads are relatively uniform around the circumference. This confirms the validity of the axisymmetrical finite element models utilized in the disc and valve seat analyses.

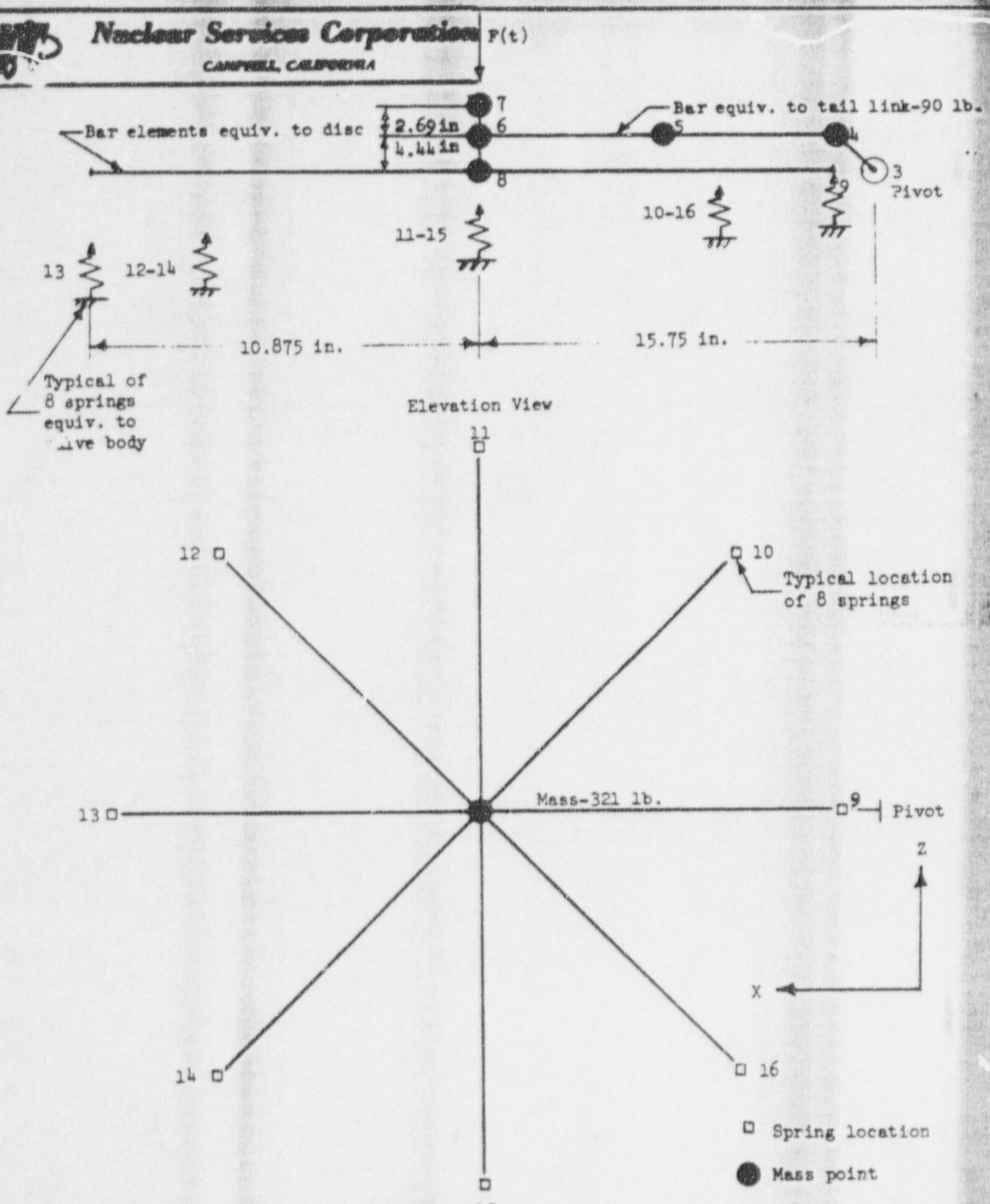

MODEL OF MULTI-DEGREE OF FREEDOM MODEL

Figure A.4.2-1

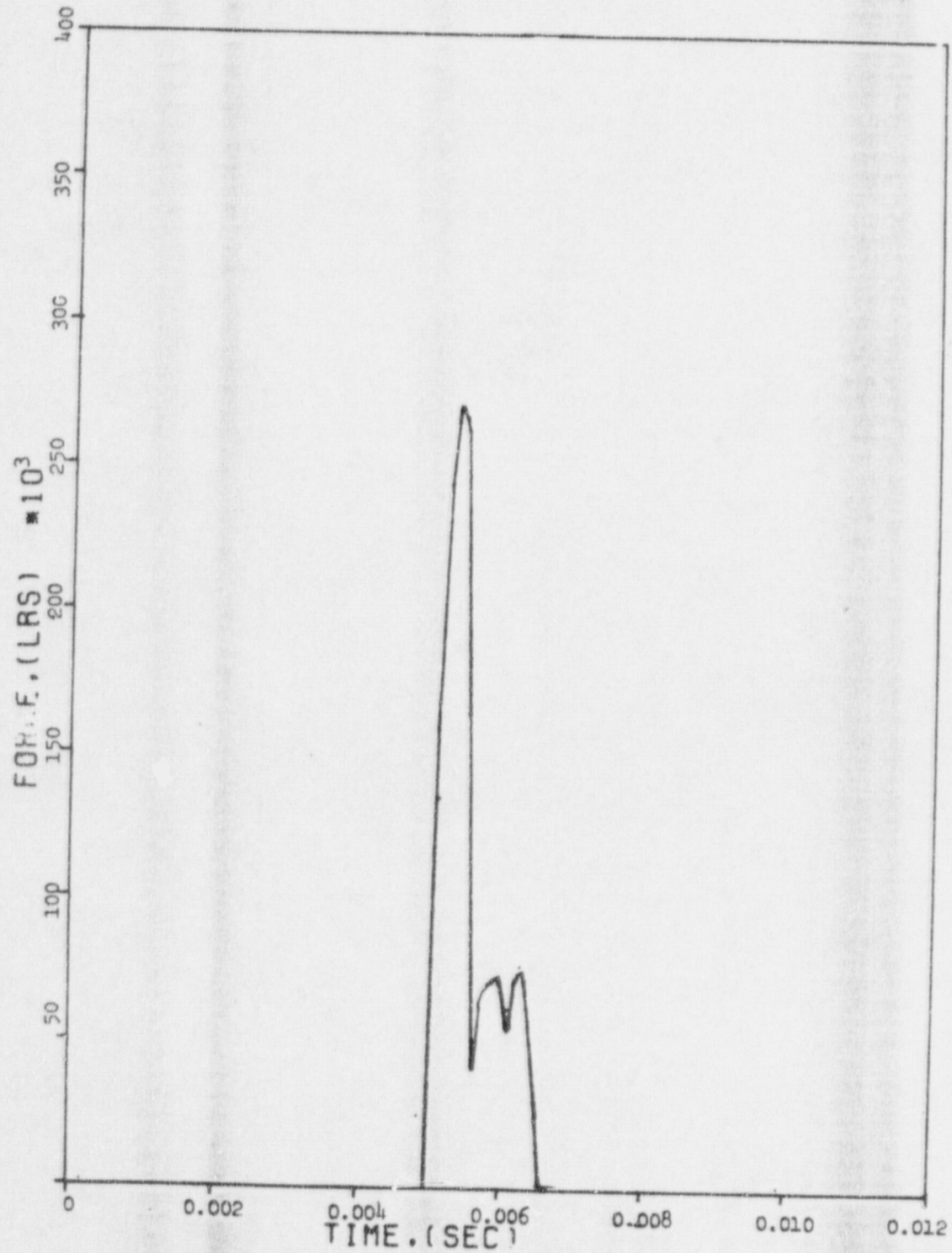

RESPONSE OF DISC-VALVE IMPACT LOAD AT NODE 9
Figure A.4.2-2

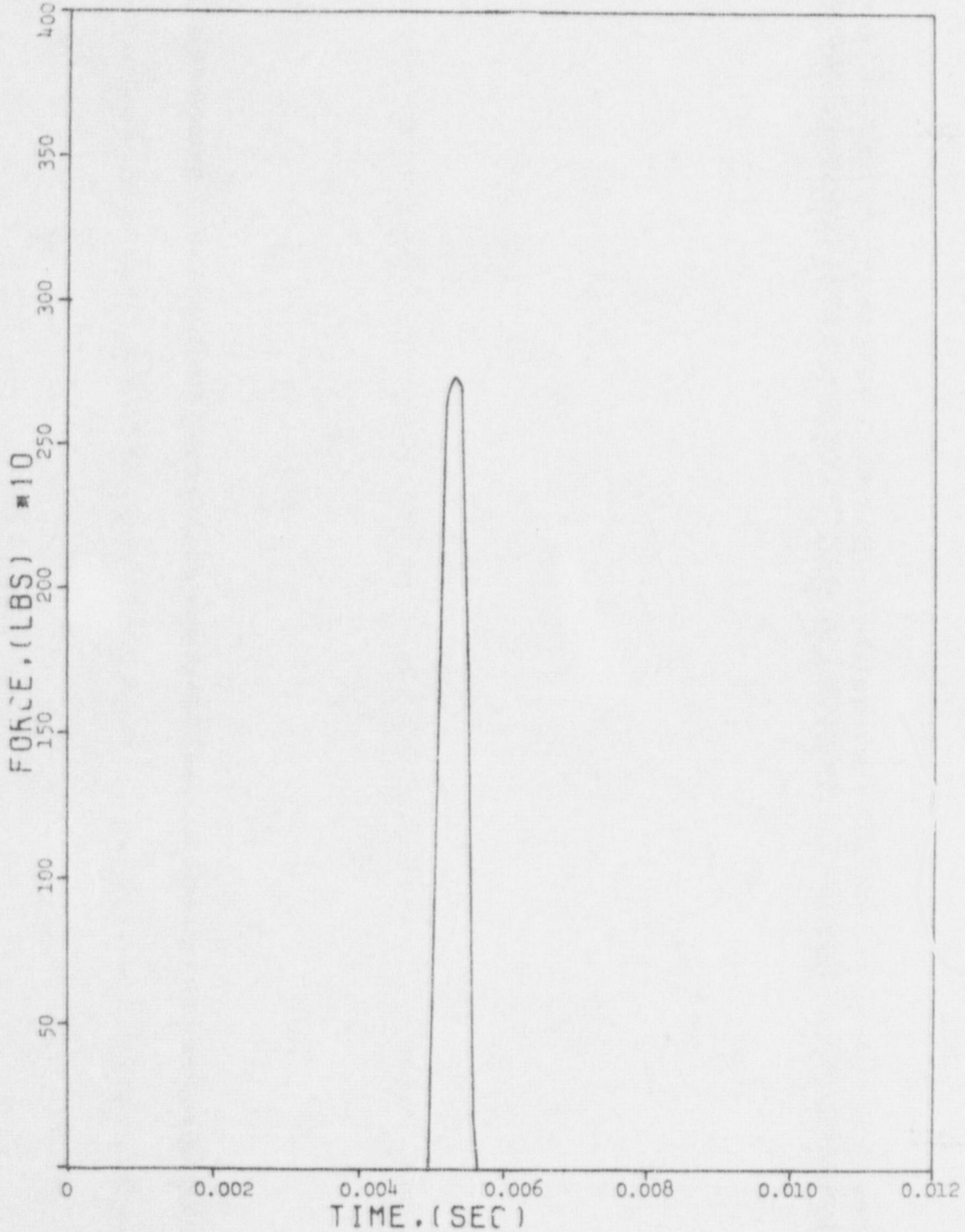

RESPONSE OF DISC-VALVE IMPACT LOAD AT NODE 10 & 16

Figure A.4.2-3

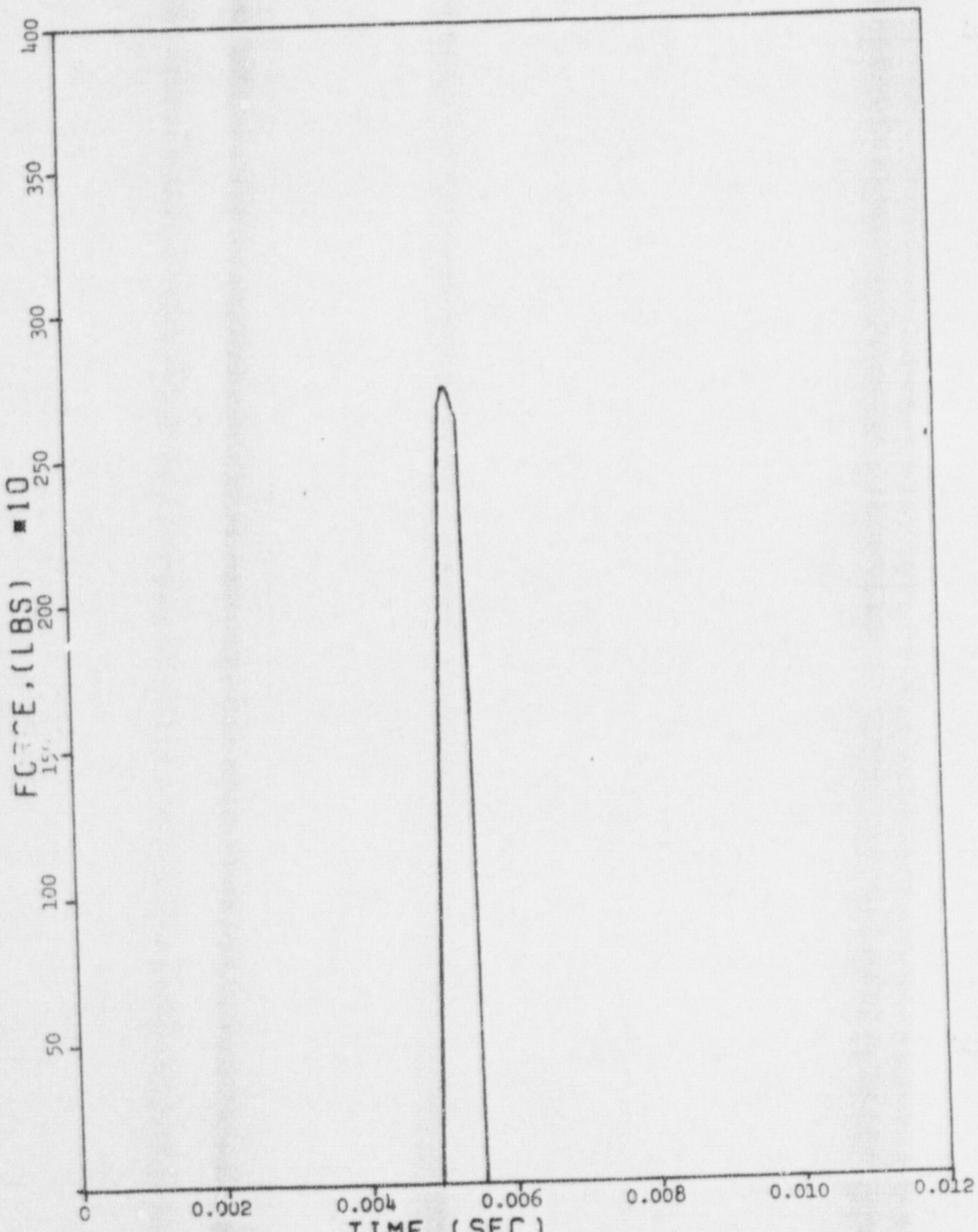

RESPONSE OF DISC-VALVE IMPACT LOAD AT NODE 11 & 15
Figure A.4.2-4

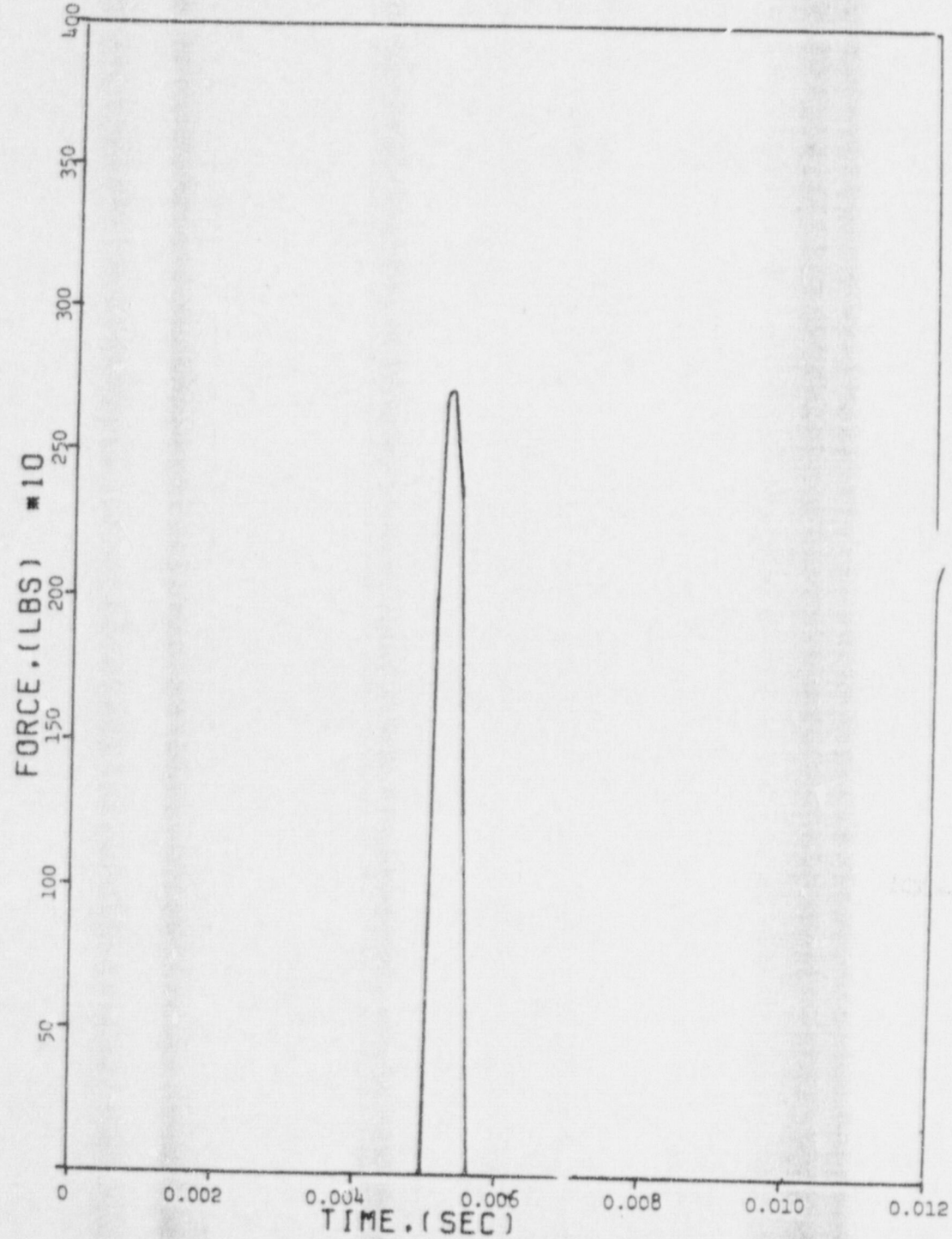

RESPONSE OF DISC-VALVE IMPACT LOAD AT NODE 12 & 14
Figure A.4.2-5

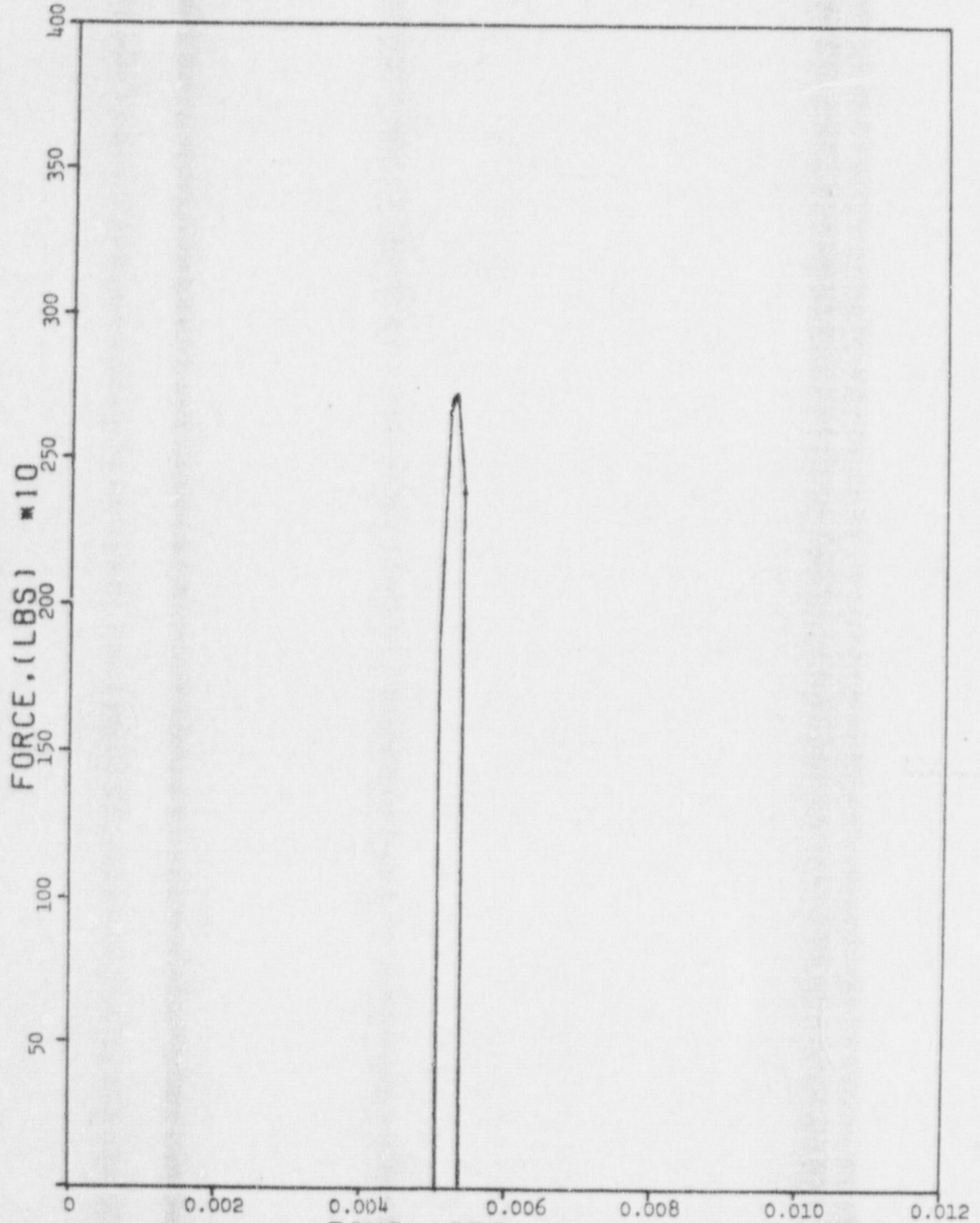

RESPONSE OF DISC-VALVE IMPACT LOAD AT NODE 13
Figure A.4.2-6

APPENDIX B

Analysis of the Tail Link

TABLE OF CONTENTS

B.1 Static Finite Element Analyses

A static analysis of the isolation tail link was performed with the aid of the finite element computer code MARC-CDC. The model shown in Figure B.1-1 was constructed from 160 quadrilateral and triangular, isoparametric plane stress elements which incorporated material strain-hardening effects. Analyses of the model were conducted for two valve closure loading conditions; that is, (1) centrifugal forces and (2) rotation restraint produced by the axial deflection at the center of the disc following impact.

The analysis of the effects of centrifugal forces was accomplished by rigidly fixing the model boundary at the disc-link interface and applying force at the rock shaft reaction point as shown in Figure B.1-1. By incrementing the applied load from zero to 148 kips, the force-deflection curve shown in Figure B.1-2 was obtained for the link. In addition, total plastic strains as a function of applied load were obtained and are shown in Figure B.1-3. Utilizing the above results and noting the appropriate relationship between centrifugal force and angular velocity shown in Figure B.1-4, relationships between maximum element strain and impact energy, and deflection and impact energy were determined and shown in Figures B.1-5 and B.1-6 respectively. Figure B.1-7 represents, schematically, the growth of the plastic zone in the link as a function of the increasing centrifugal force.

The effect of the restraint imposed upon the free arc travel of the tail link mechanism by the disc after impact was determined by conservatively

restricting the travel of the link to the axial path of the center of the disc as shown in Figure B.1-8. Reaction for the restraint force was supplied at the rock shaft. A deflection, simulating the axial center deflection of the disc, was applied along the restricted path and was incremented to establish strain deflection curves.

Analyses were performed for two operating conditions. One was for the link initially unstressed which approximates the spurious trip. The resulting strain axial deflection relationship is shown in Figure B.1-9. Figure B.1-10 represents, schematically, the growth of the plastic zone in the link as a function of the axial center disc displacement for this condition. The second condition was for the link initially stressed to correspond to the design pipe break. The resulting strain axial deflection relationship is shown in Figure B.1-11. In both cases the state of strain due to the restriction of the link was related to the overall closure energy by utili? ng the disc center deflection from Figure A.1-6.

As can be seen from the results, the assumed conservative restraint imposed by the axial displacement of the disc after impact adds to the maximum strains resulting from the centrifugal forces.

As discussed in Section A.3, after a number of trips, the isolation valve will meet the criteria for a design pipe break if the total permanent centerline deflection of the disc is less than 0.19 inches. During impact

this corresponds to a total disc centerline deflection of 0.31 inches.

The effect of a number of trips upon the tail link can be conservatively analyzed by adding together maximum developed strains for the various events. From Figure B.1-9, it can be seen a 0.31 inch center deflection of the disc will produce 2.5% plastic strain in the tail link. Utilizing the results in Figure B.1-10 for a design pipe break and conservatively adding these results to the previous strain, the total strain of 12% is obtained. This is within the design criteria.

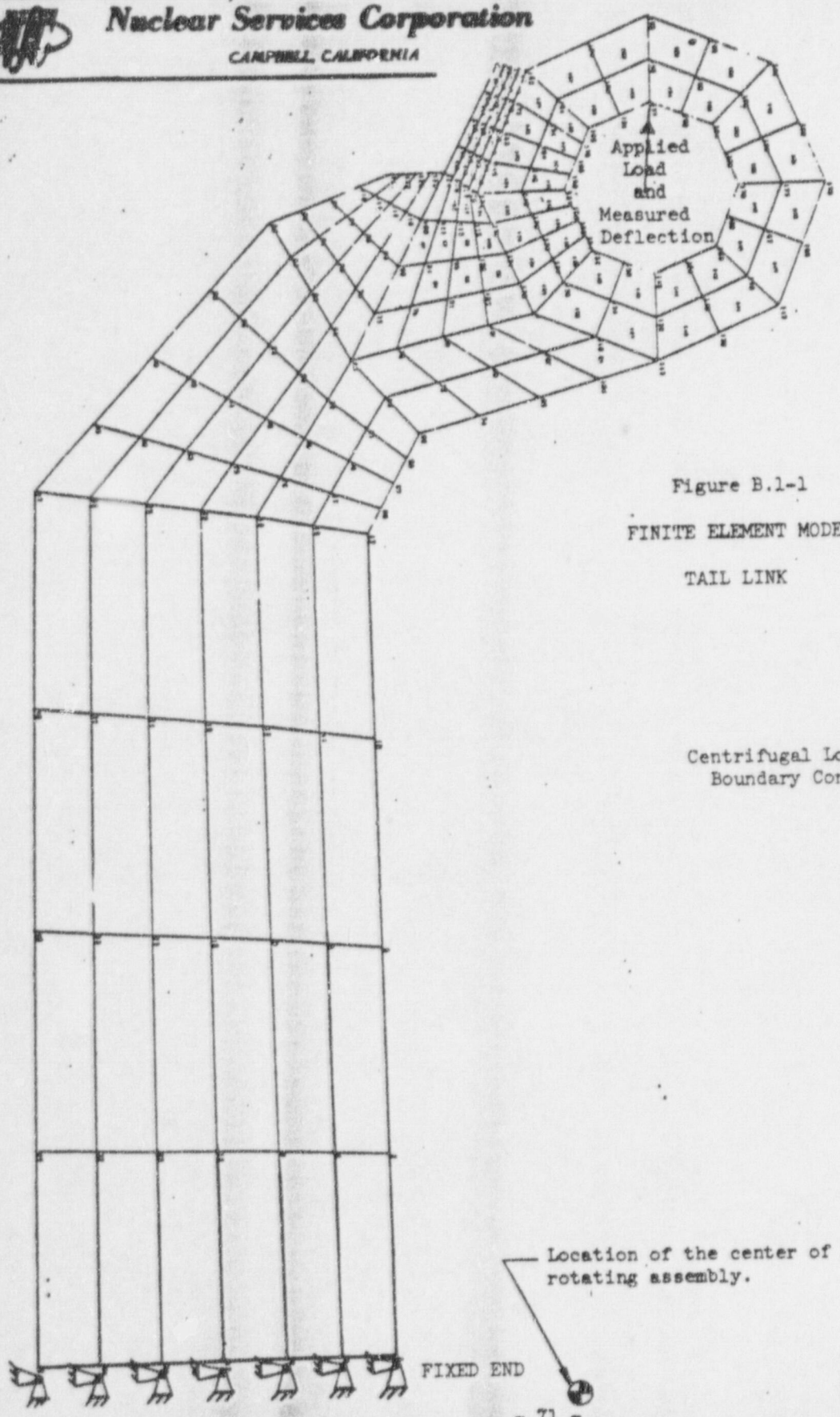

Figure B.1-1

FINITE ELEMENT MODEL

TAIL LINK

Centrifugal Loading and
Boundary Conditions

Figure B.1-2

CENTRIFUGAL LOAD VERSUS DEFLECTION

ISOLATION VALVE

TAIL LINK

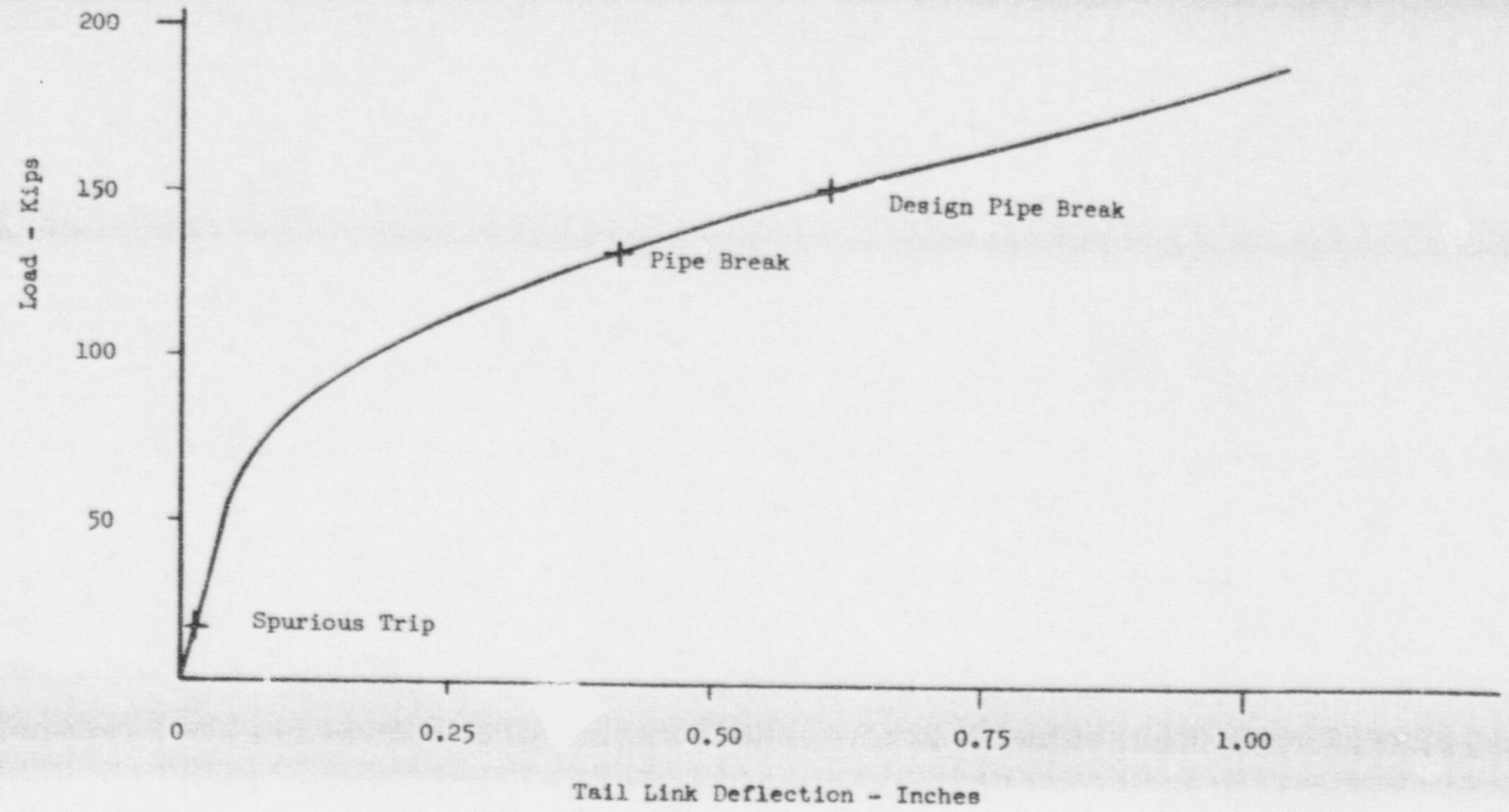

Nuclear Services Corporation
CAMPBELL, CALIFORNIA

Figure B.1-3

TOTAL STRAIN VERSUS CENTRIFUGAL FORCE

ISOLATION VALVE

TAIL LINK

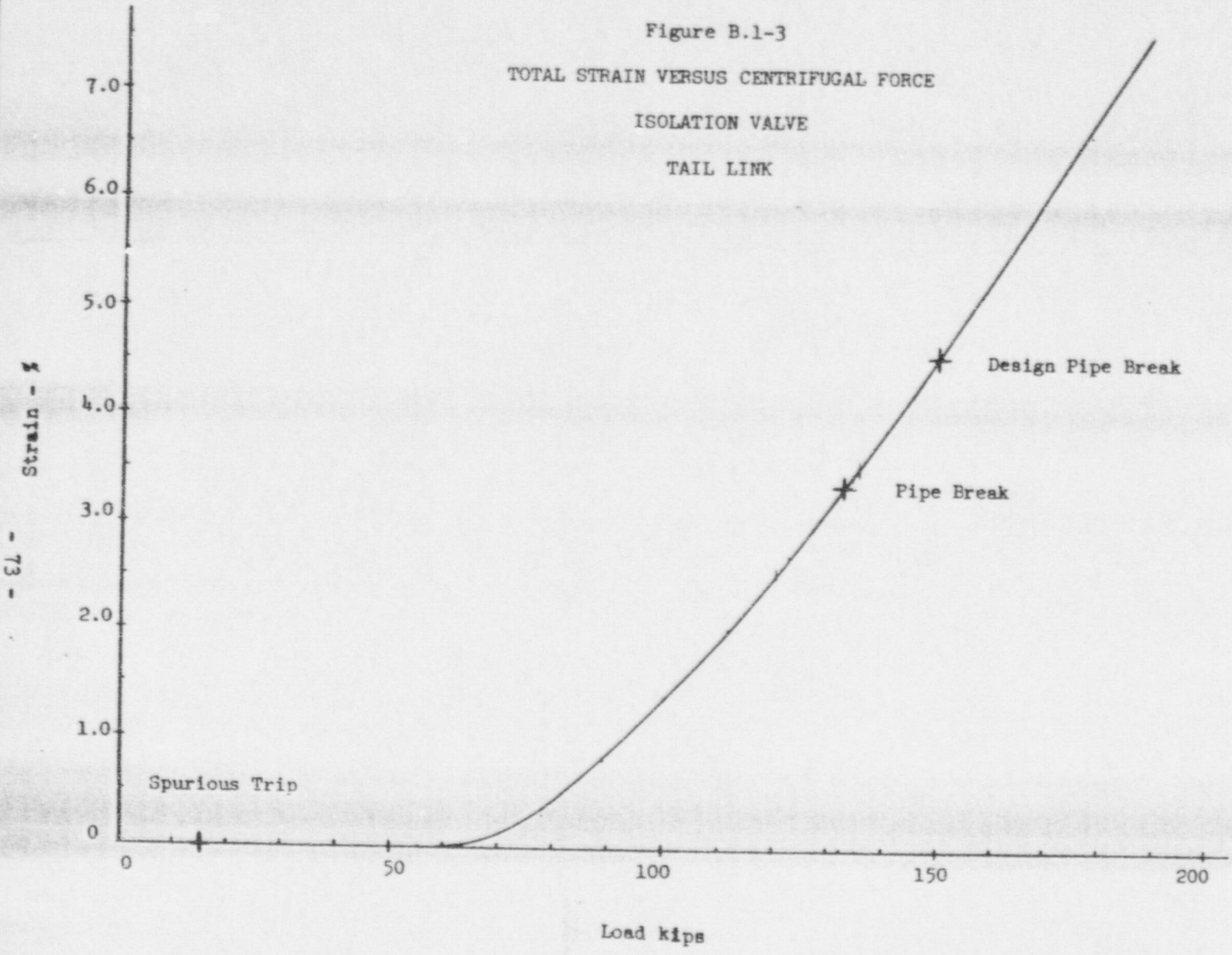

Figure B.1-4

CENTRIFUGAL FORCE VERSUS ANGULAR VELOCITY

TAIL LINK

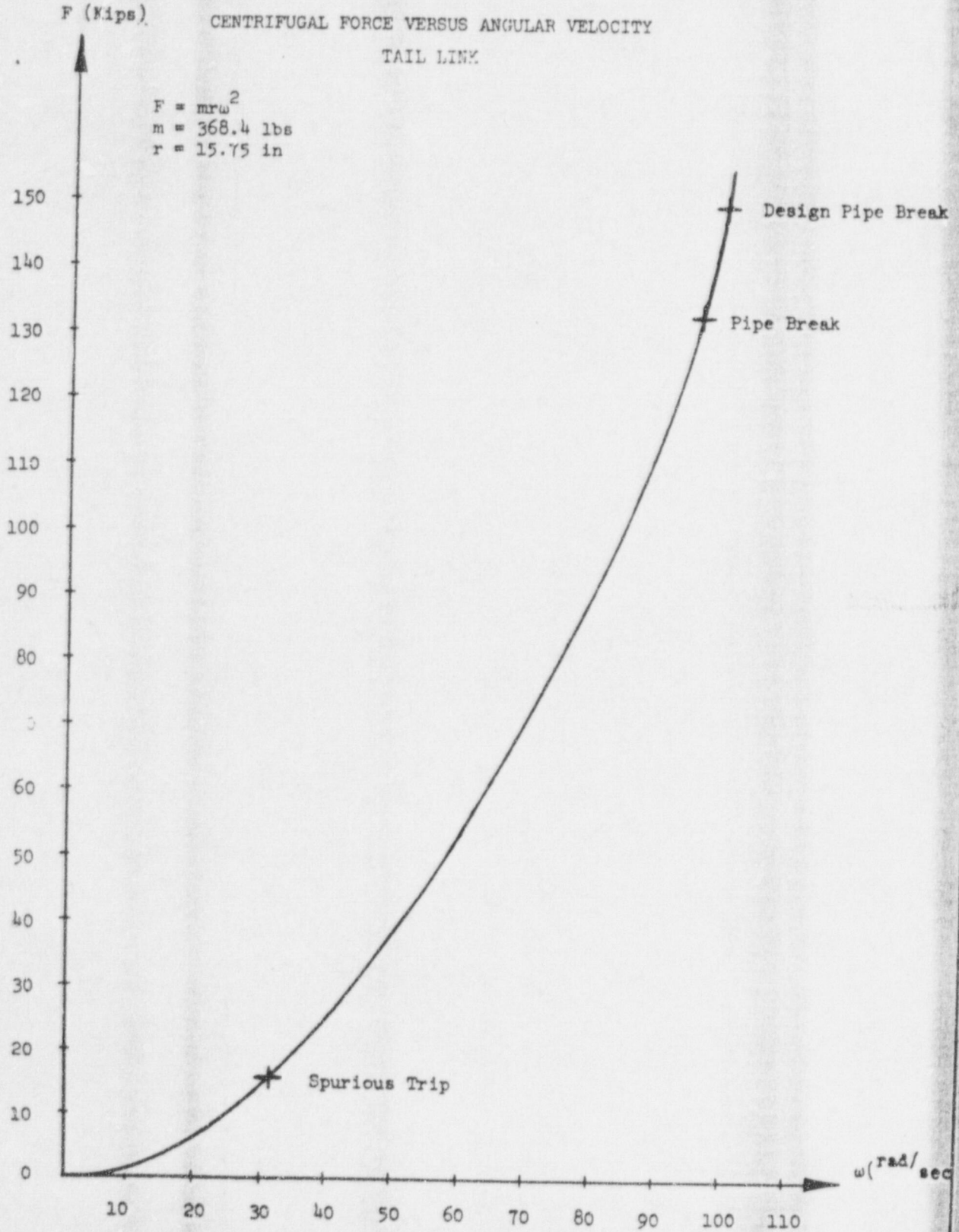

Nuclear Services Corporation
CAMPBELL, CALIFORNIA

Figure B.1-5

TOTAL STRAIN VERSUS INPUT ENERGY

ISOLATION VALVE

TAIL LINK

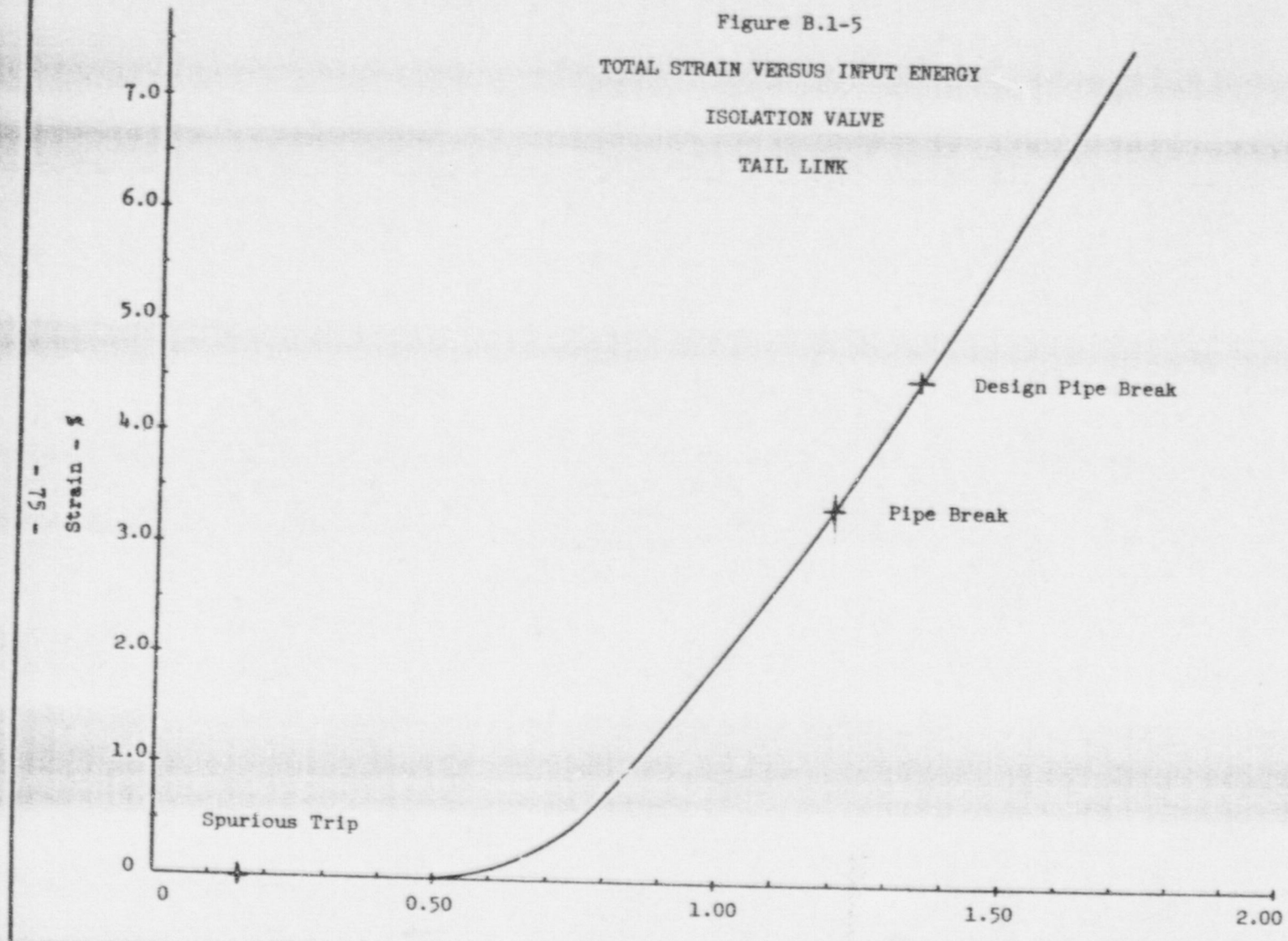

Nuclear Services Corporation
CAMPBELL, CALIFORNIA

Figure B.1-6

DEFLECTION VERSUS INPUT ENERGY

ISOLATION VALVE

TAIL LINK

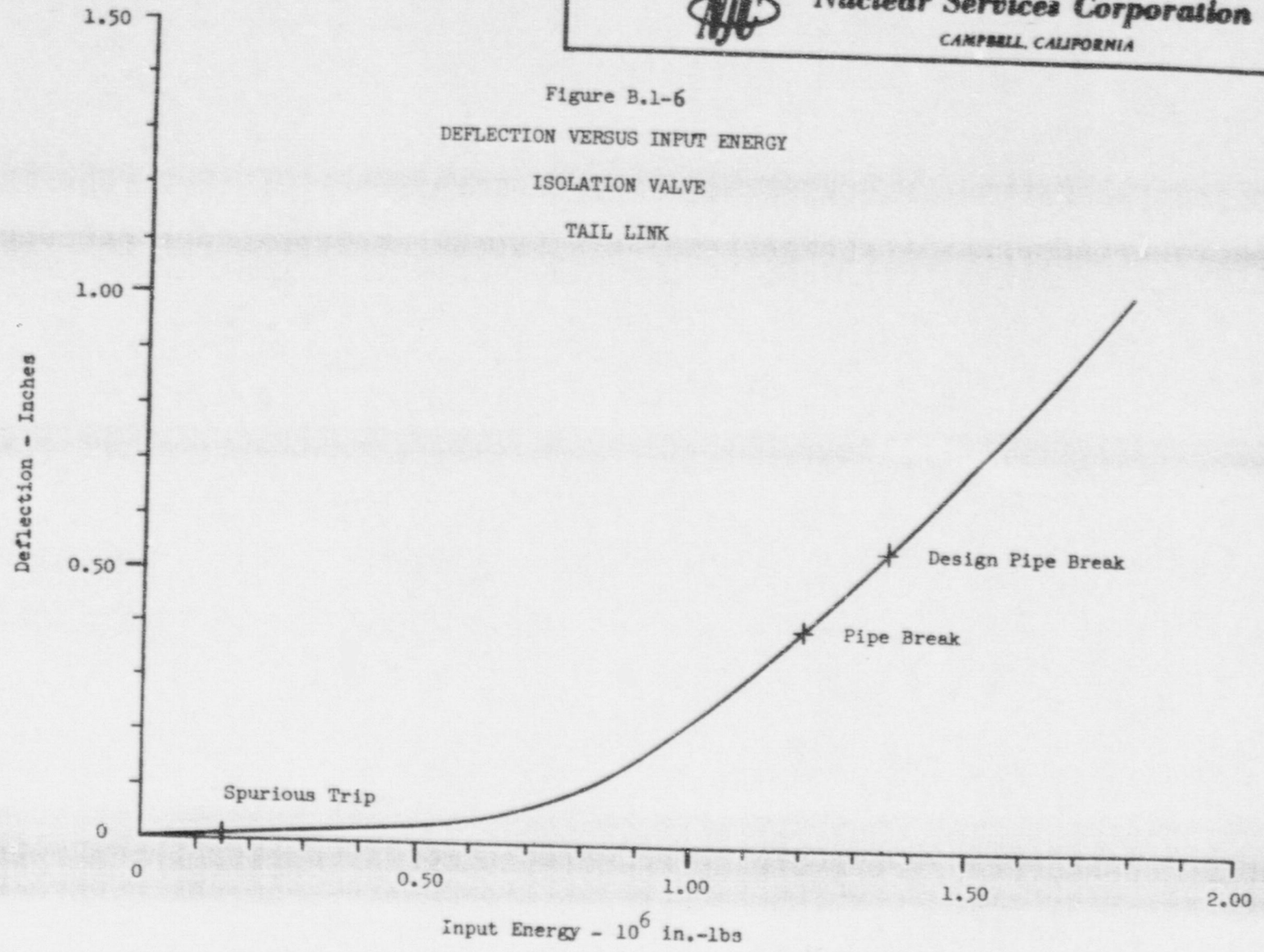

INCREMENT	LOAD x 10^3 lbs
0	55.69
1	66.83
2	77.97
3	89.12
4	100.25
5	111.39
6	122.53
7	133.67
8	144.81
9	155.95
10	167.08
11	178.22
12	189.36

LOAD DUE TO CENTIFUGAL FORCE
PRIOR TO IMPACT

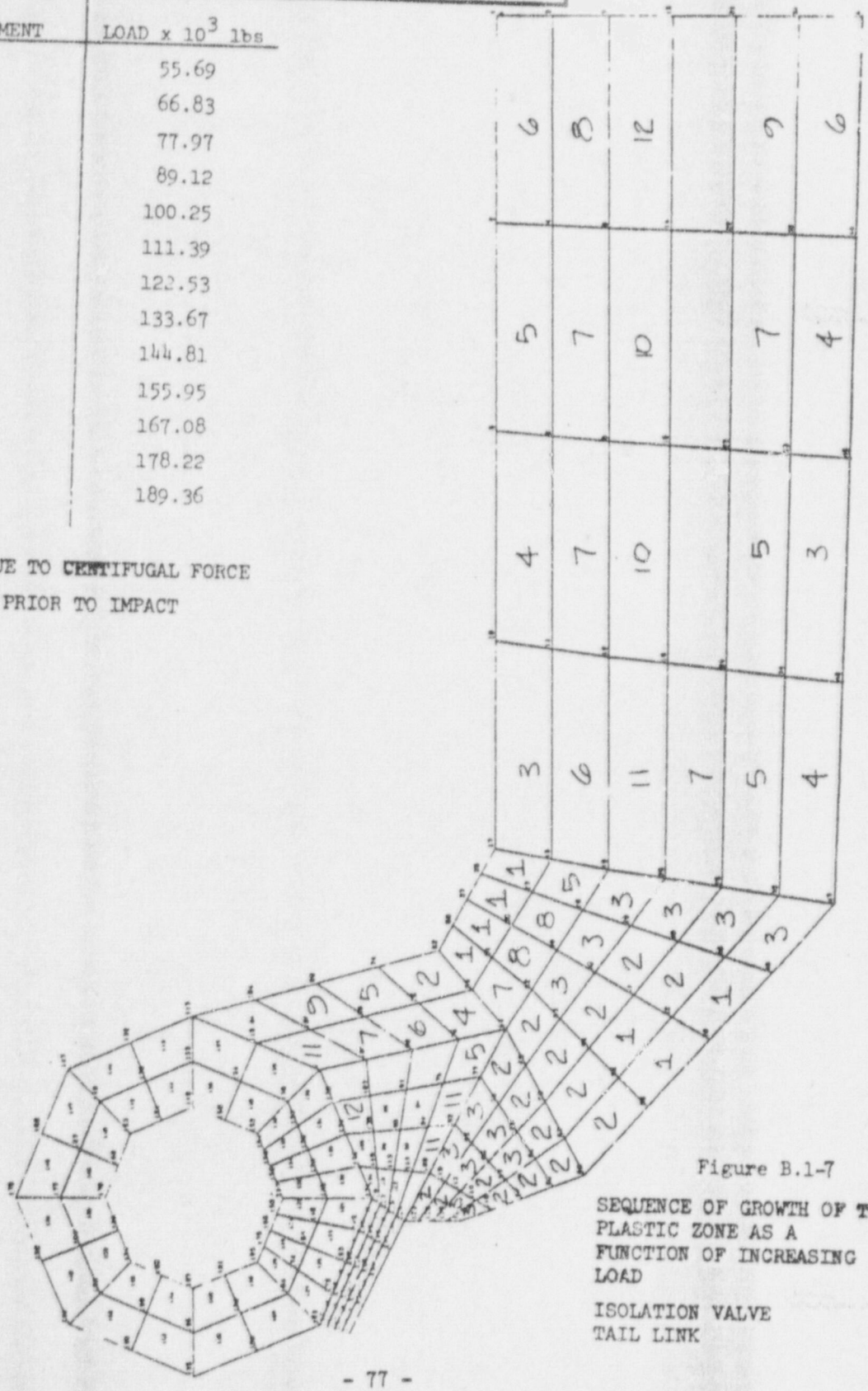

Figure B.1-7

SEQUENCE OF GROWTH OF THE PLASTIC ZONE AS A FUNCTION OF INCREASING LOAD

ISOLATION VALVE
TAIL LINK

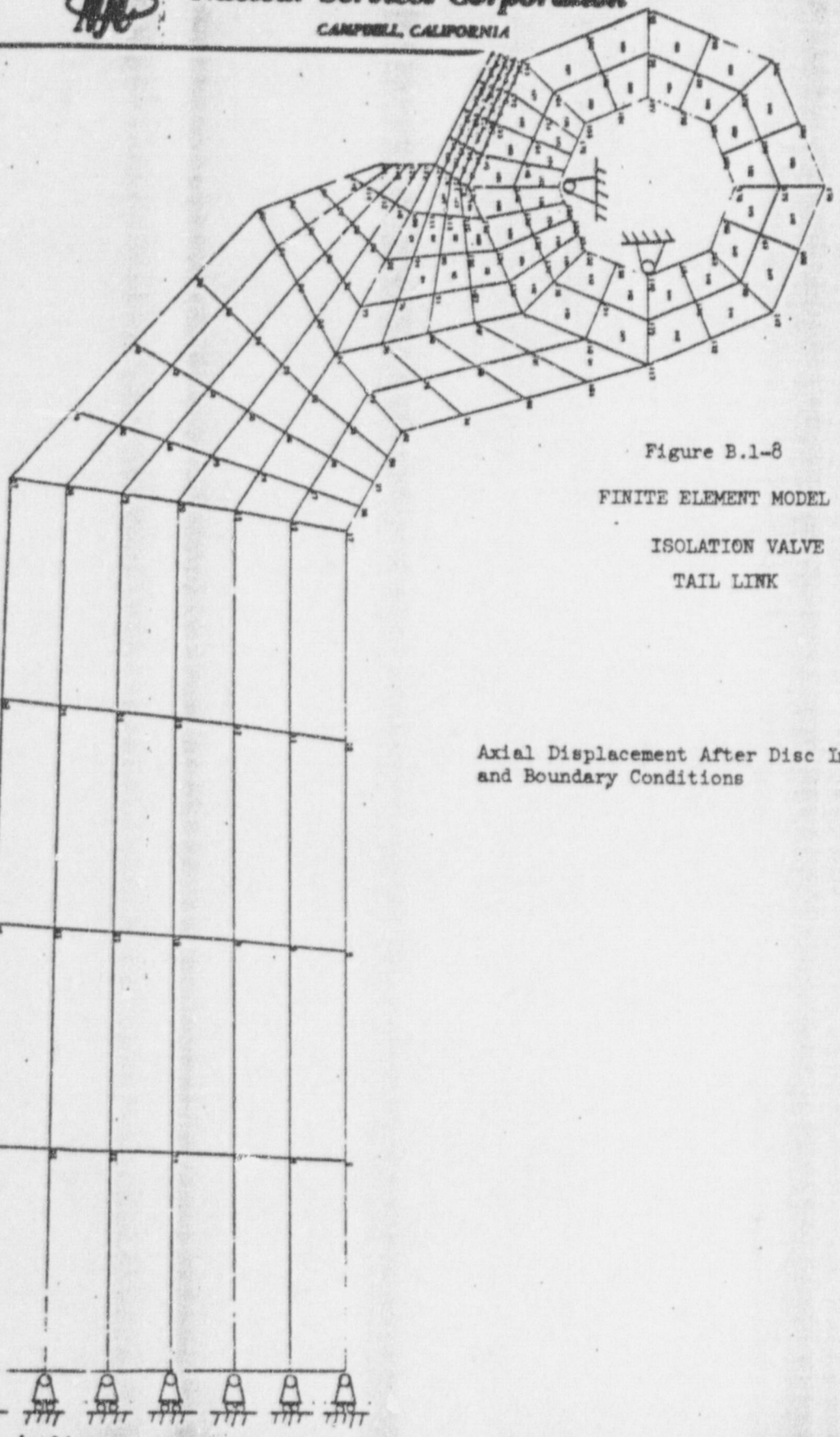

Figure B.1-8

FINITE ELEMENT MODEL

ISOLATION VALVE

TAIL LINK

Axial Displacement After Disc Impact
and Boundary Conditions

Applied Axial Deflection

Nuclear Services Corporation
CAMPBELL, CALIFORNIA

Figure B.1-9

TOTAL STRAIN VERSUS AXIAL DEFLECTION OF DISC AFTER IMPACT

ISOLATION VALVE

TAIL LINK

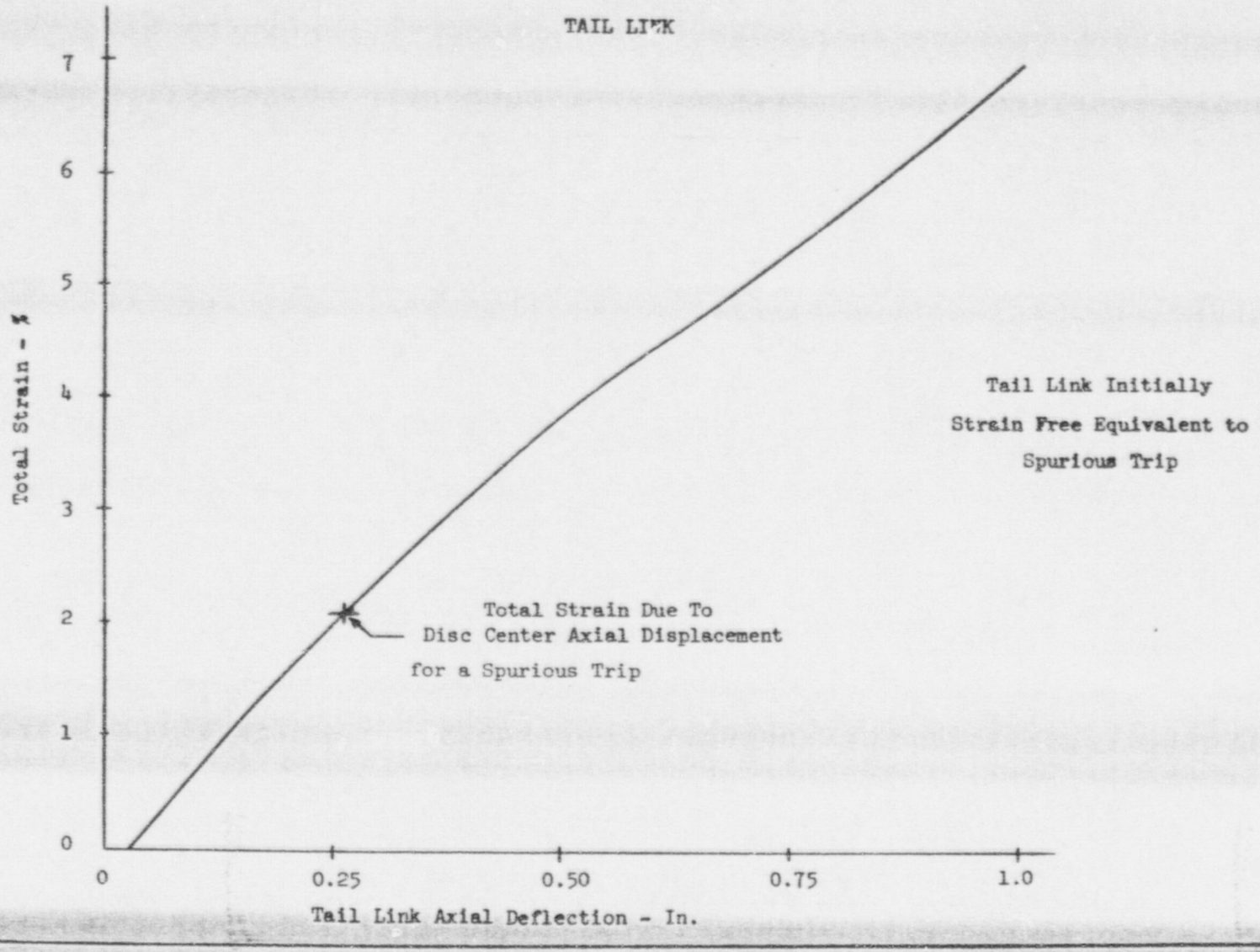

Figure B.1-10

SEQUENCE OF GROWTH OF THE PLASTIC ZONE AS A FUNCTION OF INCREASING AXIAL DISPLACEMENT AFTER IMPACT

ISOLATION VALVE
TAIL LINK

Tail Link Initially Strain Free

Increment	Displacement-in
0	.0245
1	.0305
2	.0382
3	.0491
4	.0636
5	.0837
6	.118
7	.158
8	.206
9	.268
10	.338
11	.413
12	.494
13	.582
14	.677
15	.781
16	.895
17	1.019

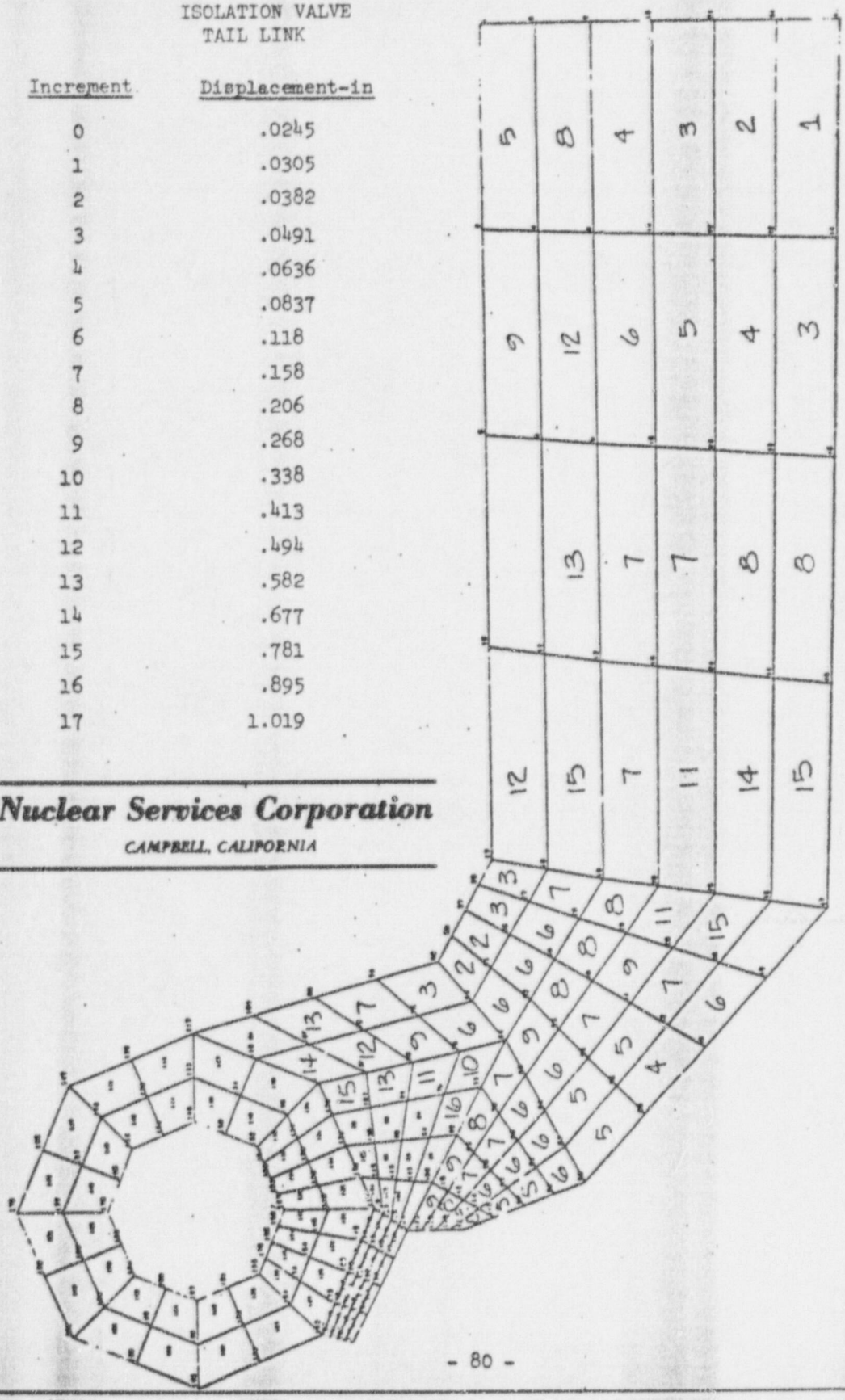

Nuclear Services Corporation
CAMPBELL, CALIFORNIA

Nuclear Services Corporation
CAMPBELL, CALIFORNIA

Figure B.1-11

TOTAL STRAIN VERSUS AXIAL DEFLECTION AFTER IMPACT

ISOLATION VALVE

TAIL LINK

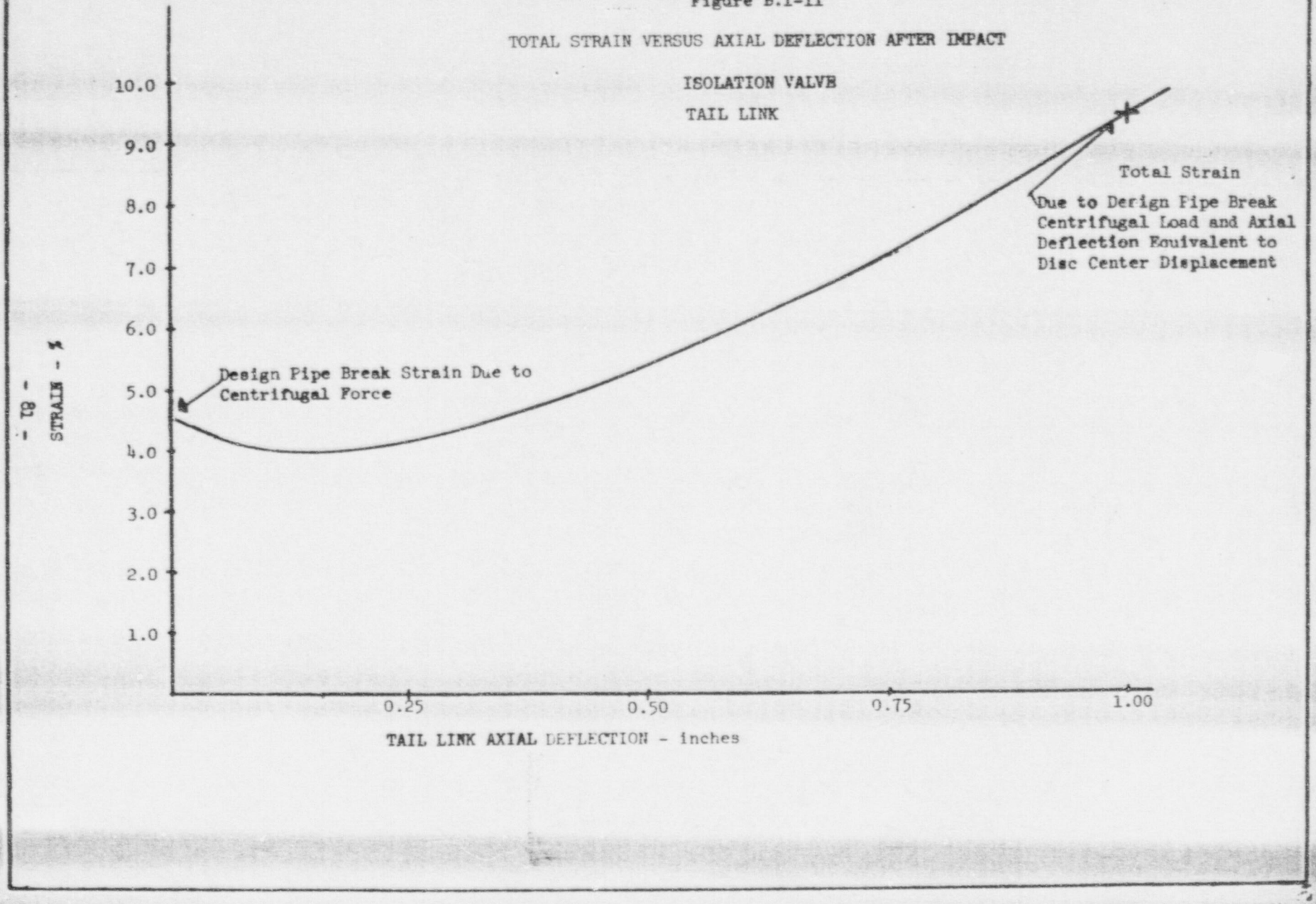

B.2 Dynamic Non-Linear Analyses

A single degree of freedom, non-linear analysis was performed on the tail link with the disc mass during the angular acceleration prior to impact. The purpose was to determine the influence of the dynamic time dependent centrifugal force upon the tail link reaction load in comparison to a static centrifugal force.

The model is as shown in Figure B.2-1. The bilinear spring stiffness was obtained from the finite element analyses of the tail link as shown in Figure B.1-2.

The centrifugal forcing function which corresponds to an impact energy of 1.07×10^6 in.-lbs. is shown on Figure B.2-2. The variation of angular velocity with time was obtained from Reference 1.

The results of the analysis shown in Figure B.2-3 indicate the maximum centrifugal force at impact is 93500 lbs. This is 21% less than the maximum force of 117800 lbs as determined from the static analysis as shown in Figure B.1-4. Since the centrifugal force from static analysis has been shown to be conservative, it has been utilized for all tail link analyses.

Figure B.2-1

MODEL OF DISC, TAIL LINK

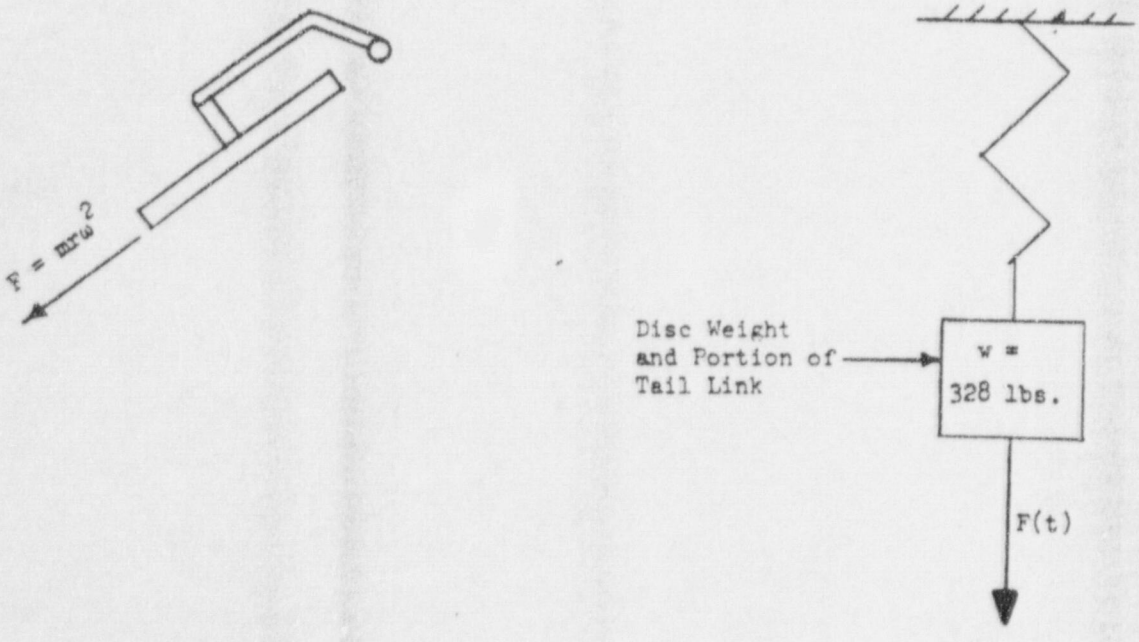

Figure B.2-2

FORCING FUNCTION

Due to Angular Velocity

$FORCE_{Max.}$	$\omega_{Max.}$	ENERGY
117,800 lb.	88.6 Rad/Sec	1.07×10^6 in-lb

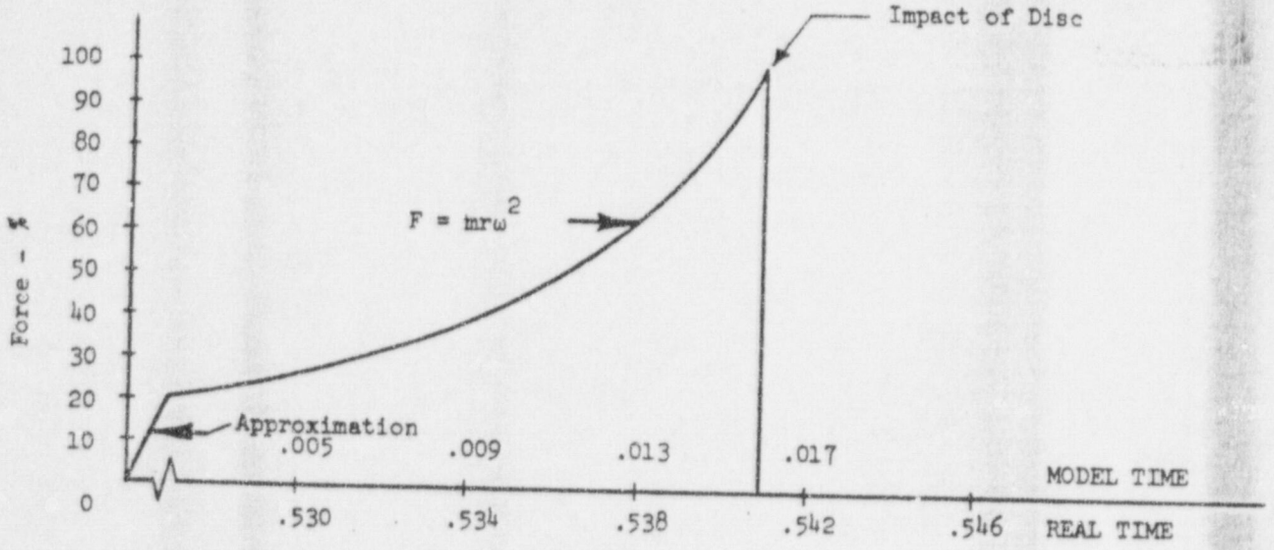

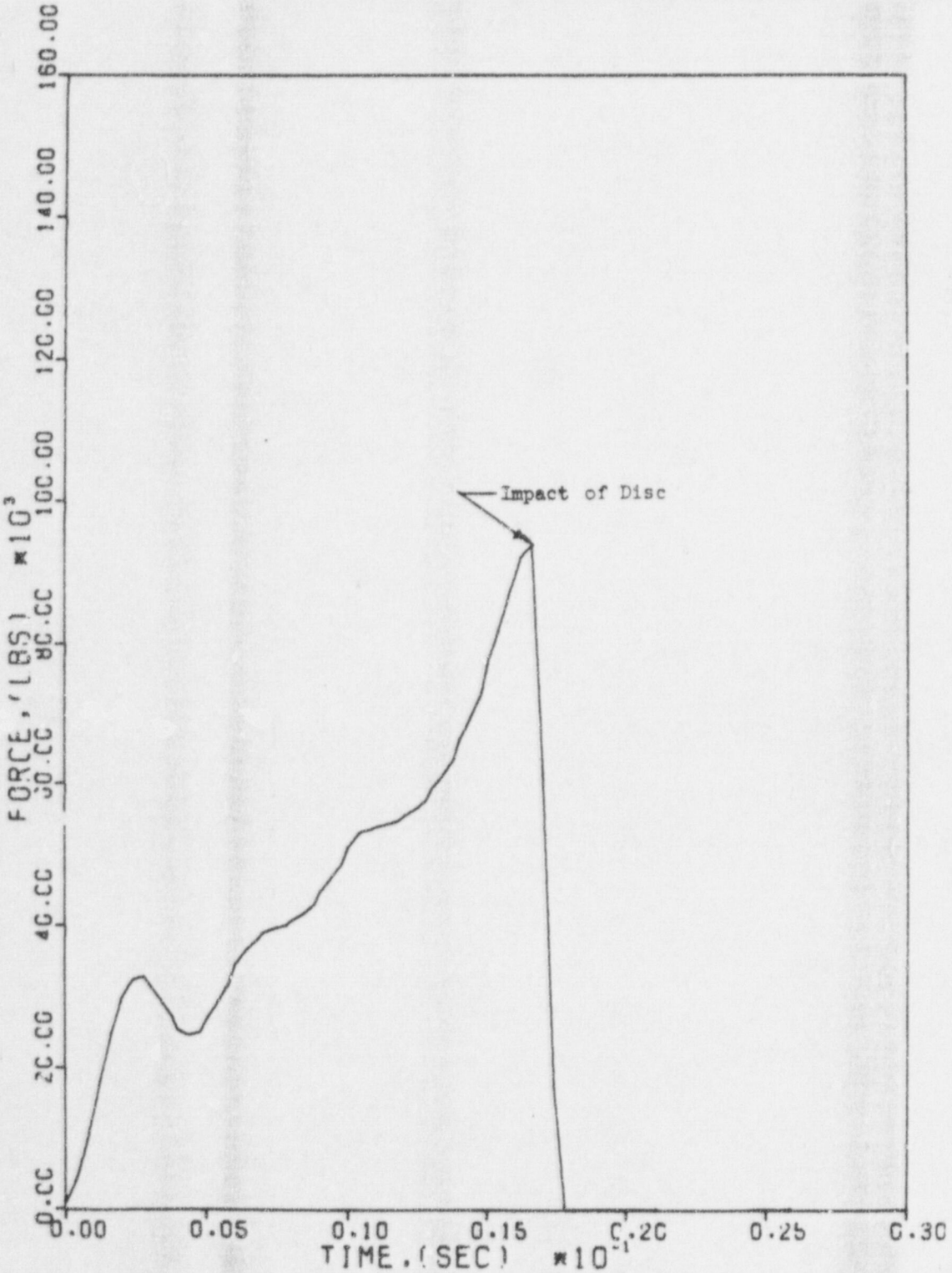

RESPONSE OF TAIL LINK REACTION LOAD

Figure B.2-3

APPENDIX C

Analysis of the

Disc & Tail Link Interaction

C. Analysis of the Disc and Tail Link Interaction

The reaction of the centrifugal force upon the disc through the disc pin is examined in the following analysis. The model is shown in Figures C-1 and C-2.

It is assumed that the pressure on the lower half ring contact area between the disc and tail link is a cosine distribution. Thus to determine effective reaction location of $\bar{P}$

$$\bar{P} = \int_A p\,da = 2p_r \int_0^{\pi/2} \cos\theta\, d\theta \int_{r_1}^{r_2} r\, dr = p\left(r_2^2 - r_1^2\right)$$

$$\bar{P}\,\bar{y} = 2p_r \int_0^{\pi/2} \cos^2\theta \int_{r_1}^{r_2} r^2\, dr = \left(\frac{p\,\pi}{2}\right)\left(\frac{r_2^3 - r_1^3}{3}\right)$$

thus

$$\bar{y} = \frac{\bar{P}\,\bar{y}}{\bar{P}} = \frac{\frac{\pi}{6}\left(r_2^3 - r_1^3\right)}{\left(r_2^2 - r_1^2\right)}$$

with

r_2 = 2.5 in.

r_1 = 1.238 in.

The location is obtained

$\bar{y}$ = 1.524

and

$\bar{P}$ = p_n x 4.7173

By examining the free body diagram in Figure C-3 the major forces are identified.

The maximum centrifugal force which corresponds to the maximum $\omega = 99.64$ rad./sec. is:

$$F = mr\,\omega^2 = \frac{302.8}{386.4} \times 15.75 \times 99.64^2$$

$$F = 122{,}536.\ \text{lb}$$

The total contact force between the tail link and disc is:

$$\overline{P} = \frac{122536. \times 1.913}{1.524} = 153813.\ \text{lb}$$

The maximum contact pressure which is the maximum normal stress of m-m becomes:

$$p_n = \frac{\overline{P}}{4.7173} = \frac{153813.}{4.7173} = 32.6\ \text{ksi}$$

Hence, the maximum stress produced due to the contact is less than the yield stress of 70 ksi per Appendix E.

To determine the stress in the disc pin the forces from equilibrium are:

$$T = \overline{P} = 153813.\ \text{lb}$$

$$S = F = 122536.\ \text{lb}$$

The maximum stress which exists at point a in Figure C-3 is:

$$\sigma_x = \frac{T}{A} = \frac{153813.}{4.827} = 31.87 \text{ ksi}$$

$$\tau_{xy} = \frac{4\ S}{3\ A} = \frac{4 \times 122536.}{3 \times 4.827} = 33.35 \text{ ksi}$$

The calculated principal stress at C are:

$$\sigma_{\substack{1\\2}} = \frac{31.87}{2} \pm \sqrt{\left(\frac{31.87}{2}\right)^2 + 33.85} = 15.94 \pm 37.41$$

$$\sigma_{\substack{1\\2}} = \begin{cases} 53.35 \text{ ksi tension} \\ -21.47 \text{ ksi compression} \end{cases}$$

$$\tau_{max} = 37.41$$

By applying the Mises yield criteria

$$\sigma_{eff} = \frac{1}{\sqrt{2}} \sqrt{(\sigma_1 - \sigma_2)^2 + (\sigma_2 - \sigma_3)^2 + (\sigma_3 - \sigma_1)^2}$$

with

$$\sigma_3 = 0$$

the effective stress is

$$\sigma_{eff} = 66.73 \text{ ksi}$$

which is below the yield strength of 70 ksi per Appendix E.

FIGURE C-1

TAIL LINK & DISC ATTACHMENT AREA

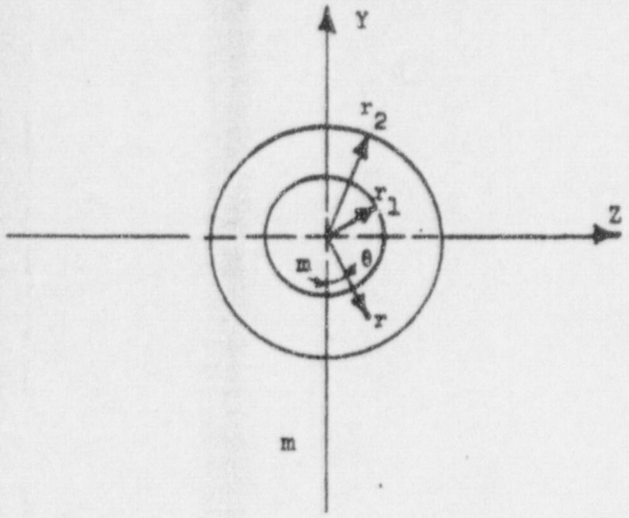

FIGURE C-2

SKEMATIC OF DISC & TAIL LINK AREA

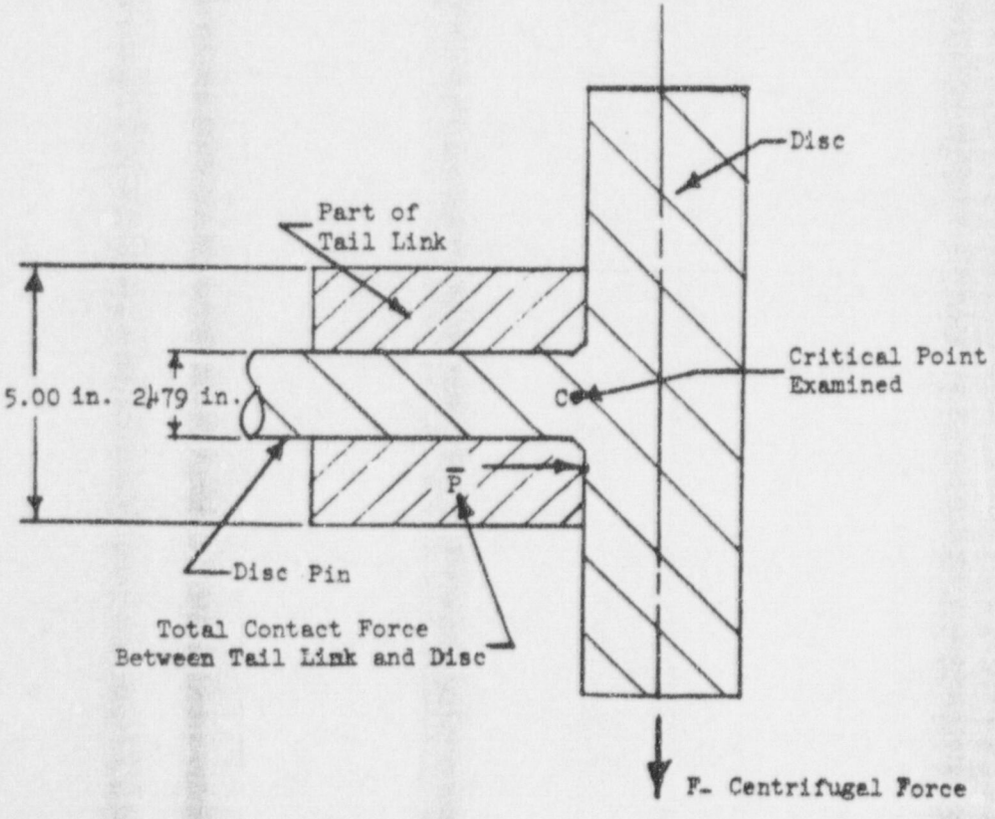

FIGURE C-3

FREEBODY DIAGRAM OF TAIL LINK
AND DISC CONTACT AREA

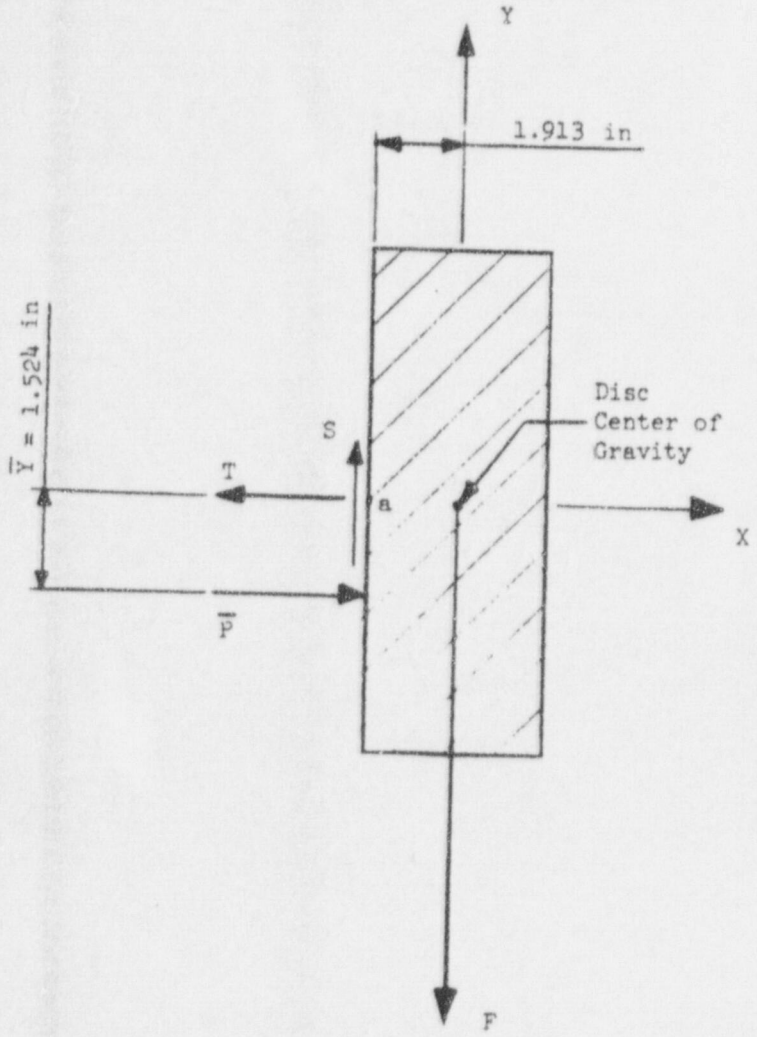

APPENDIX D

Analysis of the Rock Shaft

D. Analysis of the Rock Shaft

The effect of the centrifugal force due to the effective weight of the tail link and disc is examined in the following analysis. The model is shown in Figures D-1 and D-2.

By referring to Figure D-1, it can be seen that the torque T_1 is produced by weight and pressure and T_2 is the restraint torque produced by air pressure in the cylinder acting on the piston. After rupture of the piston in the cylinder, $T_2 = 0$, there would be no torsional stress in the rock shaft.

The maximum torsional stress produced in rock shaft occurs when T_2 is maximum. When the piston ruptures, the pressure in the cylinder = 150 psi, per Reference 8. Also 5550 lbs. on the piston stem produces 233. psi in the air cylinder. Thus the force in the piston stem is:

$$\frac{150.}{233.} \times 5550 = 3573 \text{ lbs},$$

and the maximum torsional stress is:

$$T_{2\ max} = 3573 \times 4.875 = 17418 \text{ lb.-ins.}$$

Torsional stress in the rock shaft is

$$\tau_{max} = \frac{T_{2\ max}\ r}{I_o}$$

$$I_o = \frac{\Pi}{2} r^4 = 1.57$$

$$\tau_{max} = \frac{17418 \times 1.0}{1.57} = 11.1 \text{ ksi}$$

The maximum direct shear, V, in the rock shaft due to the centrifugal force is $\frac{F_{max}}{2}$

where

$$F_{max} = m_{eff} r w^2_{max} = \frac{368.4}{386.4} \times 15.75 \times 99.64^2 = 149083 \text{ lb}$$

and

$$V = \frac{F_{max}}{2} = 74542 \text{ lb.}$$

Maximum shear stress is

$$S_{max} = \frac{4}{3}\frac{V}{A} = 4 \times \frac{74542}{3 \times 1 \text{ kI}^2} = 31.6 \text{ ksi,}$$

where

A = cross section area of the rock shaft.

By conservatively assuming that the rupture of the piston does not occur, the total maximum shearing stress = 31.6 + 11.1

= 42.7 ksi

which is also the principal shearing stress. This is below the yield stress of 85 ksi for the rock shaft.

Figure D-1

SCHEMATIC OF TORQUE PRODUCING STEMS ON ROCK SHAFT

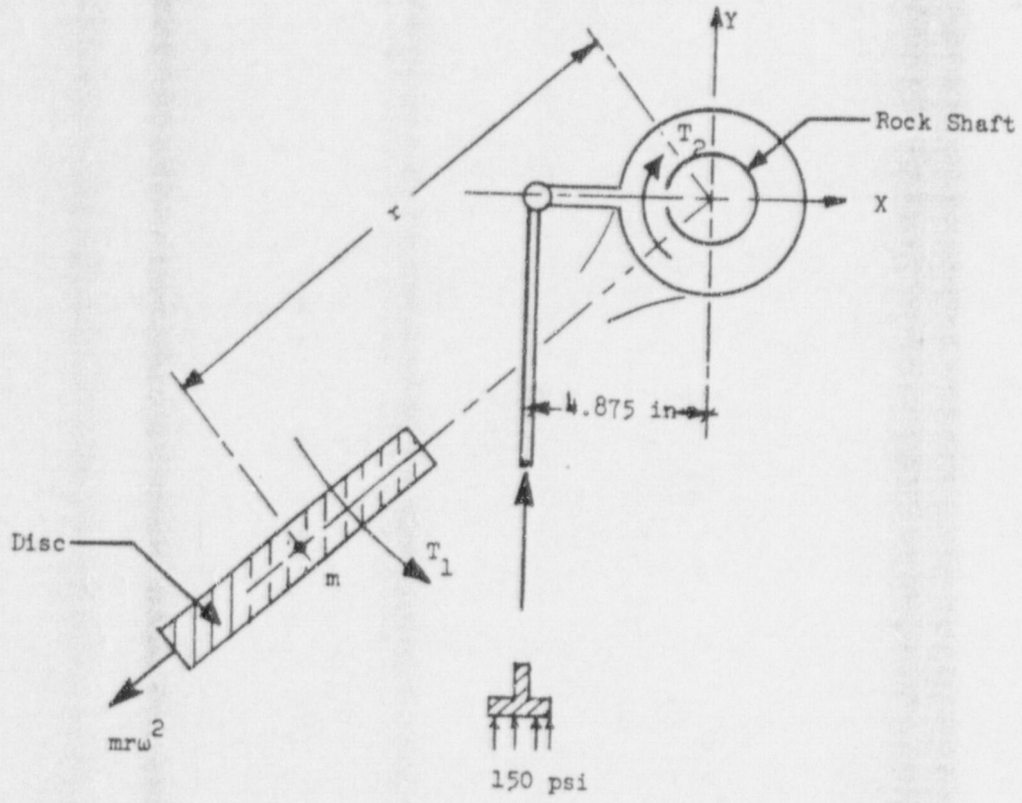

Figure D-2

SCHEMATIC OF ROCK SHAFT, TAIL LINK & VALVE BODY ASSEMBLY

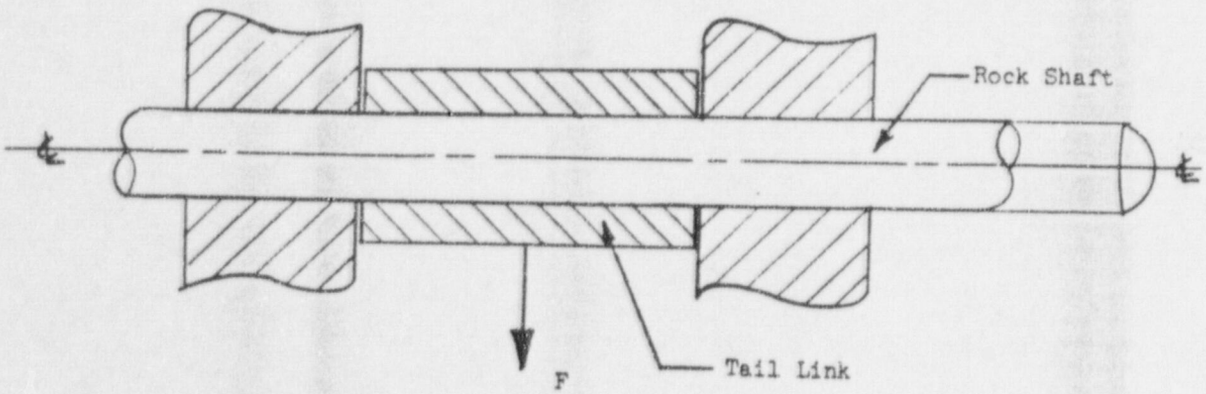

APPENDIX E

Material Properties

E. MATERIAL PROPERTIES

Since high strain rate test data at the operating temperature was not available, it was conservative not to utilize enhanced yield strengths. Temperature dependent material properties were extrapolated from room temperature lot test data and high temperature properties of identical or similar materials. Conservative bilinear approximations for the stress-strain curves as shown in Figures E-1 to E-5 were utilized for all analyses.

The details of how material properties at the operating temperature were determined are shown in the following sections.

E.1 Disc

410 CB Martensitic Stainless Steel

Per Reference 2 the following room temperature lot test data was obtained:

σ_y = 79. ksi

σ_u = 103. ksi

ϵ_u = 22. - 24.%

Per Reference 3 the following lot test data at 600°F was obtained:

σ_y = 65.9 - 67. ksi

σ_u = 81.2 - 82.2 ksi

ϵ_u = 18%

Utilizing the information from Reference 3 and Figure F3.0?12 in Reference 10, which reflects the effect of temperature on 410 CB, the following properties at 546°F are obtained:

$$\sigma_y = 65.9 + \frac{600. - 546.}{600.} \{110. - 95.\}$$

σ_y = 67.2 ksi

$$\sigma_u = 81.2 + \frac{600. - 546.}{600.} \{125. - 105.\}$$

σ_u = 83.0 ksi

$$\epsilon_u = 18 + \frac{600. - 546.}{600.} \{22. - 20.\}$$

ϵ_u = 18.5%

The elastic modulus obtained from Reference 9, Figure 17 at 546°F is:

$E = 24.5 \times 106$

Actual properties utilized in the analysis were:

$\sigma_y = 70.$ ksi

$\sigma_u = 80.$ ksi

$\epsilon_u = 18.$ %

$E = 24.5 \times 10^6$ psi

For constructing the stress strain curve the ultimate stress was assumed to occur at $\epsilon_u - .15\ \epsilon_u$ which is typical for stainless steels.

The stress strain curve reflecting these properties is in Figure E-1.

E.2 Disc Seat

Weld E-309-Cb-15 Austentic Stainless Steel

Per Reference 12 the weld material can be treated as annealed. Annealed properties at room temperature per Reference 11 are:

σ_y = 45. - 55. ksi

σ_u = 85. - 95. ksi

ε_u = 30. - 45.%

From Figure 17, Reference 9 the elastic modulus at temperature is obtained:

$E = 24.5 \times 10^6$ psi

As 309 is a modification of 304 with similar properties, the properties at elevated temperatures for 304 in Reference 10 are applicable. From Figure 3.03132 in Reference 10 the following were obtained:

σ_y = 40. ksi

σ_u = 72. ksi

ε_u = 20.%

The actual properties utilized in the analysis were:

σ_y = 40. ksi

σ_u = 72. ksi

ε_u = 20.%

$E = 24.5 \times 10^6$ psi

The ultimate stress was assumed to occur at $\varepsilon_u - .15\ \varepsilon_u$ which is typical for stainless steels. The stress strain curve reflecting these properties is in Figure E-2.

E.3 Valve Body & Tail Link

A216 WCB Cast Carbon Steel

Per Reference 2 the following room temperature lot test data was obtained:

σ_y = 41.5 - 46. ksi

σ_u = 73.5 - 75. ksi

ϵ_u = 26.5 - 31.%

From Reference 9 the elastic modulus obtained at 546°F from Figure 16 is:

$E = 27.5 \times 10^6$ psi

Properties at the operating temperature from Reference 13 are:

$$\sigma_y = 37. - \left\{\frac{546. - 400.}{400.}\right\} \{37. - 25.\}$$

σ_y = 32.6 ksi

$$\sigma_u = 70. - \left\{\frac{546. - 400.}{400.}\right\} \{70. - 65.\}$$

$_u$ = 68. ksi

$$\epsilon_u = 30. + \left\{\frac{546. - 400.}{400.}\right\} \{38. - 30.\}$$

ϵ_u = 33.%

Actual properties utilized in the analysis were:

σ_y = 36. ksi

σ_u = 65. ksi

ε_u = 24.%

E = 27.5×10^6 psi

The ultimate stress was assumed to occur at $.5\varepsilon_u$ which is a reasonable assumption for a medium carbon steel. The stress strain curve reflecting these properties is in Figure E-3.

E.4 Rock Shaft

416 Martensitic Stainless Steel

Room temperature properties per Reference 2 from lot test data were:

σ_y = 108.5 - 124. ksi

σ_u = 127.- 148. ksi

ε_u = 15.0 - 16.7%

Figure 3.03122 in Reference 10 presents data for 410 which is similar to 416. From this figure at 546° F:

σ_y = 85. ksi

which was utilized in the analysis. This information is reflected in Figure E-4.

E.5 Valve Body Seat

Weld 316 Austenitic Stainless Steel

Per Reference 12 the welded material can be treated as annealed. Typical room temperature properties for 316 were obtained from Reference 9 and noted below:

σ_y = 35. ksi

σ_u = 80. ksi

ε_u = 65.%

Also from Reference 9 typical tensile properties at operating temperature are obtained for 316.

$$\sigma_y = 25.0 - \left\{\frac{546. - 500}{200.}\right\} \left\{25. - 23.\right\}$$

σ_y = 24.9 ksi

$$\sigma_u = 73.0 - \left\{\frac{546. - 500}{200.}\right\} \left\{73. - 72.5\right\}$$

σ_u = 72.8 ksi

$$\varepsilon_u = 49. - \left\{\frac{546. - 500}{200.}\right\} \left\{49. - 47.\right\}$$

ε_u = 48.5%

and

E = 24.5×10^6 per Figure 17

The actual properties utilized in the analyses were:

σ_y = 19. ksi

σ_u = 61. ksi

ε_u = 40. %

E = 24.5×10^6 psi

The ultimate stress was assumed to occur at $\varepsilon_u - .15\ \varepsilon_u$ which is typical for stainless steels. The stress strain curve reflecting these properties is in Figure E-5.

At Room Temp
(Ref. 2),

σ_y = 79 ksi

σ_u = 103 ksi

ε_u = 22-24%

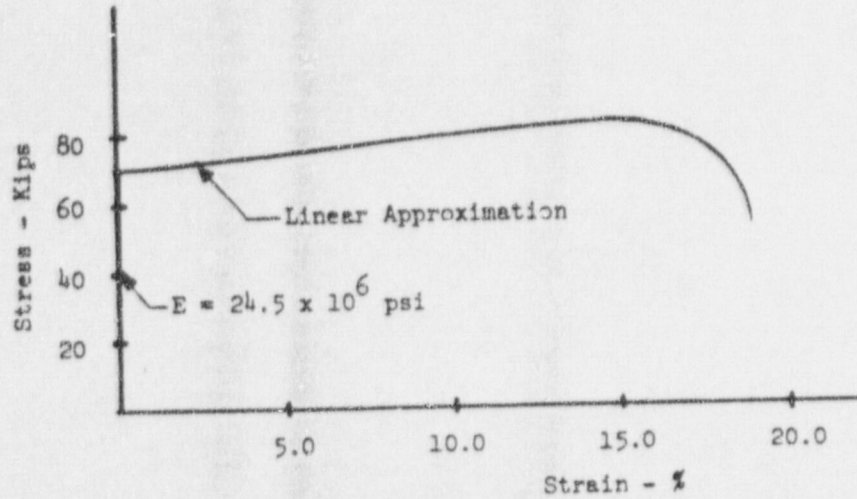

Stress Strain Curve for 410-Cb (Disc) at 546°F from References 3, 9, & 10

Figure E-1

At Room Temp
(Ref. 11 and 12),

σ_y = 45-55 ksi

σ_u = 89-95 ksi

ε_u = 30-45%

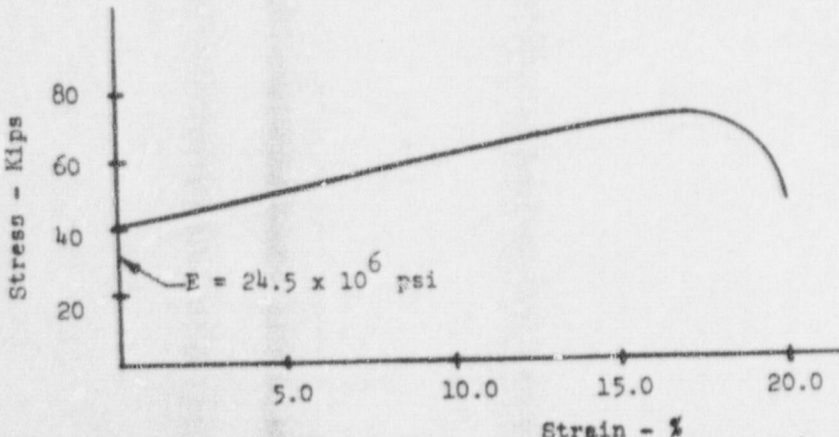

Stress Strain Curve for E-309-Cb-15 (Disc Seat) at 546°F, from References 9 & 10

Figure E-2

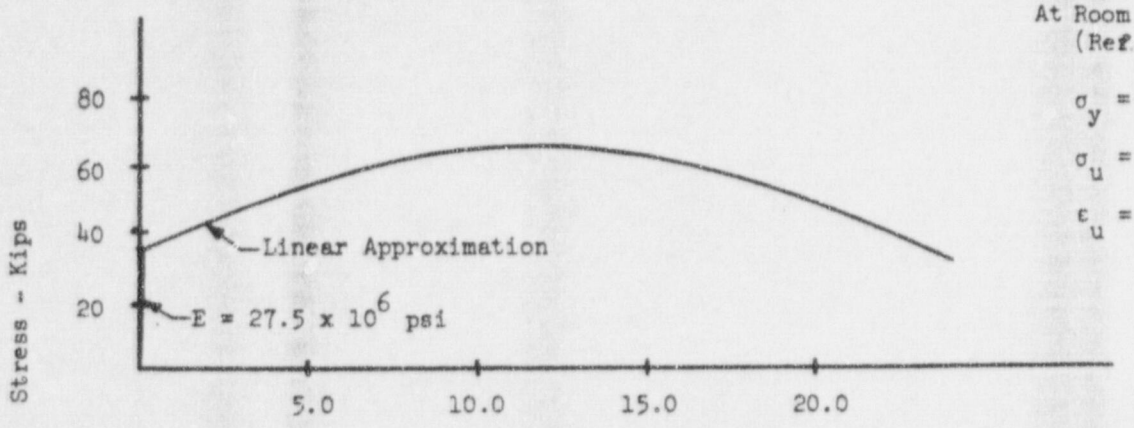

At Room Temp (Ref. 2),

σ_y = 41.5-46.0 ksi

σ_u = 73.5-77.5 ksi

ϵ_u = 26.5-30.0%

Stress Strain Curve for A216-WCB (Valve Body & Tail Link) at 546°F from References 9 & 13

Figure E-3

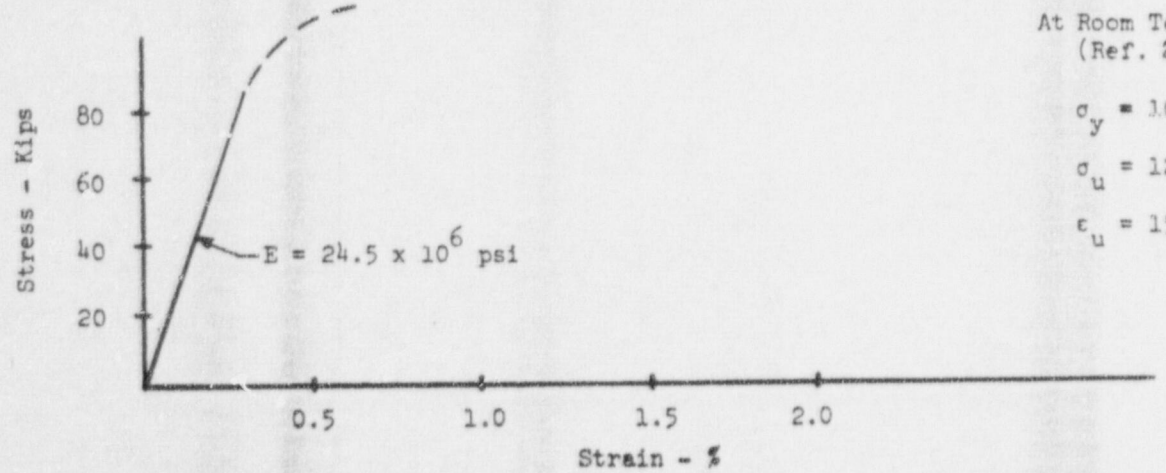

At Room Temp (Ref. 2),

σ_y = 108.5-124 ksi

σ_u = 127-148 ksi

ϵ_u = 15.0-16.7%

Stress Strain Curve for 416 (Rock Shaft) at 546°F from References 9 & 10

Figure E-4

At Room Temp
(Ref. 9 & 12),

σ_y = 34-42 ksi

σ_u = 81 ksi

ϵ_u = 50-55%

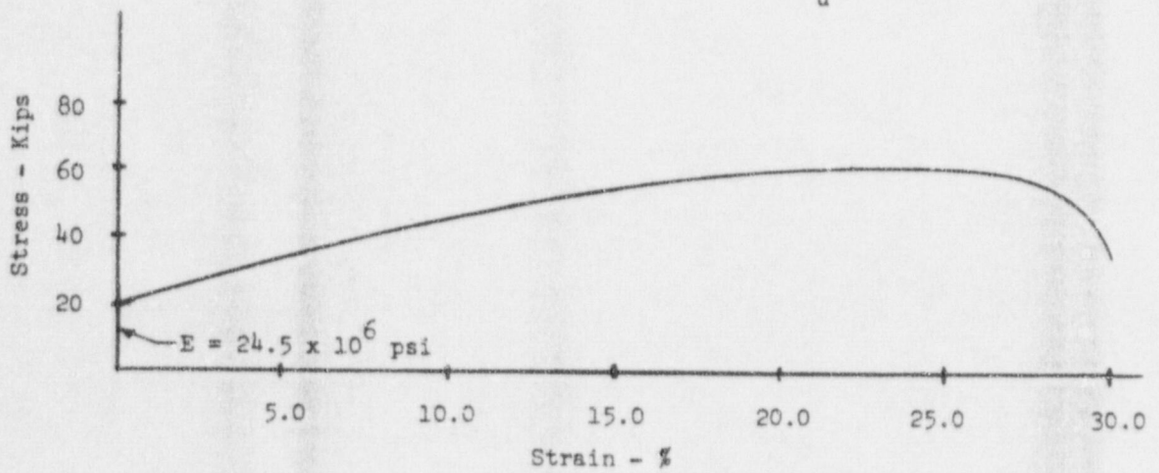

Stress Strain Curve for 316 (Valve Body Seat) at 546°F from Reference 9

Figure E-5